# LATTICE-GAS AUTOMATA AND LATTICE BOLTZMANN EQUATIONS FOR TWO-DIMENSIONAL HYDRODYNAMICS

# A THESIS

Presented to

The Academic Faculty

by

Li-Shi Luo

In Partial Fulfillment
of the Requirements for the Degree of
Doctor of Philosophy in Physics

Georgia Institute of Technology

April, 1993

# LATTICE-GAS AUTOMATA AND LATTICE BOLTZMANN EQUATIONS FOR TWO-DIMENSIONAL HYDRODYNAMICS

A	PPROVED:	
Kurt A. Wiesenfeld, Chairman		Cyrus K. Aidun
Gary D. Doolen		Ronald F. Fox
Edmund J. Mansky, II		T. A. Brian Kennedy
Data Appr	roved by Chairr	APSON

# Acknowledgements

I would like to express my most sincere gratitude to my thesis advisor at Los Alamos National Laboratory, Dr. Gary D. Doolen, for his constant guidance, support and encouragement. This work would have been impossible without his insight and enthusiasm for the subject. I would also like to thank my thesis advisor at Georgia Institute of Technology, Dr. Kurt A. Wiesenfeld, for his concern, support and encouragement throughout the years.

I would like to express my sincere gratitude to my mentors at Los Alamos National Laboratory, among them Drs. Yee-Chun Lee, Harvey A. Rose and Robert H. Kraichnan. Their hands were always available when difficulties arose. I have learned a lot from them.

Throughout the course of my thesis work, I have been helped by many of my colleagues and friends, especially by Drs. Hudong Chen of the Dartmouth College and Yue-Hong Qian of the Princeton University. The proof of the H-theorem for the linear lattice Boltzmann equations in Chapter 5 is due to our close collaboration. I am grateful to Ms. Shuling Hou, Drs. Shiyi Chen, Xiaowen Shan, Qisu Zou, Bruce Boghosian, Zhengsu She, Brosl Hasslacher, Frank Alexander, Daniel O. Martinéz, Jim Sterling, Mario Ancona and Basil Nichols for many stimulating conversations. I am also very grateful to Dr. Jeremy Margulies for his editorial assistance.

I would also like to acknowledge Drs. Cyrus K. Aidun of the Institute of Paper Science and Technology, Ronald F. Fox, T. A. Brian Kennedy and Edmund J. Mansky, II of the School of Physics, Georgia Institute of Technology, for their interest in my work as members of my thesis committee, and for their critical comments. I am very grateful to Dr. Mei-Yin Chou for her generosity in allowing me to use

computers in her laboratory, and for her interest in my work. I would like to thank Drs. Edward W. Thomas, Henry S. Valk and Helmut J. Biritz for their help in administrative matters throughout the years. I am also deeply in debt to my teachers in Georgia Tech. I would like to express my sincere appreciation to those who have taught me in various courses and seminars.

My greatest debt should go to Dr. John Nuttall of the University of Western Ontario. When I first came to Canada in 1982, I was determined to study physics, which I did not have an opportunity to study in my home country. At that time, I could barely speak any English at all. I remembered that, soon after I decided to study with Dr. Nuttall, he went to the Library to find some books he thought would be suitable for me. Many afternoons we spent time together; he explained those books to me, some times sentence by sentence, paragraph by paragraph. Many weekends, his quiet and beautiful farm in the countryside provided a sanctuary for my lonely soul. I also learned farming with modern machinery in his farm. Besides his personal concern, what also really impressed me was Dr. Nuttall's serious attitude toward science. His rigorous and uncompromising manner of conducting scientific research has been, and will always be, the best example for me to follow in my life. I would like to dedicate this thesis to Dr. John Nuttall and Mrs. Suzanne Nuttall.

I would like to acknowledge the financial support of the School of Physics of Georgia Institute of Technology, and of the Center for Nonlinear Studies of Los Alamos National Laboratory. I am also grateful for access to computing resources at the Advance Computing Laboratory of Los Alamos National Laboratory, and for the frequent assistance of the ACL staff.

Finally, I am deeply grateful for the enduring support of my family.

# List of Tables

3.2.1	The collision table for the 6-bit FHP models	56
3.4.1	The collision table for the 7-bit FHP models. Shown here are only the binary collision rules involving a rest particle. The seventh bit of	
	a binary number represents the occupation number of the rest particle.	61

# List of Figures

3.1.1	Two-body (head-on) collision rules of the HPP model	52
3.2.1	Triangular-lattice space for FHP models. In this Figure, two successive microscopic configurations of the FHP lattice-gas automaton are shown. Each arrow represents a discrete particle with the momentum directing as the arrow. The solid arrows are particles at time $t$ ; and the hollow arrows are those at time $t+1$ , after a collision and an advection process	53
3.2.2	The collision rules for the 6-bit FHP lattice-gas automata. In the left column are input states, and in the right are output states	55
3.4.1	The two-body collision rules including rest particle for the 7-bit FHP lattice-gas automata. In the left column are incoming states, and in the right are outgoing states. The solid circle represents the presence of a rest particle	61
3.4.2	The three-body collision rules including rest particle for the 7-bit FHP lattice-gas automata. In the left column are incoming states, and in the right are outgoing states. The solid circle represents the presence of a rest particle	63
4.4.1	Kinematic viscosity $\nu(\mathbf{k})$ , bulk viscosity $\zeta(\mathbf{k})$ and sound speed $c_s(\mathbf{k})$ vs. $\mathbf{k}$ for density = 0.2, and $\theta = 0$ (solid line), $\pi/12$ (dotted line) and $\pi/6$ (dashed line): (a) $\nu(\mathbf{k})$ vs. $\mathbf{k}$ ; (b) $\zeta(\mathbf{k})$ vs. $\mathbf{k}$ ; (c) $c_s(\mathbf{k})$ vs. $\mathbf{k}$ .	. 119
4.5.1	The power spectra to determine sound speed $c_s$ with various values of $k$ and $\theta = \pi/6$ . The histograms represent the data of the power spectra, the thin solid lines are three-point-averaged smoothed results of the spectra, and the thick solid lines are the fitting results of the smoothed ones by the Lorentzian form given by Eq. (4.5.5). (a) $N_y = 128$ , $T = 2^{15} = 32768$ ; (b) $N_y = 64$ , $T = 2^{15} = 32768$ ; (c) $N_y = 32$ , $T = 2^{13} = 8192$ ; (d) $N_y = 16$ , $T = 2^{12} = 4096$	123
4.5.2	Sound speed $c_s(\mathbf{k})$ vs. $k$ for density $d = 0.2$ and $\theta = \pi/6$ . The analytic result is represented by the solid line and the LGA simulations by $+$ . The relative differences between the LGA simulation and the analytic result are less than 1%. Nonlinear effects must explain the differences	124
4.6.1	Forcing rules of FHP 7-bit models. In the left column are states before the forcing. Those in the right column are after forcing. The rules in the first four rows add one unit of momentum to the system, whereas the rule in the fifth row adds two units. The solid arrows indicate occupied states while the hollow ones indicate vacant states. States not indicated may be either occupied or vacant	125

4.6.2	Momentum profile of Poiseuille flow for density $d=0.2$ and a channel width of 16 lattice sites. To obtain steady state, $10^6$ time iterations were run before the average. The momentum $p_x$ is averaged over $L_y$ and over $2 \times 10^6$ time iterations. The analytic result (Eq. $(4.6.9)$ ) is represented by the solid line and the LGA simulation by $\Box$ . The graph is rescaled so that $p_{max}=1$ . Note the agreement for the non-zero momentum at the walls due to finite mean free path. The simulation was run on CRAY Y-MP, with $F_0=1.0641\times 10^{-3}$	128
4.6.3	Velocity profile of plane Couette flow for density per link $d=0.2$ and a channel width of 16 lattice sites. The system size $N_x \times N_y = 16384 \times 32$ . The probability of applying forcing is 0.06. To obtain a steady state, $10^3$ time iterations were run before the average. The velocity, $v_x$ , is averaged over $N_x$ and over $2 \times 10^3$ time iterations. The analytic result of Eq (4.6.15) is represented by the solid line and the LGA simulation by "+". The graph is rescaled so that $v_{max} = 1$ . The simulation was run on a CM-200 computer	131
6.1.1	A schematic two-dimensional plot of the flow channel in the experiment.	146
6.1.2	Geometry of boundary walls used in the simulations	147
6.2.1	The contours of the stream function for the channel flow with square wall. Fig. (a) illustrates the symmetric flow pattern before the symmetry-breaking bifurcation occurs. Figs. (b), (c) and (d) illustrate the asymmetric flow patterns developed after the symmetry-breaking bifurcation occurs	150
6.2.2	The same as the Fig. (6.2.1), with the sinusoidal walls	151
6.2.3	Bifurcation diagram of the symmetry-breaking bifurcation for flow in the symmetric sudden-expansion channel. $\times$ represents the values of $\chi$ with the sinusoidal walls; $\square$ represents $\chi$ with the sinusoidal walls and with random force at the entry; $\bigcirc$ represents $\chi$ with the square walls.	152

# Summary

This thesis contains seven chapters. The discussion in Chapter 1 motivates the study of lattice-gas automata and lattice Boltzmann equations. Chapter 2 briefly reviews the essentials of hydrodynamics and kinetic theory. The hydrodynamic equations, i.e., the Euler equations and the Navier-Stokes equations, are derived from both the continuum and the kinetic point of view. A useful technique to solve the Boltzmann equation, the Chapman-Enskog procedure, is discussed and summarized. Chapter 3 studies the statistical mechanics of the two-dimensional lattice-gas automata due to Frisch, Hasslacher and Pomeau (FHP) in detail. The Chapman-Enskog technique is applied to obtain the Euler equations and the Navier-Stokes equations with the corresponding transport coefficients, i.e., the kinematic and the bulk viscosity and the sound speed, for the FHP lattice-gas automata. Chapter 4 analytically solves the linearized lattice Boltzmann equation. Generalized hydrodynamics of the lattice-gas automata is studied. Also, analytic results of some simple flows such as the Poiseuille flow and the plane Couette flow are obtained. Chapter 5 studies the linear lattice Boltzmann equations. H-theorems for the system are proved. Chapter 6 studies and simulates nonlinear flow phenomena in a 2-D symmetric sudden-expansion channel by the method of the linear lattice Boltzmann equation. A symmetry-breaking bifurcation is observed, and the critical Reynolds number is obtained via the simulations. The results are compared with experimental observations and results by other numerical simulation techniques. Chapter 7 summarizes and concludes the thesis.

# Table of Contents

Ackno	wledg	ements	iii
List o	f Table	es	$\mathbf{v}$
List o	f Figu	res	vi
Summ	nary		viii
Chapte	er 1. I	ntroduction	1
1.1	The N	Intivation of Computational Fluid Dynamics	4
1.2		el Computing	5
1.3		ic Background	7
	1.3.1	Cellular Automata	7
	1.3.2	Discrete Velocity Models	8
	1.3.3	Lattice-Gas Automata	10
1.4	Outlin	ne of This Thesis	13
Chapte	er 2. I	Hydrodynamics and Kinetic Theory	15
2.1	Conti	nuum Description of Hydrodynamics	16
2.2	The S	ymmetries of the Navier-Stokes Equation	22
2.3	Kinet	ic Theory, the Boltzmann Equation and Hydrodynamics	23
	2.3.1	The Distribution Function and Its Hydrodynamic Moments	24
	2.3.2	The Liouville Equation, the BBGKY Hierarchy and Kinetic Transport Equation	25
	2.3.3	The Boltzmann Equation	27
	2.3.4	Conservation Laws and Summational Invariant	29
	2.3.5	Equilibrium and Boltzmann's $H$ -Theorem	30
	2.3.6	From the Boltzmann Equation to the Euler Equations	32
2.4	The C	Shapman-Enskog Procedure and the Navier-Stokes Equation	34
	2.4.1	The Chapman-Enskog Expansion and the Normal Solution of the Boltzmann Equation	35
	2.4.2	The First-Order Solution	39
	2.4.3	The Second Order Solution, the Navier-Stokes Equation and Transport Coefficients	40
	$2\ 4\ 4$	The Validity of the Chapman-Enskog Procedure	42

	2.4.5 Some Further Developments	43
2.5	Some Dimensionless Parameters, the Law of Similarity and Asymptotic Ordering in Hydrodynamics	44
Chapte	er 3. The FHP Lattice-Gas Automata	49
3.1	Prelude: The HPP Lattice-Gas Model	51
3.2	Evolution, Microscopic Equation and Conservation Laws	53
3.3	The Collision Operator, $\mathcal{C}_{\alpha}$	57
3.4	The FHP Model with Rest Particles	60
3.5	Spurious Conserved Quantities	62
3.6	Lattice Symmetries and Tensor Structures	66
3.7	The Equilibrium Distribution Function and Necessary Collisions	68
3.8	The Lattice Boltzmann Equation	73
3.9	The Local and Global $H$ -Theorem	75
3.10	The Solution of the Lattice Boltzmann Equation, the Chapman-Enskog Procedure and Hydrodynamic Equations	78
	3.10.1 The Chapman-Enskog Procedure and the Perturbative Solution of the Lattice Boltzmann Equation	78
	3.10.2 The First Order Solution and the Euler Equations	81
	3.10.3 The Second Order Solution and the Incompressible Navier-Stokes Equations	86
	3.10.4 The Viscosity due to Collisions	91
3.11	Rest Particles and the Compressible Navier-Stokes Equations	93
	3.11.1 The Euler Equations	94
	3.11.2 The Compressible Navier-Stokes Equations	96
	3.11.3 Evaluation of the Coefficients of Viscosity	98
3.12	Normal Mode Frequencies of the LGA Hydrodynamics	100
3.13	Epilogue	102
Chapte	er 4. The Linearized Lattice Boltzmann Equation	105
4.1	The Linearized Lattice Boltzmann Equation and the Linearized Collision Operator	107
4.2	The Circulant Matrix	108
4.3	The Eigenvalues and Eigenvectors of the Linearized Collision Operator	110
4.4	The Solution of the Linearized Lattice Boltzmann Equation and Generalized Hydrodynamics	113
4.5	A Numerical Test of the Dispersion Relation of the Sound Speed	120
	4.5.1 The Green-Kubo Formula	120

	4.5.2 The Simulation	121
4.6	Analytic Solutions for Simple Flows	122
	4.6.1 Poiseuille Flow	126
	4.6.2 Plane Couette Flow	129
Chapte	r 5. The Linear Lattice Boltzmann Equation 1	32
5.1	The Linear Collision Operator and the Equilibrium Distribution 1	133
5.2	Lattice BGK Model	137
	5.2.1 The Single Relaxation Time Approximation	137
	5.2.2 Lattice BGK model	139
5.3	The $H$ -Theorem for Linear Lattice Boltzmann Equations	140
	5.3.1 The Local $H$ -Theorem for Spatially Homogeneous Systems 1	140
	5.3.2 The Global $H$ -Theorem for Spatially Inhomogeneous Systems . $1$	142
Chapte	r 6. Flow in a 2-D Symmetric Sudden-Expansion Channel 1	45
6.1	The Description of the System and the Arrangement of the Simulation 1	46
6.2	Numerical Results for the Steady State Symmetry-Breaking Bifurcation 1	l48
Chapte	r 7. Conclusion and Discussion	53
Refere	nces 1	55
Vita	1	72

## CHAPTER ONE

## INTRODUCTION

This thesis deals with the theoretical basis, and several specific numerical applications to hydrodynamic systems, of two emerging methodologies in studies of complex systems: those of the lattice-gas automata (LGA) and the lattice Boltzmann equations (LBE).

Traditionally, in dealing with physical systems, one would first derive the partial differential equation(s) for the systems when it is possible, then one solves the equation(s) either analytically or numerically. Hydrodynamics is such an example. In the description of partial differential equations, the underlying physical systems are viewed as based on a continuum, despite the fact that the real physical systems could be genuinely discrete. For instance, matter consists of individual molecules. Thus, the density, velocity and other fields in fluids should also be discrete. Therefore, the concept of continuum is an idealization, an approximation of physical reality for fluids.

For many interesting physical systems, the partial differential equations are nonlinear ones. For most nonlinear partial differential equations (with appropriate boundary conditions), analytic solutions are rarely available. Hence, numerical solutions become necessary. However, for certain nonlinear partial differential equations, even numerical solutions are difficult to obtain. The difficulty is inherently associated with the nonlinearity of the equations. One cannot completely face this difficulty without giving up the approach of partial differential equations and the view point of the

continuum.

The approach of using lattice-gas automata and lattice Boltzmann equations is a serious attempt to provide effective alternatives to study complex systems. These alternatives are drastically different from traditional numerical methods for solving partial differential equations, because the concept of the continuum is completely abandoned in this approach. Physical systems are treated at the kinetic level computationally, rather than at the macroscopic level. As we shall see, lattice-gas automata can be viewed as extremely simplified versions of molecular dynamics (MD). Moreover, the phase-space and time are completely discretized. For the sake of computational efficiency, there are usually only a small number of velocities allowed. These methods begin by formulating the mathematical laws of physical systems as simple evolutionary rules for discrete automata. These rules consist of the minimum symmetry criteria for the correct macroscopic dynamics, and neglect a great deal of fine details of the true microscopic physics. However, by having such a drastic simplification, one can still mimic the correct generic macroscopic behavior of some physical systems. But, one would not be able to capture some specific fine details of a particular physical system. This conceptual step has been fruitful in practical applications, because it is the basis for constructing very efficient algorithms to simulate complex systems using modern, massively parallel computers.

Although kinetic theory also treats gases and liquids as systems consisting of individual molecules, the primary goal of kinetic theory is to build a bridge between the microscopic and macroscopic dynamics, rather than to deal with macroscopic dynamics directly. In other words, the goal is to derive macroscopic equations from microscopic dynamics by means of statistics, rather than to solve macroscopic equations. Much of modern research in statistical mechanics is based on attempts to solve either the Boltzmann equation or similar equations for the particle distribution functions. Once the distribution functions are obtained, the hydrodynamic equations

can be derived. One should keep in mind that the Boltzmann equation is a nonlinear integro-differential equation, which is very difficult to solve either analytically or numerically. Therefore, one is not better off dealing with complex systems at the kinetic level by directly solving the Boltzmann equation. On the other hand, molecular dynamics simulates physical systems from the first principles. It directly computes trajectories or wave functions for systems with a large number of particles and with realistic inter-particle interactions (such as the Leonard-Jones potential). Molecular dynamics is computationally very intensive even with some approximations made, and the computational intensity limits the number of particles in, and the length of evolution time scale for a system. Thus, the applicability of molecular dynamics is also limited. In contrast with kinetic theory and molecular dynamics, the methods of the lattice-gas automata and the lattice Boltzmann equations not only provide a simple framework to study complex physical systems in theory, but also offer effective and efficient algorithms for realistic simulations in practice.

In order to motivate the consideration of these parallel methods, this chapter provides a quick look at the objectives and demands of computational fluid dynamics (CFD). This is followed by a discussion of modern parallel computing, and of the somewhat longer history of the lattice-gas automata and their antecedents. The chapter closes with an overview of the balance of the thesis, including a brief description of the original results presented here.

Although the applications of these methods to hydrodynamical systems have been emphasized through out this thesis, these methods are certainly not limited to hydrodynamic systems, and indeed, these methods have been successfully applied to study complex physical systems other than hydrodynamics. These applications shall be mentioned, and the relevant references shall be cited later in this chapter.

# 1.1 The Motivation of Computational Fluid Dynamics

Hydrodynamics is one of the oldest subjects in the realm of physical science. Hydrostatics was studied by Archimedes in the time of the Greek antiquity (circa 200 B.C.). Euler's equation for inviscid fluids was obtained by Euler in the eighteenth century. The governing equation of viscous fluids, the Navier-Stokes equation, has been studied for over a century. The most challenging problem of the subject is the theory of turbulence. Despite great advances in the physical sciences, there has only been small progress towards a better understanding of turbulence. No complete quantitative theory of turbulence has yet evolved; rather, what is known are some qualitative results [1]. The theory of turbulence could be the last frontier in the field of classical physics.

The theory of turbulence deserves serious attention, because turbulence occurs in almost every situation involving the motion of fluids. It affects the resistance of bodies such as automobiles, aircraft, boats, etc. to motion in fluids. A quantitative theory of turbulence would advance our ability to effectively control turbulence in engineering applications.

One obstacle to the development of a theory of turbulence is the fact that the Navier-Stokes equations are a set of nonlinear partial differential equations. These equations are merely a statement of (mass, momentum and energy) conservation laws and cannot be solved analytically in general. The nonlinearity of the equations leads to a rich complexity of the system. Indeed, hydrodynamic flows can exhibit an extremely rich variety of complex phenomena, such as bifurcations and period-doubling phenomena [1]. These phenomena are so rich that, in many respects, fluid flows can be considered as an excellent paradigm of complexity in natural systems.

Analytic solutions of the Navier-Stokes equations are very difficult to obtain, except for a few simple cases. Thus, it is inevitable to use either experimental or

computational means to study hydrodynamic systems. Only within the last decade or so have computers become powerful enough to begin solving the Navier-Stokes equations, albeit for highly simplified flow situations. Now, numerically generated turbulence information is being accepted by discriminating scientists with the same degree of confidence as afforded to empirical observations. In fact, numerical work is providing new insights into the interrelationships of the many flow variables. One of these is the relationship between pressure and strain in a fluid, for which no measurement is yet possible [2]. Despite this computational progress, current computers are not yet powerful enough, in either memory or speed, to simulate flows over entire aircraft. An estimate based upon traditional algorithms and a Reynolds number of 10<sup>8</sup> suggests that one needs exa-bytes (10<sup>18</sup>) of memory and exa-FLOPs of speed for such a simulation [2]. Current computers can only offer giga-bytes of memory and giga-FLOPs of speed, although a tera-FLOP (10<sup>12</sup>) machine may be realized in the near future. The computational needs of the scientific and engineering communities demand drastic improvement in both computer hardware and software. Some important issues in computational physics, especially in computational fluid dynamics [3], have been addressed in March 1993 issue of Physics Today, a special issue dedicated to high-performance computing and physics.

# 1.2 Parallel Computing

In the past decade, the advance in computer technology has been enormous. A desk-top workstation nowadays is just as, or almost as, powerful as a supercomputer a decade ago. Yet, the fastest supercomputer available now, such as the CRAY Y-MP, still by no means satisfies the demand from the scientific community. Many challenges, such as weather forecasting and computational field theory, are still outstanding in terms of our computational capability. As discussed in the preceding section, one particular long-standing challenge to physical science is the understanding of turbu-

lence. A hydrodynamic system with a high Reynolds number (> 10<sup>5</sup>, say) is a highly nonlinear dynamical system with many degrees of freedom. The numerical simulation of such systems is many orders of magnitude beyond the capacity of existing computing resources [2]. There are similar limitations on our ability to simulate many other multi-dimensional field theories [4].

An important development in recent years has been the emergence of parallel computers and algorithms. Massively parallel computers, such as the Connection Machines [5,6], the Hypercube, the Delta Touchstone and the Paragon (the last three machines are made by Intel), and parallel algorithms have provided a hope to break through a limitation set by the traditional computers with serial-architectures. Recently, a spectral code with a grid-size of 512<sup>3</sup> to simulate turbulence (currently this is the largest grid-size) has been implemented on a Connection Machine 200 (CM-200) at the Advanced Computing Laboratory, Los Alamos National Laboratory. This code is running on CM-200 at a speed of approximately 30 seconds per-time-step, which is equivalent to 5-6 giga-FLOPs [7]. This speed is three times of the reported speed achieved by a CRAY Y-MP computer with four processors (2 giga-FLOPs). The new Connection Machine 5 (CM-5) is expected to advance the speed one order of magnitude faster. Because parallel computing will certainly become dominant in the 90's and well into next century, there is an urgent need to develop fully parallel algorithms. The methods of the lattice-gas automata and the lattice Boltzmann equations are such parallel algorithms, suitable for solving many difficult problems which can be described by nonlinear partial differential equations, including the Navier-Stokes equations.

### 1.3 Historic Background

In what follows, we give a quick review of the history of cellular automata, discrete velocity models of gases and lattice-gas automata. The connections between these subjects are somewhat obvious. The lattice-gas automata belong to a special class of cellular automata. The lattice-gas automata and discrete velocity models have the similarity in modeling collision processes with finite number of discrete velocities.

#### 1.3.1 Cellular Automata

In the early 1950's, in the beginning of the computer era, Stanislaw Ulam [8] and John von Neumann [9] had foreseen the use of a totally discrete model for natural phenomena. Von Neumann's primary aim was to devise a simple system capable of reproducing itself in the manner of a living organism. The best-known model of the kind, the "game of life" invented by John H. Conway, has a biological aspect, as the name suggests; cells are born, live or die depending on the local population density. The model, now referred to as a cellular automaton (CA) [10–15], is a dynamical system in which time, space and state variables are all discrete, and there is only a finite number of states on each site of the discrete space. The evolution of the automaton is fully determined by a set of prescribed rules, which only involve the states at the preceding time step. The updating rules are usually simple. A precise definition of cellular automata can be stated as follows. Let  $A_i^t$  be a state variable at a moment of discrete time t and a site i of discrete space, the evolution of  $A_i^t$  is determined by

$$A_{i}^{t+1} = f(\{A_{i+j}^{t} | \|j\| \le r\}), \tag{1.3.1}$$

where r is the radius of interaction. Typical rules, which determine the form of f, are local (for instance, involving only the nearest neighbor interactions, that is, r = 1).

Although the updating rules of cellular automata can be very simple, the evo-

lution, or patterns, exhibited by cellular automata can have an amazing complexity [15,16]. The complex behavior of cellular automata is believed to be physically related to a variety of natural phenomena, including self-organization phenomena, and fluid flows [15,17]. Cellular automata can also be viewed as the idealization of partial differential equations arising from mathematical physics [17–19]. Some classes of cellular automata have been shown to be capable of universal computation, *i.e.*, beginning with a particular initial state, the evolution of some automata could implement any chosen finite algorithm [16]. Owing to their simple construction and discrete nature, cellular automata are very suitable models to implement on digital computers. Nowadays, cellular automata are becoming widely studied and have had broad applications to many disciplines in science and engineering [15,19–22].

#### 1.3.2 Discrete Velocity Models

While the lattice-gas automata are perhaps the simplest discrete-velocity models to simulate fluid motion, there exist other discrete-velocity models. A reference in a 1964 paper by Broadwell [23] to an 1890 paper of J. C. Maxwell [24] has spawned the erroneous notion, often stated in recent literature [25–27], that consideration of discrete velocity models dates from Maxwell's 1890 paper. The earliest discrete gas model known to the author is the one which can be found in the 1954 textbook by Hirschfelder, Curtiss and Bird [28, pages 2–5]. Their model consists of particles residing in cubic lattice space. The model is only used to derive the equation of state for gases.

Several discrete velocity models exist in the literature. Some of them are reviewed briefly in M. H. Ernst's article in Physics Reports [29]. These models are mentioned here only in a historical perspective. For further details, there are exten-

<sup>&</sup>lt;sup>1</sup>The author is grateful to Prof. James E. Broadwell at Cal. Tech. for bringing this fact to the author's attention.

sive reviews of the subject [30,26].

One of the simplest discrete velocity models is the one proposed by T. Carleman [31]. The Carleman model considers only particles with velocities v = +1 or -1in one dimension. The dynamics is defined by binary collisions: A pair of particles with +1 velocity collide and become a pair of particles with -1 velocity, and vice versa. Another similar model is the McKean model [32,33]. The McKean model and the Carleman model differ from each other in their binary collisions. In the McKean model, the binary collisions are that a pair of particles with +1 and -1 velocities collide and become a pair of particles with -1 velocity, and vice versa. The general solutions of the nonlinear Boltzmann equations for both the Carleman and the McKean models are unknown, except for certain special cases [29, 34]. Macroscopically, these two models conserve the total number of particles and total energy (trivially, as a consequence of the particle number conservation), but violate momentum conservation. The total momentum in both models decays to zero, as  $t \to \infty$ . These two models can also be related to each other by a partial differential equation, the telegrapher's equation [29]. Furthermore, the Carleman and the McKean models are special cases of a more general two-velocity model, the Illner model [35,36], which includes the most general quadratic (binary) collisions. For the Illner model, some soliton solutions can be found analytically [34]. The Carleman, the McKean and the Illner models are also called two-velocity models.

In 1964, Broadwell proposed two discrete gas models with six ( $\mathbf{v} = (\pm 1, 0, 0)$ ,  $(0, \pm 1, 0)$  and  $(0, 0, \pm 1)$ ) and eight velocities ( $\mathbf{v} = (\pm 1, \pm 1, \pm 1)$ ) allowed, respectively, and with continuous space-time, to study rarefied gas dynamics [23,37]. Broadwell solved the Boltzmann equations analytically for these two models, obtained solutions for some simple flows, and computed shock structure for one of the models. There also exist many other models of this type [25].

In 1968, Kadanoff and Swift used a master-equation with continuous time, dis-

crete space and momentum to study hydrodynamics (propagation of sound waves) in a spin system [38].

It should be stressed that most of the models mentioned here have been studied only within the framework of the Boltzmann equation. They provide various model equations for the Boltzmann equation, which are easier to deal with than the Boltzmann equation. They are very helpful in studies of some important issues in kinetic theory, such as fluctuation theory. Neither the derivation of correct macroscopic equations from microscopic dynamics in simple models, nor the utilization of the model equations of the Boltzmann equation as effective algorithms are the primary concern in the previous studies of these models. Most studies in the field of discrete velocity models are concerned with the exact solutions (or the analytic properties of the solutions) of the Boltzmann model equations [23, 37, 25, 39-41, 34, 42, 26, 43]. However, in studies of the lattice-gas automata and the lattice Boltzmann equations, the primary goal is to use these simple models to simulate complex systems. In order to do so, two criteria must be satisfied: First, these models must lead to the correct macroscopic equations. Second, they must be simple enough in construction that they can be used as fast algorithms for difficult physical problems. These features of the methods of the lattice-gas automata and the lattice Boltzmann equations clearly distinguish themselves from other models.

#### 1.3.3 Lattice-Gas Automata

The lattice-gas automata [44–50] belong to a special class of cellular automata designed to study various physical systems. The lattice-gas automata and their floating-point-number counterparts, the lattice Boltzmann equations, have been successfully applied to physical systems such as single- or multi-phase/component fluids [51–58], chemically reactive systems [59–65], non-ideal gases [66, 67], phase transition phenomena [68, 69, 58], magnetohydrodynamics (MHD) [70–73], and semiconductor de-

vice [74,75]. The lattice-gas automata and the lattice Boltzmann equations can be used to "solve" partial differential equations arising from physics, such as the Navier-Stokes equations [44], Burgers' equation [76], the wave equation [77], Poisson's equation [78], reaction-diffusion equations [59,79], and the transport equation of electrons in semiconductors [74,75]. Models of various lattice-gas automata share some common advantages. First of all, the updating rules are local (the nearest neighbor interactions only, for instance). Thus the system can be updated synchronously. In other words, computer programs of lattice-gas models are completely parallel. Second, the rules can be implemented either by simple Boolean logic operations (bit operations) or by table look-up. Therefore the algorithm is very fast. Third, since the LGA algorithm involves only integer (or logical) operations, the utilization of memory can be highly efficient. Fourth, since the updating rules are logical, thus they are exact and have no roundoff error. Hence, the conservation laws can be exactly satisfied and the algorithm is unconditionally stable. Last, the method is capable of efficiently handling complicated boundary geometries, which are difficult to implement using conventional methods.

The LGA also possess some inherent shortcomings. One problem is that with only a few particle speeds allowed, the range of velocities is severely limited. A second problem is that because of the discreteness of the model, Galilean invariance is lost. Also the lattice-gas equation of state is velocity-dependent. A fourth problem is that the results tend to be noisy, with significant density and velocity fluctuations occurring. Nevertheless, most of these shortcomings can be overcome by an alternative method — the method of the lattice Boltzmann equations, a floating-point-number variation of the lattice-gas automata. We will discuss in detail both the lattice-gas automata and the lattice Boltzmann equations in later chapters.

The first totally discrete model, a lattice-gas automaton in two-dimensional square-lattice space, was proposed by Hardy, Pomeau and de Pazzis (HPP) in 1972

[80–83]. The HPP model, a discussion of which shall be postponed to §3.1, is a simple model introduced to analyze fundamental questions in statistical mechanics such as ergodicity and the divergence of transport coefficients in two dimensions. The HPP model has some useful features. For instance, it leads to sounds waves; it also gives the correct result on the divergence of transport coefficients in two dimensions. However, it does not satisfy symmetry criteria required for a correct hydrodynamic equation. Like all of those aforementioned discrete-velocity models, the HPP model only has been used for theoretical analysis. It cannot be used as an effective algorithm to simulate realistic physical systems. Therefore, it has not had an extensive impact on practical applications.

The serious use of the lattice-gas automata as a practical algorithm to simulate complex systems only began in the mid-80's, after Frisch, Hasslacher, Pomeau (FHP) [44,46] and Wolfram [45] invented the lattice-gas automaton in two-dimensional triangular lattice space which leads to the Navier-Stokes equation. The FHP model later was adapted to three-dimensional space by d'Humières, Lallemand, and Frisch [84,46]. The lattice-gas automata, which are integer models, later also evolved to their floating-point number counterpart, the lattice Boltzmann methods [85,86].

In recent years, lattice-gas automata have distinguished themselves from other discrete-velocity models because they can be used to solve complicated and practically important problems which are very difficult for traditional methods, such as multi-phase or multi-component fluids flowing through porous media. Even in simulations of some standard benchmarking problems, such as flow past a cylinder in three-dimensional space, lattice-gas automata have provided some results which are in excellent agreement with experimental results and, indeed, have superseded the accuracy of the recent numerical results obtained by traditional methods of computational fluid dynamics simulation [87]. There are other encouraging facts supporting the new methods. It is not an overstatement that, together with massively parallel

computers such as the Connection Machines, the methods of the lattice-gas automata and the lattice Boltzmann equations have become useful algorithms for numerical simulations.

#### 1.4 Outline of This Thesis

This thesis is solely devoted to the methods of the lattice-gas automata and the lattice Boltzmann equations. These subjects, newly emerged in 1980's, utilize the statistical mechanics of simple discrete models to simulate complex physical systems. This thesis contains both theoretical and computational aspects of the lattice-gas automata and the lattice Boltzmann equations. The theory of lattice-gas automata and the lattice Boltzmann equations in two-dimensional space is reviewed in detail so that those who are new to the field can use it as an overview. One new contribution we have made here is contained in Chapter 4. We have solved the linearized lattice Boltzmann equation valid for the entire range of the Knudsen number, and have demonstrated its usefulness by obtaining analytic solutions for simple flows. In Chapter 5, we prove H-theorems for the linear lattice Boltzmann equations. In Chapter 6, we also provide an original study of simulations using the linear lattice Boltzmann equation: The symmetry-breaking bifurcation phenomenon of flow past a two-dimensional, symmetric sudden-expansion channel. Comparisons of our results with experimental ones and those by other numerical methods are made.

This thesis is arranged as follows: In Chapter 2, hydrodynamic and kinetic theory are reviewed very briefly. This chapter provides the theoretical background for the later chapters. The hydrodynamic equations are derived from both the continuum and the kinetic point of view. A key technique for solving the Boltzmann equation and for evaluating the transport coefficients, the Chapman-Enskog procedure, is discussed in detail. In Chapter 3, the theory of lattice-gas automata is given

in extensive detail. The properties associated with the evolution of the lattice-gas automata are studied: The conservation laws and the symmetries of various models. The lattice Boltzmann equation and the related H-theorems for the LGA systems are shown. The macroscopic equations with the corresponding transport coefficients for the LGA are obtained via the Chapman-Enskog procedure. The normal-mode analysis of the hydrodynamic equation derived from the lattice-gas automata is presented. In Chapter 4, a rigorous analysis of the linearized lattice Boltzmann equation is given with results on generalized hydrodynamics and solutions for some special flows. In Chapter 5, the linear lattice Boltzmann equations are studied. The linear lattice Boltzmann equations can be used as an efficient algorithm for simulation. The H-theorems for the linear Boltzmann equation with continuous space and time, but with discrete velocity are proved. In Chapter 6, numerical results of flow in a two-dimensional, symmetric sudden-expansion channel by the linear lattice Boltzmann equation are presented. Finally, in Chapter 7, conclusions and discussions on future studies are presented.

## CHAPTER TWO

## HYDRODYNAMICS AND KINETIC THEORY

Fluid motions are described by the Euler equations for ideal fluids and by the Navier-Stokes equations for dissipative fluids [88,1]. These hydrodynamic equations can be derived by two different methods: the continuum method and kinetic theory [47]. In the continuum approach, individual molecules are ignored. The fluid is viewed as continuous matter. At each point of this continuous fluid, unique values of the density, velocity, pressure and temperature field are assumed to exist. The fact that this continuous fluid must obey the conservation laws of mass, momentum and energy gives rise to a set of partial differential equations governing the field variables. The solution to these differential equations then defines the spatial variation and temporal evolution of each field variable. These continuous field variables are assumed to be the mean values of the molecular magnitudes of corresponding field variable at each position and time.

The alternative method, *i.e.*, kinetic theory, treats the fluid as consisting of molecules whose motion is governed by the laws of dynamics. Kinetic theory attempts to derive the macroscopic behavior of the fluid from the laws of mechanics and probability theory. Kinetic theory can obtain the same set of partial differential equations governing the field variables, as by the continuum method, provided that the fluid is near equilibrium and the constitutive relation between stress and strain is assumed. In addition, this method yields expressions for the transport coefficients, such as coefficients of viscosity and thermal conductivity, in terms of molecular quantities such

as the interacting forces between molecules or the mean free path of molecules.

The validity of these two methods lies in two different, but overlapping, domains. The continuum approach is appropriate only if the microscopic scale, *i.e.*, the mean free path of molecules, is negligible compared to the smallest physical length scale of the flow field. Kinetic theory is useful when the concept of the continuum is no longer valid, that is, when the effect of the mean free path cannot be ignored, such as in rarefied gases.

The remains of this chapter review the essential basics of hydrodynamics and kinetic theory. In the next two sections, the Euler equations and the Navier-Stokes equations are derived from continuum point of view and the symmetry properties of the Navier-Stokes equation are discussed. In §2.3, basic concepts of kinetic theory are briefly introduced. In §2.4, the Chapman-Enskog procedure to obtain the normal solutions of the Boltzmann transport equation, the Navier-Stokes equation with the corresponding transport coefficients is studied.

# 2.1 Continuum Description of Hydrodynamics

In this section, we will derive hydrodynamical equations using the concept of the continuum fields. To do so, we only need to apply Gauss' theorem for a vector field,  $\mathbf{A}$ , in D-dimensional space,

$$\int_{\partial V} \mathbf{A} \cdot \hat{\mathbf{n}} dS = \int_{V} \nabla \cdot \mathbf{A} dV, \qquad (2.1.1)$$

and the Reynold's transport theorem [88]

$$\frac{d}{dt} \int_{V} B dV = \int_{V} \left( \frac{\partial B}{\partial t} + \nabla \cdot (B \mathbf{v}) \right) dV \tag{2.1.2}$$

to the conserved quantities: mass, momentum and energy. The Euler equations for the ideal fluid can thus be obtained:

$$\frac{\partial \rho}{\partial t} + \nabla \cdot \rho \mathbf{v} = 0, \qquad (2.1.3a)$$

$$\rho \frac{\partial \mathbf{v}}{\partial t} + \rho(\mathbf{v} \cdot \nabla) \mathbf{v} = -\nabla P, \qquad (2.1.3b)$$

$$\rho \frac{\partial \varepsilon}{\partial t} + \rho(\boldsymbol{v} \cdot \nabla)\varepsilon = -P(\nabla \cdot \boldsymbol{v}), \qquad (2.1.3c)$$

where P is the hydrodynamic pressure,  $\rho$ ,  $\boldsymbol{v}$  and  $\varepsilon$  are the mass density, the (macroscopic) velocity and the internal energy density per unit mass, respectively. These fields are the fundamental thermodynamical variables specifying a thermodynamical system. Eqs. (2.1.3) are differential forms of mass, momentum and energy conservation laws for ideal fluids (non-dissipative fluids).

For fluids with dissipation, *i.e.*, the viscous fluids, the continuity equation (2.1.3a) remains the same. However, the equations for momentum and energy are different from Eqs. (2.1.3b) and (2.1.3c). Let's rewrite Euler's equation (2.1.3b) as

$$\frac{\partial}{\partial t}(\rho v_i) = -\frac{\partial \Pi_{ij}}{\partial x_i},\tag{2.1.4}$$

where the momentum flux density tensor,

$$\Pi_{ij} = P\delta_{ij} + \rho v_i v_j \,, \tag{2.1.5}$$

represents the completely reversible momentum transfer due to the pressure forces exerted on the fluid and to mechanical mass transfer for ideal fluid. For dissipative fluids, viscosity causes irreversible momentum transfer in the direction opposite to the velocity gradient. The equation of motion for viscous fluids can be obtained by

adding a viscous term,  $-\sigma'_{ij}$ , to the momentum flux density tensor for the ideal fluid

$$\Pi_{ij} = P\delta_{ij} + \rho v_i v_j - \sigma'_{ij} = \rho v_i v_j - \sigma_{ij}. \tag{2.1.6}$$

The tensor,

$$\sigma_{ij} = -P\delta_{ij} + \sigma'_{ij}, \qquad (2.1.7)$$

is the stress tensor, and  $\sigma'_{ij}$  is the viscous stress tensor. For a Newtonian fluid, the stress tensor must satisfy the following conditions:

- 1. The stress tensor,  $\sigma_{ij}$ , is isotropic, so that the fluid properties are point functions.
- 2. The stress tensor,  $\sigma_{ij}$ , linearly depends only on the deformation-rate tensor  $\tau_{ij} \equiv \frac{\partial v_i}{\partial x_j}$ .
- 3. When the fluid is in linear uniform motion or in solid-body rotation, the viscous stress tensor,  $\sigma'_{ij}$ , must vanish, so that the stress is hydrostatic and the pressure exerted by the fluid is the thermodynamic one.

Using symmetry considerations, the viscous stress tensor,  $\sigma'_{ij}$ , for the Newtonian fluid in a D-dimensional Cartesian coordinate system can be written as (For details see the derivation in Ref. [1]),

$$\sigma'_{ij} = \eta_1 \left( \frac{\partial v_i}{\partial x_j} + \frac{\partial v_j}{\partial x_i} - \frac{2}{D} \delta_{ij} \frac{\partial v_k}{\partial x_k} \right) + \eta_2 \delta_{ij} \frac{\partial v_l}{\partial x_l}$$

$$= (\eta_1 S_{ijkl} + \eta_2 \delta_{ij} \delta_{kl}) \frac{\partial v_k}{\partial x_l},$$
(2.1.8)

where the tensor  $S_{ijkl}$  is defined as follows:

$$S_{ijkl} \equiv \delta_{ik}\delta_{jl} + \delta_{il}\delta_{jk} - \frac{2}{D}\delta_{ij}\delta_{kl}, \qquad (2.1.9)$$

and,  $\eta_1$  and  $\eta_2$  are coefficients of viscosity:  $\eta_1$  is the dynamic shear viscosity and  $\eta_2$  the dynamic bulk viscosity. In the definition of the viscous stress tensor, Eq. (2.1.8), the Einstein convention for summation is used, *i.e.*, repeated indices are summed. This convention is used unless confusion may occur. Note that  $\sigma'_{ij}$  is constructed so that the expression in the bracket proportional to  $\eta_1$  is traceless. The tensor  $S_{ijkl}$  is isotropic and has the following symmetry properties

$$S_{ijkl} = S_{jikl} = S_{jilk}, (2.1.10a)$$

$$\sum_{i} S_{iikl} = \sum_{k} S_{ijkk} = 0. \tag{2.1.10b}$$

Then, from Euler's equation (2.1.4) and Eq. (2.1.6), the general form of the compressible Navier-Stokes equation can be written as the following

$$\rho \frac{\partial v_i}{\partial t} + \rho v_j \frac{\partial v_i}{\partial x_j} = -\frac{\partial P}{\partial x_i} + \frac{\partial}{\partial x_j} \left( \eta_1 S_{ijkl} + \eta_2 \delta_{ij} \delta_{kl} \right) \frac{\partial v_k}{\partial x_l}. \tag{2.1.11}$$

The coefficients of viscosity are usually functions of density,  $\rho$ , pressure, P, and temperature, T, which in general are not constant throughout the fluid.

Similarly, we can obtain the energy equation for fluids with dissipation:

$$\rho \frac{\partial \varepsilon}{\partial t} + \rho(\boldsymbol{v} \cdot \nabla) \varepsilon = \sigma_{ij} \frac{\partial v_i}{\partial x_j} + \nabla \cdot (\kappa \nabla T)$$

$$= -P \nabla \cdot \boldsymbol{v} + (\eta_1 S_{ijkl} + \eta_2 \delta_{ij} \delta_{kl}) \frac{\partial v_i}{\partial x_j} \frac{\partial v_k}{\partial x_l} + \nabla \cdot (\kappa \nabla T), \qquad (2.1.12)$$

where  $\kappa$  is the thermal conductivity. Here the constitutive relation between heat-flux,  $\mathbf{Q}$ , and temperature gradient,  $\nabla T$ ,  $\mathbf{Q} = -\kappa \nabla T$ , has been used. In above equation,  $\sigma_{ij} \frac{\partial v_i}{\partial x_j}$  represents the work done by the surface force, and  $\nabla \cdot (\kappa \nabla T)$  represents the

<sup>&</sup>lt;sup>1</sup>Some care must be taken when the Einstein convention is in use: The convention is valid only for product terms, for example, the term  $\delta_{ij}\delta_{jk}$  implies  $\sum_{j}\delta_{ij}\delta_{jk}$ . However, for a single tensor, the repeated indices do not imply the sum, for example,  $\delta_{ii} \neq \sum_{i,j=i}\delta_{ij}$ 

energy transfer due to heat conduction. The term  $-P\nabla \cdot \boldsymbol{v}$  represents the reversible transfer of energy due to compression. The other two terms related to the coefficients of viscosity measure the rate at which mechanical energy is being irreversibly converted into thermal energy. Collectively they define the dissipation function:

$$\Phi = \sigma'_{ij} \frac{\partial v_i}{\partial x_j} = (\eta_1 S_{ijkl} + \eta_2 \delta_{ij} \delta_{kl}) \frac{\partial v_i}{\partial x_j} \frac{\partial v_k}{\partial x_l}$$

$$= (\eta_2 - \frac{2}{D} \eta_1) (\nabla \cdot \boldsymbol{v})^2 + \eta_1 \left( \frac{\partial v_i}{\partial x_j} + \frac{\partial v_j}{\partial x_i} \right) \frac{\partial v_i}{\partial x_j}$$

$$= (\eta_2 - \frac{2}{D} \eta_1) (\nabla \cdot \boldsymbol{v})^2 + \frac{1}{2} \eta_1 \left( \frac{\partial v_i}{\partial x_j} + \frac{\partial v_j}{\partial x_i} \right)^2,$$
(2.1.13)

which is positive definite for Newtonian fluids [88]. The positivity of  $\Phi$  manifests itself for the fact that the energy transfer caused by the viscous effects is indeed irreversible.

To summarize, we have obtained a set of partial differential equations in *D*-dimensional Euclidean space:

$$\frac{\partial \rho}{\partial t} + \frac{\partial}{\partial x_i} (\rho v_i) = 0, \tag{2.1.14a}$$

$$\rho \frac{\partial v_i}{\partial t} + \rho v_j \frac{\partial v_i}{\partial x_j} = -\frac{\partial P}{\partial x_i} + \frac{\partial}{\partial x_j} (\eta_1 S_{ijkl} + \eta_2 \delta_{ij} \delta_{kl}) \frac{\partial v_k}{\partial x_l}, \tag{2.1.14b}$$

$$\rho \frac{\partial \varepsilon}{\partial t} + \rho v_i \frac{\partial \varepsilon}{\partial x_i} = -P \frac{\partial v_i}{\partial x_i} + (\eta_1 S_{ijkl} + \eta_2 \delta_{ij} \delta_{kl}) \frac{\partial v_i}{\partial x_j} \frac{\partial v_k}{\partial x_l} + \frac{\partial}{\partial x_i} \left( \kappa \frac{\partial T}{\partial x_i} \right). \quad (2.1.14c)$$

Together with the thermal and caloric equations of state

$$P = P(\rho, T), \qquad (2.1.15a)$$

$$\varepsilon = \varepsilon(\rho, T),$$
 (2.1.15b)

this set of equations governs the motion of Newtonian fluids, provided that the transport coefficients,  $\eta_1$ ,  $\eta_2$  and  $\kappa$  are given. In situations where the variations of  $\rho$ , P and T are negligible, then the transport coefficients  $\eta_1$ ,  $\eta_2$  and  $\kappa$  can be approximately treated as constants, and Eqs. (2.1.14b) and (2.1.14c) can be simplified:

$$\rho \frac{\partial \mathbf{v}}{\partial t} + \rho(\mathbf{v} \cdot \nabla)\mathbf{v} = -\nabla P + \eta_1 \nabla^2 \mathbf{v} + (\eta_2 + \frac{(D-2)}{D}\eta_1)\nabla(\nabla \cdot \mathbf{v}), \tag{2.1.16a}$$

$$\rho \frac{\partial \varepsilon}{\partial t} + \rho \mathbf{v} \cdot \nabla \varepsilon = -P \nabla \cdot \mathbf{v} + (\eta_1 S_{ijkl} + \eta_2 \delta_{ij} \delta_{kl}) \frac{\partial v_i}{\partial x_j} \frac{\partial v_k}{\partial x_l} + \kappa \nabla^2 T.$$
 (2.1.16b)

For incompressible fluids which satisfy

$$\frac{D\rho}{Dt} \equiv \frac{\partial\rho}{\partial t} + \boldsymbol{v} \cdot \nabla\rho = 0, \qquad (2.1.17)$$

thus

$$\nabla \cdot \boldsymbol{v} = 0, \qquad (2.1.18)$$

the momentum equation reduces to the incompressible Navier-Stokes equation

$$\frac{\partial \boldsymbol{v}}{\partial t} + (\boldsymbol{v} \cdot \nabla) \boldsymbol{v} = -\frac{1}{\rho} \nabla P + \nu \nabla^2 \boldsymbol{v}, \qquad (2.1.19)$$

where  $\nu = \eta_1/\rho$  is the kinematic viscosity. Accordingly, the energy equation for the incompressible fluid becomes

$$\rho \frac{\partial \varepsilon}{\partial t} + \rho \mathbf{v} \cdot \nabla \varepsilon = \eta_1 \left( \frac{\partial v_i}{\partial x_i} + \frac{\partial v_j}{\partial x_i} \right) \frac{\partial v_i}{\partial x_j} + \nabla \cdot (\kappa \nabla T). \tag{2.1.20}$$

Eqs. (2.1.18), (2.1.19) and (2.1.20) constitute the governing equations for incompressible fluids, the incompressible Navier-Stokes equations.

If  $\rho = \text{constant}$ , the divergence of Eq. (2.1.19) leads to the Poisson equation for the pressure:

$$\nabla^2 P = -\rho \frac{\partial v_i}{\partial x_j} \frac{\partial v_j}{\partial x_i}.$$
 (2.1.21)

This equation can be used to eliminate the pressure term from the set of equations.

# 2.2 The Symmetries of the Navier-Stokes Equation

Besides the conservation laws, Newtonian mechanics possesses symmetries (invariances) under the following transformations: continuous spatial-temporal translations, time reversal, space reversal, arbitrary 3-D rotations (isotropy) and Galilean transformation. Inevitably, the Navier-Stokes equation inherits some of the symmetries of Newtonian mechanics. Indeed, the Navier-Stokes equation has all of the symmetries of Newtonian mechanics except time reversal because of the dissipation. The invariances of continuous spatial-temporal translations and space reversal are rather obvious in the Navier-Stokes equation. The other two invariances, *i.e.*, isotropy and Galilean invariance, are less trivial.

The isotropy of the Navier-Stokes equation is reflected in the structure of the viscous stress tensor

$$\sigma'_{ij} = (\eta_1 S_{ijkl} + \eta_2 \delta_{ij} \delta_{kl}) \frac{\partial v_k}{\partial x_l},$$

which in turn depends on the structure of the tensor  $S_{ijkl}$  and  $\delta_{ij}\delta_{kl}$ . It can be shown that the most general isotropic tensor of the fourth order must consist of products of Kronecker delta symbols with pairs in indices [89], *i.e.*,

$$c_{ijkl} = a\delta_{ij}\delta_{kl} + b\delta_{ik}\delta_{jl} + c\delta_{il}\delta_{jk}, \qquad (2.2.1)$$

where a, b and c are constants. Then it is obvious that  $\sigma'_{ij}$  is isotropic, because both  $S_{ijkl}$  and  $\delta_{ij}\delta_{kl}$  are.

Galilean invariance uniquely determines the form of the nonlinear term  $\rho vv$ , *i.e.*, the factor in front of the nonlinear term is unity. Suppose  $\Pi_{ij} = P\delta_{ij} + g\rho v_i v_j$ , where g is a constant. Then in the new inertial frame of reference where  $\mathbf{x}' = \mathbf{x} - \mathbf{u}t$ , and  $\mathbf{v}' = \mathbf{v} - \mathbf{u}$ , we have

$$\Pi'_{ij} = P\delta_{ij} + g\rho(v_i - u_i)(v_j - u_j)$$
(2.2.2)

and

$$\left(\frac{\partial(\rho \mathbf{v})}{\partial t}\right)' = \left(\frac{\partial}{\partial t} + \mathbf{u} \cdot \nabla\right) (\rho \mathbf{v} - \rho \mathbf{u}). \tag{2.2.3}$$

Consequently, the equation

$$\left(\frac{\partial(\rho \mathbf{v})}{\partial t}\right)' = -\frac{\partial\Pi'_{ij}}{\partial x_j} \tag{2.2.4}$$

leads to

$$\frac{\partial(\rho \mathbf{v})}{\partial t} = -\frac{\partial}{\partial x_i} (P\delta_{ij} + g\rho v_i v_j - (g-1)\rho(v_i u_j + v_j u_i - u_i u_j)). \tag{2.2.5}$$

Now, it is apparent that if and only if g = 1, the above equation is independent of u, that is, the equation is Galilean invariant. Therefore, g = 1 is a necessary condition for Galilean invariance.

# 2.3 Kinetic Theory, the Boltzmann Equation and Hydrodynamics

In contrast to the continuum field approach, kinetic theory assumes that a fluid is made of a huge number of molecular constituents, whose motions obey Newtonian mechanics. Directly solving the system with a large number of degrees of freedom, which is in the order of the Avogadro's number ( $10^{23}$ ), is impossible. Moreover, the objective is not to know the motion of every individual molecular constituents. Rather, one is interested in the collective behavior of such systems. Therefore, a statistical description of the system becomes inevitable. One fundamental assumption in kinetic theory is that complete information for the statistical description of a fluid at, or near, thermal equilibrium is contained in the single-particle distribution function  $F_1(\mathbf{r}, \Gamma, t)$  for the molecular constituents of the system, where variables  $\mathbf{r}$ ,  $\Gamma$  and t denote space coordinates, the rest of the phase-space coordinates complementary to space coordinates  $\mathbf{r}$  (such as linear and angular momenta) of the molecules, and time,

respectively. The moments of the distribution function are the macroscopic quantities, which are observables.

The central problem of kinetic theory is to formulate and solve the transport equation, which is the equation of the distribution function, with different collision processes dictated by the nature of the interactions between molecules. The solution of the transport equation provides the equations of the moments, which are the macroscopic equations such as the Navier-Stokes equations, with relevant transport coefficients, such as the shear and bulk viscosities which are unknowns in the Navier-Stokes equations. One particular transport equation is the celebrated Boltzmann equation. In this section, the Boltzmann equation is formulated, and in the next section, a perturbative technique for solving the Boltzmann equation, the Chapman-Enskog procedure, is reviewed.

#### 2.3.1 The Distribution Function and Its Hydrodynamic Moments

We define the number density

$$n(\mathbf{r}, \Gamma, t) = NF_1(\mathbf{r}, \Gamma, t), \qquad (2.3.1)$$

and the mass density

$$f(\mathbf{r}, \Gamma, t) = m_0 N F_1(\mathbf{r}, \Gamma, t), \qquad (2.3.2)$$

where  $m_0$  is the mass of a single molecule and N is the number of molecules.

The macroscopic quantities, namely the mass density,  $\rho(\mathbf{r}, t)$ , the macroscopic velocity,  $\mathbf{v}(\mathbf{r}, t)$  and the internal energy density,  $\varepsilon(\mathbf{r}, t)$ , are moments of the mass density distribution function  $f(\mathbf{r}, \Gamma, t)$ :

$$\rho(\mathbf{r}, t) = \int f(\mathbf{r}, \Gamma, t) d\Gamma, \qquad (2.3.3a)$$

$$\rho \mathbf{v}(\mathbf{r}, t) = \int \boldsymbol{\xi} f(\mathbf{r}, \Gamma, t) d\Gamma, \qquad (2.3.3b)$$

$$\rho \varepsilon(\mathbf{r}, t) = \frac{1}{2} \int (\boldsymbol{\xi} - \boldsymbol{v})^2 f(\mathbf{r}, \Gamma, t) d\Gamma, \qquad (2.3.3c)$$

where  $\boldsymbol{\xi}$  is the *microscopic* velocity. The first five moments of  $f(\boldsymbol{r}, \Gamma, t)$ , given by the above equations, are the hydrodynamic moments. The equipartition assumption gives the following relation between the temperature, T, and the energy density,  $\varepsilon$ :

$$\varepsilon = \frac{D_0}{2}RT = \frac{D_0}{2m_0}k_BT, \qquad (2.3.4)$$

where  $D_0$  is the number of the degrees of freedom of individual molecules, R is the ideal gas constant, and  $k_B$  is the Boltzmann constant. In what follows, we will only consider point-like molecules, *i.e.*, the molecules without structure; thus  $D_0 = 3$ , and  $\Gamma = m_0 \boldsymbol{\xi} = \boldsymbol{p}$  ( $\boldsymbol{p}$  is the momentum), or  $\Gamma = \boldsymbol{\xi}$ , whichever is convenient in the context.

# 2.3.2 The Liouville Equation, the BBGKY Hierarchy and Kinetic Transport Equation

The basic equation of kinetic theory is the evolution equation for  $f(\mathbf{r}, \Gamma, t)$  in the presence of molecular collisions. Conservation of phase-space volume (Liouville's theorem) leads to the transport equation,

$$\frac{Df}{Dt} \equiv \frac{\partial f}{\partial t} + \boldsymbol{\xi} \cdot \nabla f = \mathcal{C}(f), \qquad (2.3.5)$$

where C(f), a collision operator, models the rate of change of the distribution function  $f(\mathbf{r}, \Gamma, t)$  due to collisions, of which the details are yet to be determined. We will derive Eq. (2.3.5) for a particular form of C(f) in what follows.

For the sake of completeness, we shall start with a derivation of the BBGKY hierarchy of equations. Given a system of N particles, with the N-particle distribution

function,  $F_N$ , the M-particle reduced distribution function,  $F_M$ , is defined as

$$F_{M}(\boldsymbol{r}_{1}, \dots, \boldsymbol{r}_{M}, \Gamma_{1}, \dots, \Gamma_{M}, t) =$$

$$\int d\boldsymbol{r}_{M+1} \dots d\boldsymbol{r}_{N} d\Gamma_{M+1} \dots d\Gamma_{N} F_{N}(\boldsymbol{r}_{1}, \dots, \boldsymbol{r}_{N}, \Gamma_{1}, \dots, \Gamma_{N}, t) . \qquad (2.3.6)$$

Specifically, for M = 1, 2, we have

$$F_{1}(\boldsymbol{r}_{1}, \Gamma_{1}, t) =$$

$$\int d\boldsymbol{r}_{2} \cdots d\boldsymbol{r}_{N} d\Gamma_{2} \cdots d\Gamma_{N} F_{N}(\boldsymbol{r}_{1}, \dots, \boldsymbol{r}_{N}, \Gamma_{1}, \dots, \Gamma_{N}, t), \qquad (2.3.7a)$$

$$F_{2}(\boldsymbol{r}_{1}, \boldsymbol{r}_{2}, \Gamma_{1}, \Gamma_{2}, t) =$$

$$\int d\boldsymbol{r}_{3} \cdots d\boldsymbol{r}_{N} d\Gamma_{3} \cdots d\Gamma_{N} F_{N}(\boldsymbol{r}_{1}, \dots, \boldsymbol{r}_{N}, \Gamma_{1}, \dots, \Gamma_{N}, t). \qquad (2.3.7b)$$

The Liouville equation for  $F_N$  is

$$\frac{\partial F_N}{\partial t} + \sum_{i=1}^N \left[ \dot{\boldsymbol{r}}_i \cdot \frac{\partial F_N}{\partial \boldsymbol{r}_i} + \dot{\boldsymbol{p}}_i \cdot \frac{\partial F_N}{\partial \boldsymbol{p}_i} \right] = 0.$$
 (2.3.8)

With the substitution

$$\dot{\boldsymbol{p}}_{i} = -\sum_{\substack{j=1\\j\neq i}}^{N} \frac{\partial V_{ij}}{\partial \boldsymbol{r}_{i}}, \qquad (2.3.9)$$

where  $V_{ij} = V_{ij}(\|\mathbf{r}_i - \mathbf{r}_j\|)$  is the pair-wise potential, we can obtain the BBGKY hierarchy of equations (for details see Refs. [90–92]):

$$\frac{\partial F_{M}}{\partial t} + \sum_{i=1}^{M} \dot{\boldsymbol{r}}_{i} \cdot \frac{\partial F_{M}}{\partial \boldsymbol{r}_{i}} - \sum_{\substack{i,j=1\\i\neq j}}^{M} \frac{\partial V_{ij}}{\partial \boldsymbol{r}_{i}} \cdot \frac{\partial F_{M}}{\partial \boldsymbol{p}_{i}} =$$

$$(N - M) \int d\boldsymbol{r}_{M+1} d\Gamma_{M+1} \sum_{i=1}^{M} \frac{\partial V_{iM+1}}{\partial \boldsymbol{r}_{i}} \cdot \left(\frac{\partial F_{M+1}}{\partial \boldsymbol{p}_{i}} - \frac{\partial F_{M+1}}{\partial \boldsymbol{p}_{M+1}}\right) . \tag{2.3.10}$$

This equation was named after Bogoliubov, Born, Green, Kirkwood, and Yvon, who

independently and originally derived the equation. Of particular interest are the first two equations in the hierarchy:

$$\frac{\partial F_1}{\partial t} + \dot{\boldsymbol{r}}_1 \cdot \frac{\partial F_1}{\partial \boldsymbol{r}_1} = (N-1) \int d\boldsymbol{r}_2 d\Gamma_2 \frac{\partial V_{12}}{\partial \boldsymbol{r}_1} \cdot \left( \frac{\partial F_2}{\partial \boldsymbol{p}_1} - \frac{\partial F_2}{\partial \boldsymbol{p}_2} \right) , \qquad (2.3.11a)$$

$$\frac{\partial F_2}{\partial t} + \dot{\boldsymbol{r}}_1 \cdot \frac{\partial F_2}{\partial \boldsymbol{r}_1} + \dot{\boldsymbol{r}}_2 \cdot \frac{\partial F_2}{\partial \boldsymbol{r}_2} - \frac{\partial V_{12}}{\partial \boldsymbol{r}_1} \cdot \left( \frac{\partial F_2}{\partial \boldsymbol{p}_1} - \frac{\partial F_2}{\partial \boldsymbol{p}_2} \right) =$$

$$(N-2) \int d\boldsymbol{r}_3 d\Gamma_3 \left[ \frac{\partial V_{13}}{\partial \boldsymbol{r}_1} \cdot \left( \frac{\partial F_3}{\partial \boldsymbol{p}_1} - \frac{\partial F_3}{\partial \boldsymbol{p}_2} \right) + \frac{\partial V_{23}}{\partial \boldsymbol{r}_2} \cdot \left( \frac{\partial F_3}{\partial \boldsymbol{p}_2} - \frac{\partial F_3}{\partial \boldsymbol{p}_2} \right) \right] . \quad (2.3.11b)$$

Obviously, the equation for  $F_M$  is not closed, and so is the equation for  $f(\mathbf{r}, \Gamma, t)$ . The complete BBGKY hierarchy is equivalent to the Liouville equation, or the Hamiltonian equations of the system.

#### 2.3.3 The Boltzmann Equation

The celebrated Boltzmann equation [90, 91, 93, 92] is a specific closed equation for  $f(\mathbf{r}, \Gamma, t)$ . Boltzmann assumed molecular chaos (stosszahlansatz). The immediate implication of this assumption is the fact that the molecules entering a collision process do not have any correlation with each other so that the following factorization can be realized:

$$F_2(\mathbf{r}_1, \mathbf{r}_2, \Gamma_1, \Gamma_2, t) = F_1(\mathbf{r}_1, \Gamma_1, t) F_1(\mathbf{r}_2, \Gamma_2, t).$$
 (2.3.12)

To justify the assumption of molecular chaos, we must also assume:

- 1. The density is sufficiently low so that only binary collisions need to be considered;
- 2. The spatial dependence of gas properties is sufficiently slow so that collisions can be thought of as being localized in physical space;

3. The inter-particle potential is of sufficiently short range so that the assumption of low density is meaningful.

With all these assumptions, and with the Boltzmann gas limit (BGL):

$$N \to \infty$$
 (2.3.13a)

$$m_0 \to 0$$
 (2.3.13b)

$$r_0 \to 0 \tag{2.3.13c}$$

$$Nm_0 = \text{constant}$$
 (2.3.13d)

$$Nr_0^2 = \text{constant}$$
 (2.3.13e)

where  $r_0$  is the interaction range, the Boltzmann equation, which is a nonlinear integro-differential equation of  $f(\mathbf{r}, \Gamma, t)$ , can be obtained (for details see [90,91,94]):

$$\frac{\partial f}{\partial t} + \boldsymbol{\xi} \cdot \frac{\partial f}{\partial \boldsymbol{r}} = \frac{1}{m_0} \int dS d\boldsymbol{\xi}_1 \|\boldsymbol{\xi}_1 - \boldsymbol{\xi}\| \left( f' f'_1 - f f_1 \right) , \qquad (2.3.14)$$

where  $f' \equiv f(\mathbf{r}, \boldsymbol{\xi}', t)$ ,  $f'_1 \equiv f(\mathbf{r}, \boldsymbol{\xi}'_1, t)$ ,  $f \equiv f(\mathbf{r}, \boldsymbol{\xi}, t)$  and  $f_1 \equiv f(\mathbf{r}, \boldsymbol{\xi}_1, t)$ , respectively. In the above equation, dS is the collision cross section; in particular, it is here the area-element of the disc of radius,  $r_0$ , perpendicular to the vector  $(\boldsymbol{\xi}_1 - \boldsymbol{\xi})$ ;  $\boldsymbol{\xi}'$  and  $\boldsymbol{\xi}'_1$  are the velocities before a binary collision, which become  $\boldsymbol{\xi}$  and  $\boldsymbol{\xi}_1$  after the collision;  $\boldsymbol{\xi}'$  and  $\boldsymbol{\xi}'_1$  are related to  $\boldsymbol{\xi}$  and  $\boldsymbol{\xi}_1$  by momentum and energy conservation constraints. The Boltzmann equation (2.3.14) is a specific form of the transport equation (2.3.5).

It should be noted that, historically, the Boltzmann equation was studied long before the BBGKY hierarchy. Boltzmann studied the equation in 1872 [95]. It was not until 1946 that Bogoliubov and others studied the BBGKY hierarchy. However, mathematically it is logical to include the Boltzmann equation as the first order

truncated and closed equation in the BBGKY hierarchy. This is the reason we choose to present the Boltzmann equation and the BBGKY hierarchy in a nonchronological order.

#### 2.3.4 Conservation Laws and Summational Invariant

Let h denote a function of velocity  $\xi$  with the property that the sum of its values for the two particles is the same before and after a collision:

$$h(\boldsymbol{\xi}_1) + h(\boldsymbol{\xi}_2) = h(\boldsymbol{\xi}_1') + h(\boldsymbol{\xi}_2').$$
 (2.3.15)

Such a quantity is called a summational invariant.

It can be shown that the collision operator C(f) in Eq. (2.3.14) conserves mass, momentum and energy [96], *i.e.*,

$$\int h\mathcal{C}(f)d\Gamma = 0, \qquad (2.3.16)$$

where

$$h = c_0 + \boldsymbol{c}_{\xi} \cdot \boldsymbol{\xi} + c_{\varepsilon} \xi^2 , \qquad (2.3.17)$$

 $c_0$  and  $c_{\varepsilon}$  are arbitrary constants, and  $c_{\xi}$  is an arbitrary *D*-dimensional constant vector.

It can also be shown that mass, momentum and energy are the only summational invariants for structureless molecules. (For molecules with structures, angular momentum is a summational invariant, too.) Because, the conservation of momentum and energy imposes four conditions relating  $\xi'$  and  $\xi'_1$  to  $\xi$  and  $\xi_1$  (with given  $\xi$  and  $\xi_1$ ), and specification of the scattering angles imposes two more. Then there is no freedom remaining for additional constraints.

#### 2.3.5 Equilibrium and Boltzmann's H-Theorem

In most cases, the Boltzmann equation is difficult to solve. However, even without solving the Boltzmann equation, a great deal of significant information can be extracted from it. For instance, one can obtain the hydrodynamic equations from it. Also the *H*-theorem, a result first proved by Boltzmann, can be shown.

In equilibrium, f is independent of time and, if there is no external force, it is independent of position. Then the Boltzmann equation (2.3.14) reduces to C(f) = 0. It can be shown that

$$\int d\boldsymbol{\xi} \ln f \mathcal{C}(f, f_1) = \frac{1}{4m_0} \int d\boldsymbol{\xi} d\boldsymbol{\xi}_1 dS \|\boldsymbol{\xi}_1 - \boldsymbol{\xi}\| \left(f' f_1' - f f_1\right) \ln \left(\frac{f f_1}{f' f_1'}\right) = 0. \quad (2.3.18)$$

For any positive x and y the function  $(y - x) \ln(x/y)$  is never positive. Therefore, the above integral vanishes if and only if

$$f'f_1' = ff_1. (2.3.19)$$

This implies that  $\ln f$  is indeed a summational invariant, that is,  $f = \exp(h)$ , where h is given by Eq. (2.3.17). Because of the hydrodynamic moments, given by Eqs. (2.3.3), the equilibrium distribution function, denoted by  $f_0$ , is

$$f_0 = \rho \left[ \frac{m_0}{2\pi k_B T} \right]^{\frac{D}{2}} \exp\left( -\frac{m_0}{2k_B T} (\boldsymbol{\xi} - \boldsymbol{v})^2 \right).$$
 (2.3.20)

The distribution function,  $f_0$ , is call the Maxwell-Boltzmann distribution function, which was first obtained by Maxwell. The above derivation is due to Boltzmann. It should be noted that in the above equation,  $\rho$ ,  $\boldsymbol{v}$  and T are independent of  $\boldsymbol{x}$  and t, as  $f_0$  is an absolute global equilibrium.

Now, define the quantity

$$H = \int d\boldsymbol{\xi} f \ln f. \tag{2.3.21}$$

And, consider a spatially uniform system, with f depending on t only. Then the Boltzmann equation for the system becomes

$$\frac{\partial f}{\partial t} = \mathcal{C}(f). \tag{2.3.22}$$

The time derivative of H is

$$\frac{dH}{dt} = \int d\boldsymbol{\xi} (1 + \ln f) \frac{\partial f}{\partial t} = \int d\boldsymbol{\xi} (1 + \ln f) \mathcal{C}(f), \qquad (2.3.23)$$

which can be written as

$$\frac{dH}{dt} = \frac{1}{4m_0} \int d\xi d\xi_1 dS \|\xi_1 - \xi\| (f'f_1' - ff_1) \ln \left(\frac{ff_1}{f'f_1'}\right). \tag{2.3.24}$$

By the same argument used in deriving  $f_0$ , the integrand is never positive, and we have Boltzmann's H-theorem:

$$\frac{dH}{dt} \le 0, (2.3.25)$$

where the equality holds if and only if  $f = f_0$ .

The above theorem states that the quantity H is a non-increasing function of time. It can be shown that H has a lower bound. Consider a nonequilibrium distribution function, f, such that

$$\int d\xi (f - f_0)h = 0 \tag{2.3.26}$$

where h is any summational invariant. Let  $H_0$  be the value of the functional H at

$$f = f_0$$
:  
 $H_0 = \int d\xi f_0 \ln f_0.$  (2.3.27)

Obviously,  $H_0$  is a constant, because for a spatially uniform system at equilibrium,  $\rho$ ,  $\boldsymbol{v}$  and T are constants. Also, because of Eq. (2.3.26) and the form of  $f_0$ , we have

$$\int d\xi f \ln f_0 = \int d\xi f_0 \ln f_0 , \qquad (2.3.28)$$

and it immediately follows that

$$H - H_0 = \int d\xi f \ln(f/f_0) = \int d\xi f_0 \left( 1 + \frac{f}{f_0} \left( \ln(f/f_0) - 1 \right) \right). \tag{2.3.29}$$

Because the quantity  $(1 - x + x \ln x)$  is non-negative for non-negative x, therefore, as a consequence of the above equation,

$$H \ge H_0$$
. (2.3.30)

Thus, H is a monotonic function of time and is bounded from below, then H must approach a limit, or an equilibrium. At the limit,  $\frac{\partial H}{\partial t} = 0$ , which implies f is a Maxwell-Boltzmann distribution. Since  $\rho$ ,  $\boldsymbol{v}$  and T are constants, the particular (global) equilibrium f approaches must be the one constrained by Eq. (2.3.26). Therefore, f approaches  $f_0$  as  $t \to \infty$ .

The H-theorem can be extended to spatially non-uniform system. The result would then be the local Maxwell-Boltzmann distribution. However, the details of this aspect will not be discussed here, and readers should be referred to Ref. [96].

#### 2.3.6 From the Boltzmann Equation to the Euler Equations

The Euler equations (2.1.3) can be easily derived from the transport equation (2.3.5), independent of the details of the collision operator, C(f), as long as certain sym-

metries, such as conservation laws, are preserved. We can immediately see that the zeroth order moment of Eq. (2.3.5) with respect to velocity  $\boldsymbol{\xi}$  yields the continuity equation (2.1.3a); the first order moment yields Euler's equation (2.1.3b); and the second order moment yields Eq. (2.1.3c), provided that  $f(\boldsymbol{r}, \Gamma, t)$  is the local Maxwell-Boltzmann distribution.

We will derive the Euler equations (2.1.3) in detail. Note the fact that r,  $\xi$  and t are independent variables, therefore  $\xi$  commutes with the operator  $\nabla$  and  $\partial/\partial t$ . The zeroth order moment of the transport equation (2.3.5) immediately leads to the continuity equation of mass:

$$\int \left(\frac{\partial f}{\partial t} + \boldsymbol{\xi} \cdot \nabla f\right) d\boldsymbol{\xi} = \frac{\partial}{\partial t} \int f d\boldsymbol{\xi} + \nabla \cdot \int \boldsymbol{\xi} f d\boldsymbol{\xi} = \frac{\partial \rho}{\partial t} + \nabla \cdot (\rho \boldsymbol{v}) = 0.$$
 (2.3.31)

Next, we compute the first order moment of the transport equation (2.3.5) to obtain the momentum equation. Decompose  $\pmb{\xi}$  as

$$\boldsymbol{\xi} = \boldsymbol{\xi}_0 + \boldsymbol{v}, \tag{2.3.32}$$

then

$$\int \boldsymbol{\xi} \frac{\partial f}{\partial t} d\boldsymbol{\xi} = \frac{\partial}{\partial t} \int \boldsymbol{\xi} f d\boldsymbol{\xi} = \frac{\partial}{\partial t} (\rho \boldsymbol{v}), \qquad (2.3.33)$$

and

$$\int \boldsymbol{\xi}(\boldsymbol{\xi} \cdot \nabla) f d\boldsymbol{\xi} = \nabla \cdot \left[ (\rho \boldsymbol{v} \boldsymbol{v}) + \int \boldsymbol{\xi}_{\scriptscriptstyle 0} \boldsymbol{\xi}_{\scriptscriptstyle 0} f d\boldsymbol{\xi} \right] .^{2}$$
(2.3.34)

The integral  $\int \boldsymbol{\xi}_0 \boldsymbol{\xi}_0 f d\boldsymbol{\xi}$  can be identified as  $-\sigma_{ij}$ , where  $\sigma_{ij}$  is the stress tensor. If  $f(\boldsymbol{r}, \Gamma, t)$  is the local Maxwell-Boltzmann distribution function,

$$f_L = \rho \left[ \frac{m_0}{2\pi k_B T} \right]^{\frac{D}{2}} \exp\left( -\frac{m_0}{2k_B T} (\boldsymbol{\xi} - \boldsymbol{v})^2 \right), \qquad (2.3.35)$$

<sup>&</sup>lt;sup>2</sup>Note that  $\boldsymbol{v}\boldsymbol{v} \neq \boldsymbol{v} \cdot \boldsymbol{v} = \boldsymbol{v}^2 = ||\boldsymbol{v}||^2 = v^2$ . It represents a second order tensor  $v_i v_j$ .

then the integral,  $\int \boldsymbol{\xi}_0 \boldsymbol{\xi}_0 f d\boldsymbol{\xi}$ , is indeed equal to  $P\delta_{ij}$ , where P is the hydrodynamic pressure. Therefore the second order moment of  $f_L$  is the momentum flux tensor  $\Pi_{ij}$  in Eq. (2.1.5). Hence Euler's equation (2.1.3b) is obtained.

Similarly, for the second order moment of the transport equation (2.3.5), we have:

$$\frac{1}{2} \int \xi^2 \frac{\partial f}{\partial t} d\boldsymbol{\xi} = \frac{\partial}{\partial t} \left( \frac{1}{2} \rho v^2 + \rho \varepsilon \right), \tag{2.3.36}$$

and

$$\frac{1}{2} \int \xi^2(\boldsymbol{\xi} \cdot \nabla) f d\boldsymbol{\xi} = \nabla \cdot \left[ \rho \boldsymbol{v} (\frac{1}{2} v^2 + \varepsilon) + \boldsymbol{v} \cdot \int \boldsymbol{\xi}_0 \boldsymbol{\xi}_0 f d\xi + \frac{1}{2} \int \boldsymbol{\xi}_0 \xi_0^2 f d\boldsymbol{\xi} \right] . \tag{2.3.37}$$

In the above equation, it is obvious that the last term in the right-hand side can be identified as the heat-flux, Q, which vanishes if  $f = f_L$  (due to the symmetry of the integral). Therefore

$$\frac{1}{2} \int \xi^2(\boldsymbol{\xi} \cdot \nabla) f_L d\boldsymbol{\xi} = \nabla \cdot \left( \rho \boldsymbol{v} (\frac{1}{2} v^2 + \varepsilon) + P \boldsymbol{v} \right) . \tag{2.3.38}$$

Then the energy equation, (2.1.3c), follows.

So far, we have derived the Euler equations (2.1.3) from the viewpoint of kinetic theory. It is a much more difficult task to obtain the Navier-Stokes equations *via* kinetic theory. The next section is devoted to the derivation of the Navier-Stokes equations using the Chapman-Enskog procedure.

# 2.4 The Chapman-Enskog Procedure and the Navier-Stokes Equation

Much of the effort in kinetic theory has been devoted to the solutions of the transport equation, in particular, of the Boltzmann equation. There are several outstanding names associated with this effort: Boltzmann, Maxwell, Hilbert, Chapman, Enskog and Grad [90]. In this section, a perturbative method of solving the Boltzmann equation, the Chapman-Enskog procedure, is reviewed. This method provides the normal solutions of the Boltzmann equation. The normal solution is the one which is uniquely determined for t > 0 by the values at t = 0 of the five hydrodynamic moments. That is, the solution, f, is uniquely determined by the macroscopic thermofluid state.

## 2.4.1 The Chapman-Enskog Expansion and the Normal Solution of the Boltzmann Equation

The Chapman-Enskog procedure is a method of solving the Boltzmann equation (2.3.14) by asymptotic expansion. In any expansion procedure, it is necessary to formally introduce a small expansion parameter such that in certain regime of which the expansion is valid. The parameter to be used in what follows is the Knudsen number,  $K_n$ :

$$\epsilon = \frac{l}{L} \equiv K_n \,, \tag{2.4.1}$$

where l and L are the mean free path and the typical macroscopic length scale of the system. The mean free path measures the average distance a molecule travels without collisions. Clearly,  $K_n$  has to be small for the hydrodynamic description (or continuum description) to be valid. Besides l and L, other relevant physical parameters in the system are the typical macroscopic time scale,  $\tau_0$ , and the typical microscopic time scale,  $\tau$ , which is the time interval between successive collisions. If we restrict ourselves to the regime in which

$$\mathcal{O}(\boldsymbol{\xi}) = \mathcal{O}(l/\tau) = \mathcal{O}(L/\tau_0) = \mathcal{O}(\boldsymbol{v}), \qquad (2.4.2)$$

i.e., the magnitude of the microscopic velocity,  $\boldsymbol{\xi}$ , is of the same order as that of the macroscopic velocity,  $\boldsymbol{v}$ , and note that the mean free path, l, is proportional to  $(\rho r_0^2/m_0)^{-1}$ , then dimensional analysis shows that the terms on the left-hand side of the Boltzmann equation are of order  $\tau_0^{-1}$  and v/L, while the collision term is of order  $(\rho/m_0)vr_0^2 = v/l$ . Comparing both sides of the Boltzmann equation, we can introduce the small parameter,  $\epsilon$ , into the Boltzmann equation

$$\frac{Df}{Dt} \equiv \frac{\partial f}{\partial t} + \boldsymbol{\xi} \cdot \frac{\partial f}{\partial \boldsymbol{r}} = \frac{1}{\epsilon} \, \mathcal{C}(f) \,, \tag{2.4.3}$$

where the collision term, C(f), could be given by Equation (2.3.14). The parameter  $\epsilon$  is introduced for obtaining successive equations in the same order of  $\epsilon$ , and it shall be set to unity eventually.

To solve the above equation, it is assumed that the entire time dependence of  $f(\mathbf{r}, \Gamma, t)$  is solely in the thermodynamical variables,  $\rho$ ,  $\mathbf{v}$  and T; that is, instead of being a function of t, f is treated as a functional of  $\rho$ ,  $\mathbf{v}$  and T. Thus, this assumption, the Chapman-Enskog ansatz, formally leads to the replacement

$$f(\mathbf{r}, \boldsymbol{\xi}, t) \to f(\mathbf{r}, \boldsymbol{\xi}; \rho, \boldsymbol{v}, T).$$
 (2.4.4)

In the Chapman-Enskog procedure, we are seeking solutions of the form:

$$f = \sum_{n=0}^{\infty} \epsilon^n f^{(n)} \tag{2.4.5}$$

which is the normal solution, such that

$$\int d\boldsymbol{\xi} f^{(0)} \begin{bmatrix} 1 \\ \boldsymbol{\xi} \\ (\boldsymbol{\xi} - \boldsymbol{v})^2 \end{bmatrix} = \begin{bmatrix} \rho \\ \rho \boldsymbol{v} \\ 3\rho RT \end{bmatrix}, \qquad (2.4.6a)$$

$$\int d\boldsymbol{\xi} f^{(n)} \begin{bmatrix} 1 \\ \boldsymbol{\xi} \\ (\boldsymbol{\xi} - \boldsymbol{v})^2 \end{bmatrix} = 0, \qquad n \ge 1.$$
 (2.4.6b)

Of course, the  $f^{(n)}$ 's themselves depend upon  $\epsilon$ , due to Eq. (2.4.6). One should notice that f, as a function of  $\boldsymbol{r}$ ,  $\boldsymbol{\xi}$  and t, is not expanded as series of functions of  $\epsilon$ . In fact,  $f^{(n)}$  depends upon  $\epsilon$  in a complex way only through the thermodynamical variables  $\rho$ ,  $\boldsymbol{v}$  and T.

Because of the ansatz given by Eq. (2.4.4),

$$\frac{\partial f}{\partial t} = \frac{\partial f}{\partial \rho} \frac{\partial \rho}{\partial t} + \frac{\partial f}{\partial \mathbf{v}} \cdot \frac{\partial \mathbf{v}}{\partial t} + \frac{\partial f}{\partial T} \frac{\partial T}{\partial t}.$$
 (2.4.7)

Although the moments of f, *i.e.*,  $\rho$ ,  $\boldsymbol{v}$  and  $\varepsilon$ , themselves are not expansions of  $\epsilon$  due to Eq. (2.4.6), their derivatives are. By substitution of the expansion for f — Eq. (2.4.5), the equations for the moments of f can be rewritten as follows

$$\frac{\partial \rho}{\partial t} = -\nabla \cdot (\rho \mathbf{v}), \qquad (2.4.8a)$$

$$\frac{\partial v_i}{\partial t} = -\boldsymbol{v} \cdot \nabla v_i + \frac{1}{\rho} \frac{\partial}{\partial x_j} \sum_{n=0}^{\infty} \epsilon^n \sigma_{ij}^{(n)}, \qquad (2.4.8b)$$

$$\frac{\partial T}{\partial t} = -\boldsymbol{v} \cdot \nabla T + \frac{2}{3R\rho} \sum_{n=0}^{\infty} \epsilon^n \left( \sigma_{ij}^{(n)} \frac{\partial v_i}{\partial x_j} - \nabla \cdot \boldsymbol{Q}^{(n)} \right), \qquad (2.4.8c)$$

where

$$\begin{bmatrix} \sigma_{ij}^{(n)} \\ \boldsymbol{Q}^{(n)} \end{bmatrix} = \int d\boldsymbol{\xi} f^{(n)} \begin{bmatrix} -\xi_{0i}\xi_{0j} \\ \boldsymbol{\xi}_{0}\xi_{0}^{2} \end{bmatrix}. \tag{2.4.9}$$

For the purpose of proper ordering of terms in  $\mathcal{O}(\epsilon^n)$ , we introduce the operator  $\partial_n/\partial t$ :

$$\frac{\partial_0 \rho}{\partial t} = -\nabla \cdot (\rho \mathbf{v}), \qquad (2.4.10a)$$

$$\frac{\partial_n \rho}{\partial t} = 0, \qquad n \ge 1, \tag{2.4.10b}$$

$$\frac{\partial_0 v_i}{\partial t} = -\mathbf{v} \cdot \nabla v_i + \frac{1}{\rho} \frac{\partial \sigma_{ij}^{(0)}}{\partial x_j}, \qquad (2.4.10c)$$

$$\frac{\partial_n v_i}{\partial t} = \frac{1}{\rho} \frac{\partial \sigma_{ij}^{(n)}}{\partial x_i}, \qquad n \ge 1,$$
(2.4.10d)

$$\frac{\partial_0 T}{\partial t} = -\mathbf{v} \cdot \nabla T + \frac{2}{3R\rho} \left( \sigma_{ij}^{(0)} \frac{\partial v_i}{\partial x_i} - \nabla \cdot \mathbf{Q}^{(0)} \right) , \qquad (2.4.10e)$$

$$\frac{\partial_n T}{\partial t} = \frac{2}{3R\rho} \left( \sigma_{ij}^{(n)} \frac{\partial v_i}{\partial x_j} - \nabla \cdot \mathbf{Q}^{(n)} \right) , \qquad n \ge 1 .$$
 (2.4.10f)

Now, we can use the above notation and rewrite

$$\frac{\partial f}{\partial t} = \sum_{n=0}^{\infty} \epsilon^n \sum_{m=0}^n \left( \frac{\partial_m \rho}{\partial t} \frac{\partial}{\partial \rho} + \frac{\partial_m \mathbf{v}}{\partial t} \cdot \frac{\partial}{\partial \mathbf{v}} + \frac{\partial_m T}{\partial t} \frac{\partial}{\partial T} \right) f^{(n-m)}$$

$$\equiv \sum_{n=0}^{\infty} \epsilon^n \frac{\partial_n f}{\partial t} . \tag{2.4.11}$$

The left-hand side of the Boltzmann equation is

$$\frac{\partial f}{\partial t} + \boldsymbol{\xi} \cdot \frac{\partial f}{\partial \boldsymbol{r}} = \sum_{n=0}^{\infty} \epsilon^n \left( \frac{\partial_n f}{\partial t} + \boldsymbol{\xi} \cdot \frac{\partial f^{(n)}}{\partial \boldsymbol{r}} \right) \equiv \sum_{n=0}^{\infty} \epsilon^n \frac{D_n f}{Dt}, \qquad (2.4.12)$$

while the right-hand side becomes

$$\frac{1}{\epsilon}\mathcal{C}(f) = \frac{1}{\epsilon}\mathcal{C}(f^{(0)}) + \sum_{n=1}^{\infty} \epsilon^{n-1} \sum_{m=0}^{n} \mathcal{C}(f^{(m)}, f^{(n-m)}), \qquad (2.4.13)$$

where C(f) and  $C(f^{(0)})$  are defined in Eq. (2.3.14), and  $C(f^{(m)}, f^{(n-m)})$  is

$$C(f^{(m)}, f^{(n)}) = \frac{1}{m_0} \int dS d\xi_1 ||\xi_1 - \xi||$$
$$[f^{(m)}(\mathbf{r}, \xi', t) f^{(n)}(\mathbf{r}, \xi'_1, t) + f^{(n)}(\mathbf{r}, \xi', t) f^{(m)}(\mathbf{r}, \xi'_1, t) -$$

$$f^{(m)}(\mathbf{r}, \boldsymbol{\xi}, t) f^{(n)}(\mathbf{r}, \boldsymbol{\xi}_1, t) - f^{(n)}(\mathbf{r}, \boldsymbol{\xi}, t) f^{(m)}(\mathbf{r}, \boldsymbol{\xi}_1, t) ] . \tag{2.4.14}$$

Now, a set of equations for  $f^{(n)}$  can be obtained by equating the terms of like order in the small parameter  $\epsilon$ . One should notice that operator  $\frac{D_n}{Dt}$  (or  $\frac{\partial_n}{\partial t}$ ) represents the time derivative with respect to time scale of  $t_n = \epsilon^{-n}t$ , because

$$\epsilon^n \frac{D_n}{Dt} = \frac{D_n}{D(\epsilon^{-n}t)} \equiv \frac{D_n}{Dt_n}.$$
 (2.4.15)

Therefore, the appropriate physical characteristic time scales corresponding to the different order of perturbations are different. The higher the order of the perturbation is, the longer the characteristic time scale, and hence the slower the corresponding physical process. This constitutes the basic idea of the multiple time scale formalism [46].

#### 2.4.2 The First-Order Solution

By considering the terms of order  $\mathcal{O}(\epsilon^{-1})$ , we have the first order equation from the Chapman-Enskog procedure:

$$C(f^{(0)}) = 0. (2.4.16)$$

Subject to the conditions given by Eq. (2.4.6), the first-order equation immediately yields the solution that  $f^{(0)}$  is indeed the local Maxwell-Boltzmann distribution function,  $f_L$ . The first-order solution is a direct consequence of Boltzmann's H-theorem, which has been discussed in the previous section. Thus the first-order approximation leads to the usual equations for an inviscid fluid, *i.e.*, the Euler equations (2.1.3). The derivation is straightforward, as outlined in the previous section.

## 2.4.3 The Second Order Solution, the Navier-Stokes Equation and Transport Coefficients

The second-order equation is obtained by equating terms of order  $\mathcal{O}(\epsilon^0)$ , which is an equation for  $f^{(1)}$ :

$$\frac{D_0 f}{Dt} = \mathcal{C}(f^{(0)}, f^{(1)}) + \mathcal{C}(f^{(1)}, f^{(0)}) = 2\mathcal{C}(f^{(0)}, f^{(1)}) = 2f_L \mathcal{L}_{\phi}(\phi^{(1)}), \qquad (2.4.17)$$

where  $\phi^{(1)}=f^{(1)}/f_L$ , and the linear operator  $\mathcal{L}_{\phi}$  is given as follows

$$\mathcal{L}_{\phi}(\phi^{(1)}) = \frac{1}{m_0} \int dS d\boldsymbol{\xi}_1 \|\boldsymbol{\xi}_1 - \boldsymbol{\xi}\| f_L(\boldsymbol{\xi}_1) (\phi^{(1)\prime} + \phi_1^{(1)\prime} - \phi^{(1)} - \phi_1^{(1)}). \tag{2.4.18}$$

The solution of equation (2.4.17) is not as trivial as the one for the first-order equation. It is a rather tedious process. We shall omit the details of the process, which can be found in some standard references (e.g., [90, 96-98]), as they are beyond the scope of this thesis. We will only present essential results in what follows.

Because  $f^{(0)} = f_L$  is known, the term  $\frac{D_0 f}{Dt}$  depends only upon  $f^{(0)}$  and hence can be carried out explicitly in terms of  $\rho$ ,  $\boldsymbol{v}$ , T and their derivatives,

$$\frac{D_{0}f}{Dt} \equiv \left(\frac{\partial\rho}{\partial t}\frac{\partial}{\partial\rho} + \frac{\partial\boldsymbol{v}}{\partial t} \cdot \frac{\partial}{\partial\boldsymbol{v}} + \frac{\partial T}{\partial t}\frac{\partial}{\partial T} + \boldsymbol{v} \cdot \frac{\partial}{\partial\boldsymbol{r}}\right) f_{L} \qquad (2.4.19)$$

$$= \frac{f_{L}}{2RT} \left\{ \left(\xi_{0}^{2}(D+2)RT\right) \boldsymbol{\xi}_{0} \cdot \nabla \ln T + S_{ijkl} \frac{\partial v_{i}}{\partial x_{j}} \xi_{0k} \xi_{0l} \right\}$$

$$= f_{L} \left\{ \left(\frac{\xi_{0}^{2}}{2RT} - \frac{5}{2}\right) \boldsymbol{\xi}_{0} \cdot \nabla \ln T + \frac{1}{RT} \left(\xi_{0i} \xi_{0j} - \frac{1}{3} \xi_{0}^{2} \delta_{ij}\right) \frac{\partial v_{i}}{\partial x_{j}} \right\} \qquad (D=3).$$

Eq. (2.4.17), an inhomogeneous integral equation for  $f^{(1)}$ , has the solution in three-dimensional space [90,96–98]:

$$f^{(1)} = -\frac{f^{(0)}}{\rho RT} \left( A(\xi_0, T) \boldsymbol{\xi}_0 \cdot \nabla \ln T + B(\xi_0, T) \left( \xi_{0i} \xi_{0j} - \frac{1}{3} \xi_0^2 \delta_{ij} \right) \frac{\partial v_i}{\partial x_j} \right), \qquad (2.4.20)$$

where  $A(\xi_0, T)$  and  $B(\xi_0, T)$  are the solutions of

$$-\mathcal{L}_{\phi}(A\boldsymbol{\xi}_{0}) = \left(\frac{\boldsymbol{\xi}_{0}^{2}}{2RT} - \frac{5}{2}\right)\boldsymbol{\xi}_{0}, \qquad (2.4.21a)$$

$$-\mathcal{L}_{\phi}(B \cdot (\xi_{0i}\xi_{0j} - \frac{1}{3}\xi_{0}^{2}\delta_{ij})) = \xi_{0i}\xi_{0j} - \frac{1}{3}\xi_{0}^{2}\delta_{ij}.$$
 (2.4.21b)

Solving these equations is a difficult task even for simple inter-molecular potentials, e.g., the hard-sphere potential. However, it can be done by various approximation methods [90, 96, 98].

Once  $f^{(1)}$  is obtained, then  $\sigma_{ij}^{(1)}$  and  $\mathbf{Q}^{(1)}$  can be computed, and it is easy to calculate the corresponding transport coefficients — the kinematic viscosity,  $\nu$ , and the thermal conductivity,  $\kappa$ :

$$\nu = \frac{m_0}{15\rho RT} \int d\xi \xi_0^4 A f_L , \qquad (2.4.22a)$$

$$\kappa = \frac{m_0}{6RT} \int d\boldsymbol{\xi} \, \xi_0^4 B f_L \,. \tag{2.4.22b}$$

Consequently, the incompressible Navier-Stokes equations are derived with the values of transport coefficients.

The above derivation is specific to an ideal gas (i.e., particles without structures) at low density. The result implies that the bulk viscosity vanishes. The bulk viscosity is actually negligible in such case. In order to obtain the compressible Navier-Stokes equations and the corresponding transport coefficient (the bulk viscosity), one has to consider either monoatomic gases at high densities in which the correlations between colliding molecules cannot be ignored, or polyatomic gases in which particles have internal degrees of freedom (such as rotational and vibrational degree of freedom). The study of such cases is beyond the scope of this thesis, thus we refer readers to available references [98, 90, 96, 98].

We have illustrated the Chapman-Enskog procedure by carrying out the firstand the second-order solutions. One can continue the procedure to higher orders. However, the physical significance of the higher-order solutions is not clear. For certain problems the third-order solution leads to the Burnett equation [96].

In summary, the Chapman-Enskog procedure is an expansion procedure in which the distribution function is expanded as a series in the Knudsen number in which the zeroth order approximation is the local Maxwell-Boltzmann equilibrium distribution function, subject to the conditions that the higher order distribution functions have no contribution to the hydrodynamic moments of the distribution function (mass, momentum and energy densities), given by Eq. (2.4.6). The term  $f^{(n)}$  is the nthorder term of the spatial derivatives of the thermodynamical variables  $\rho$ ,  $\boldsymbol{v}$  and T. For instance,  $f^{(1)}$  is linear in the first-order spatial derivatives of  $\rho$ ,  $\boldsymbol{v}$  and T;  $f^{(2)}$ is linear in the second-order derivatives and quadratic in the first-order ones. The derivatives are multiplied by coefficients which are functions of  $\rho$ , v and T. In the Boltzmann equation, the time derivatives of  $\rho$ ,  $\boldsymbol{v}$  and T are eliminated by the hydrodynamic equations (2.4.10). The lowest-order approximation leads to the local Maxwell-Boltzmann equilibrium distribution function  $f^{(0)} = f_L$ . Then  $f^{(0)}$  is used to calculate  $\sigma_{ij}^{(0)}$  and  ${m Q}^{(0)}$ , and hence to solve  $f^{(1)}$ . Once  $f^{(1)}$  is known,  $\sigma_{ij}^{(1)}$  and  ${m Q}^{(1)}$  can be evaluated, and so can  $f^{(2)}$ . Continuing,  $\sigma^{(n)}_{ij}$  and  $Q^{(n)}$  at any stage are available to proceed to the next stage. The existence of the nth-order solution,  $f^{(n)}$ , can also be shown rigorously [97].

#### 2.4.4 The Validity of the Chapman-Enskog Procedure

Finally, we should briefly discuss the validity of the Chapman-Enskog procedure. First of all, one should notice that the Chapman-Enskog expansion is one in inverse powers of the density while the Boltzmann equation is valid at low density. The Boltzmann gas limit (2.3.13) specifies  $Nr_0^3 \ll 1$ , which leads to  $r_0 \ll l$ . On the other hand, the

expansion is valid when  $l \ll L$ , because it is an expansion of the Knudsen number,  $K_n$ . Therefore, the density must be in the range where inequalities  $r_0 \ll l$  and  $l \ll L$  hold simultaneously. That is to say, the density should be both low enough so that only binary collisions need to be considered, and high enough so that the collision mechanism is effective in establishing a local Maxwell-Boltzmann equilibrium distribution. Then  $f_L$  is a good zeroth-order approximation to f. Second, because of the dependence of the Chapman-Enskog expansion upon the spatial derivatives, the approximation is expected to be valid in the regimes where the spatial gradients of  $\rho$ ,  $\boldsymbol{v}$  and T are small. Therefore, the Chapman-Enskog expansion is valid when the system is not too far away from the thermal equilibrium, in the sense described above.

#### 2.4.5 Some Further Developments

So far we have demonstrated how to derive hydrodynamic equations from the Boltzmann equation *via* the Chapman-Enskog procedure. Two comments are in order at this point.

First, for the purpose of deriving hydrodynamics from kinetic theory, one need not start from the Boltzmann equation. One can obtain the same set of hydrodynamic equations by starting from the BBGKY hierarchy. The Chapman-Enskog procedure can be generalized and applied to the BBGKY hierarchy. This was done in 1958 by S. T. Choh [99]; the procedure is well summarized in Ref. [100, pages 135–142].

Second, there exists a more rigorous procedure, which is also equivalent to the Chapman-Enskog procedure, for deriving the hydrodynamic equations from the Boltzmann equation. This procedure is due to R. Fox, and since it is equivalent to the Chapman-Enskog procedure, it is referred to as the Fox-Chapman-Enskog procedure [101]. The Fox-Chapman-Enskog procedure is based on the contraction procedure of n stationary, Gaussian, Markov variables to m ones (n > m) [101]. One

advantage of the Fox-Chapman-Enskog procedure is that the hydrodynamic and the kinetic time scales are naturally separated; there is no need to introduce an expansion parameter (the Knudsen number,  $K_n$ ) to distinguish different time scales. Although the Fox-Chapman-Enskog procedure is more elegant and rigorous, the results obtained by it are the same as that obtained by the Chapman-Enskog procedure.

# 2.5 Some Dimensionless Parameters, the Law of Similarity and Asymptotic Ordering in Hydrodynamics

The Navier-Stokes equation can be written in a dimensionless form associated with dimensionless parameters. The order of magnitude of these dimensionless parameters qualitatively characterizes the solution of the Navier-Stokes equation. In this section, we derive these parameters and discuss some related issues.

As in the Chapman-Enskog expansion, we shall keep the Knudsen number small, i.e.,  $K_n = \frac{l}{L} = \mathcal{O}(\epsilon)$ , where  $\epsilon$  is a small parameter. Define the Mach number,  $M = \frac{U_0}{c_s} = \frac{\tau U_0}{l}$ , the Strouhal number,  $S_l = \frac{\tau_0}{\tau}$ , and the Reynolds number,  $R_e = \frac{LU_0}{\nu}$ , with  $U_0$  as the characteristic hydrodynamic velocity,  $c_s$  the sound speed, L the characteristic hydrodynamic length scale, l the mean free path,  $\tau_0$  the characteristic hydrodynamic time scale and  $\tau$  the characteristic kinetic time scale, respectively. Also, the kinetic viscosity,  $\nu$ , goes like  $\frac{l^2}{\tau}$ . Furthermore, we have  $R_e S_l = K_n^{-2}$ .

Rescaling

$$\mathbf{v} = U_0 \mathbf{u} \tag{2.5.1a}$$

$$t = \tau_0 t' \tag{2.5.1b}$$

$$\mathbf{r} = L\mathbf{r}' \tag{2.5.1c}$$

and using the isothermal equation of state

$$P = c_s^2 \rho = \sqrt{\gamma RT} \rho \,, \tag{2.5.2}$$

where  $\gamma = \frac{C_P}{C_V}$ , and  $C_P$  and  $C_V$  are specific heats with constant volume V and constant pressure P, respectively, we can rewrite the incompressible Navier-Stokes equation in dimensionless form,

$$\frac{1}{M K_n S_l} \frac{\partial \boldsymbol{u}}{\partial t'} + (\boldsymbol{u} \cdot \nabla') \boldsymbol{u} = -\frac{1}{\rho M^2} \nabla' \rho + \frac{1}{R_e} \nabla'^2 \boldsymbol{u}, \qquad (2.5.3)$$

where  $\nabla' \equiv \frac{\partial}{\partial \mathbf{r}'}$ . In order to keep every term in the above equation in the same asymptotic order in terms of the small parameter  $\epsilon$ , we must have

$$K_n \sim \mathcal{O}(\epsilon),$$
 (2.5.4a)

$$R_e \sim \mathcal{O}(\epsilon^0),$$
 (2.5.4b)

$$M \sim \mathcal{O}(\epsilon),$$
 (2.5.4c)

$$S_l \sim \mathcal{O}(\epsilon^{-2}),$$
 (2.5.4d)

$$\frac{\nabla \rho}{\rho} \sim \mathcal{O}(\epsilon^2).$$
 (2.5.4e)

That is, for hydrodynamic description to be valid, the Knudsen number,  $K_n$ , has to be small. Also, for the viscous effect to be non-negligible, the Reynolds number,  $R_e$ , has to be  $\mathcal{O}(1)$ . Consequently, the Strouhal number is  $\mathcal{O}(\epsilon^{-2})$ , which measures the characteristic time scale of the hydrodynamic effect governed by the Navier-Stokes equation. The small Mach number limit is equivalent to the incompressible limit, hence the density fluctuation  $\frac{\nabla \rho}{\rho}$  is  $\mathcal{O}(\epsilon^2)$ .

By ignoring the viscous term,  $\nu \nabla^2 \boldsymbol{v}$ , in the Navier-Stokes equation, Euler's equa-

tion can be obtained. In this case, we must have  $R_e \sim \mathcal{O}(\epsilon^{-1})$ . Similar dimension analysis will lead to the asymptotic ordering for Euler's equation

$$K_n \sim \mathcal{O}(\epsilon),$$
 (2.5.5a)

$$R_e \sim \mathcal{O}(\epsilon^{-1}),$$
 (2.5.5b)

$$M \sim \mathcal{O}(\epsilon^0),$$
 (2.5.5c)

$$S_l \sim \mathcal{O}(\epsilon^{-1}),$$
 (2.5.5d)

$$\frac{\nabla \rho}{\rho} \sim \mathcal{O}(\epsilon^0).$$
 (2.5.5e)

One can immediately notice the distinction between the Euler ordering and the Navier-Stokes ordering. Euler's equation governs inviscid fluids, and the viscous effect should be negligible. Therefore,  $R_e \sim \mathcal{O}(\epsilon^{-1})$ . Consequently, we have  $M \sim \mathcal{O}(1)$  and  $S_l \sim \mathcal{O}(\epsilon^{-1})$ . Because  $M \sim \mathcal{O}(1)$  and thus  $\frac{\nabla \rho}{\rho} \sim \mathcal{O}(1)$ , the system described by the Euler equations is further away from equilibrium than that described by the Navier-Stokes equations. Also,  $S_l \sim \mathcal{O}(\epsilon^{-1})$  suggests that the process governed by the Euler equations is much faster than that by the Navier-Stokes equations. This is somewhat obvious, because the Euler equations are obtained in the order of  $\mathcal{O}(\epsilon^{-1})$  and the corresponding time scale is  $\epsilon t$ , while the Navier-Stokes equations are in the order of  $\mathcal{O}(1)$ . Thus, the related time scales should also follow the ordering accordingly.

Usually, the given characteristic physical quantities for a hydrodynamic system are L,  $U_0$  and  $\nu$ . The only dimensionless quantity constructed from the above three is the Reynolds number,  $R_e$ . Furthermore, the ratio between the magnitude of the non-linear convective term,  $(\boldsymbol{v}\nabla)\boldsymbol{v}$ , and that of the viscous term,  $\nu\nabla^2\boldsymbol{v}$ , is just the Reynolds number,  $R_e$ . Thus, the Reynolds number,  $R_e$ , measures the relative strength of the nonlinearity. Under this circumstance, the incompressible Navier-Stokes equation in

dimensionless form, Eq. (2.5.3), can be written as

$$\frac{\partial \boldsymbol{u}}{\partial t'} + (\boldsymbol{u} \cdot \nabla') \boldsymbol{u} = -\nabla' P' + \frac{1}{R_e} \nabla'^2 \boldsymbol{u}, \qquad (2.5.6)$$

where  $t' = \frac{U_0}{L}t$ , and the dimensionless pressure  $P' = \frac{P}{\rho U_0^2}$ . The solution of the above equation has the general form

$$\boldsymbol{u} = \boldsymbol{u}(\boldsymbol{r}', t'; R_e) \tag{2.5.7}$$

for flows of the same type, (e.g., flows with the same geometric boundary conditions but with different viscosity, etc.) i.e., the dimensionless velocities,  $\boldsymbol{u}$ , for flows of the same type are the same functions of  $\boldsymbol{r}'$  and t', if the Reynolds number,  $R_e$ , is the same. In other words, the flows of the same type are similar to each other if the Reynolds number,  $R_e$ , is the same for each flow. This is the law of similarity [1].

In Eq. (2.5.6), the Reynolds number,  $R_e$ , can be treated as an adjustable parameter, which measures the relative strength of the nonlinearity. Then, flows with large enough Reynolds number can be turbulent. Thus, the Reynolds number,  $R_e$ , also qualitatively characterizes a flow, whether it is a steady state, a time dependent state, or a turbulent state.

If the system were driven by an external force with period T, then, besides the Reynolds number, another dimensionless number characterizing the flow, the Strouhal number,  $S_l = \frac{U_0 T}{L}$ , can be defined. Consequently, by rescaling the time, t = Tt', the incompressible Navier-Stokes equation in dimensionless form, Eq. (2.5.3), can be written as

$$\frac{1}{S_l} \frac{\partial \boldsymbol{u}}{\partial t'} + (\boldsymbol{u} \cdot \nabla') \boldsymbol{u} = -\nabla' P' + \frac{1}{R_e} \nabla'^2 \boldsymbol{u}. \tag{2.5.8}$$

Thus, similar to the previous case, the solution of the above equation should have the

general form

$$\boldsymbol{u} = \boldsymbol{u}(\boldsymbol{r}', t'; R_e, S_l) \tag{2.5.9}$$

for flows of the same type. It should be noted that although the Navier-Stokes equation can be written in a dimensionless form, the characteristic quantities of a system still play important roles. That is, the Reynolds number and other dimensionless parameters cannot fully determine the physics of a system. For instance, there are boundary layers near boundaries. Moreover, the boundary layers are different for different velocities. Hence, the effects due to the boundary layers are different with different velocities.

## CHAPTER THREE

### THE FHP LATTICE-GAS AUTOMATA

Before studying the details of the lattice-gas model proposed by Frisch, Hasslacher and Pomeau (FHP) [46], first of all we should re-emphasize the motivation of using simple cellular automata models to study hydrodynamical systems. The possibility of using such a simplistic model as the lattice-gas automaton to simulate hydrodynamic systems, which are highly nonlinear and high-dimensional complex systems, is based upon the following observations [4]: The first is that studies of molecular dynamics have demonstrated that hydrodynamics applies quantitatively on a microscopic scale. Therefore, instead of  $10^{24}$  particles, only  $10^3$ – $10^8$  particles (or, in other words, an equivalent number of simultaneous equations of motion), depending on the hydrodynamic problem to be investigated, are needed for simulations for hydrodynamical systems.

The second observation is that one does not need to solve a set of the exact equations of motion, rather one can choose to solve a simplified system. The reason is the following [102,4]: The physical content of the Navier-Stokes equations is nothing but the conservation laws supplemented by the definition of the transport coefficients. The form of the hydrodynamic equations is very much determined by the symmetries of Newtonian mechanics and by the conservation laws. Such symmetries are, for instance, continuous spatial-temporal translational invariance, rotational invariance (isotropy), parity invariance and Galilean invariance. So long as these symmetries, together with the conservation laws, are preserved in the underlying microdynamics,

then the hydrodynamics should be the emerging collective behavior of the system governed by the microdynamics. For discrete models, the question which should be asked is whether the discrete models can be constructed so that these invariance properties are relaxed by necessity and without losing the proper hydrodynamic behavior. The FHP lattice-gas automata have been shown to be successful in this regard. We will study this model in detail in the subsequent sections.

The final observation is that lattice-gas automata can be thought as the extremely simplified models of molecular dynamics. This simplification has gained an enormous computational advantage, owing to the fully parallel nature of FHP lattice-gas automata. Lattice-gas automata run very fast on parallel computers such as Connection Machines. On a quarter machine of CM-200, a speed about 300 million site updates per second has been achieved at the Center for Nonlinear Studies, Los Alamos National Laboratory. It has been speculated that it is possible to obtain a speed of  $6 \times 10^{15}$  site updates per second on a specialized dedicated computer based on existing technology, which is  $10^8$  times faster than CRAY-2 computers [103].

We will mathematically justify the validity of using the FHP lattice-gas models to simulate hydrodynamical systems in this chapter. The remaining materials in this chapter is organized as follows: §3.1 briefly discusses the HPP lattice-gas automaton in a square lattice space. §3.2 presents the microdynamics of the FHP lattice-gas automata. §3.3 explicitly derives the collision operator of the FHP lattice-gas automata. §3.4 studies the FHP lattice-gas automata with rest particles. §3.5 discusses the spurious conserved quantities associated with the microdynamics of the FHP models. §3.6 analyzes the symmetries of the underlying lattice space and the associated tensor structures. §3.7 computes the equilibrium distribution function of the particle number through the usual analysis of the equilibrium statistical mechanics. As a consequence of the equilibrium, a set of necessary collisions to thermalize the system are also derived. §3.8 derives the lattice Boltzmann equation. §3.9 proves the

H-theorems for the FHP models with the Boltzmann approximation. §3.10 and §3.11 derive the macroscopic equations with the transport coefficients for the FHP latticegas automata with and without rest particles via the Chapman-Enskog procedure. §3.12 provides the normal modes analysis for the lattice-gas hydrodynamics. Finally, §3.13 concludes this chapter.

#### 3.1 Prelude: The HPP Lattice-Gas Model

In 1972, J. Hardy, Y. Pomeau and O. de Pazzis (HPP) proposed a two-dimensional lattice-gas automaton model to study two-dimensional hydrodynamics [80–83]. Their motivation was to study fundamental questions in statistical mechanics such as ergodicity and the divergence of transport coefficients in two dimensions (the long time tails of the time correlation functions), in the simplest possible model. In particular, they studied a class of equilibrium states and the time correlation functions of the model. They were able to evaluate the transport coefficients via the Green-Kubo formula. The HPP model consists of a two-dimensional square lattice space with unit lattice constant and with discrete time. Each particle has unit mass and unit speed. The four possible directions of a particle's momentum are those of the links to the nearest neighboring sites. On each site at each time step, there can be either one or zero particles with a particular momentum (exclusion principle). The evolution of the system has two steps: Collision and advection. At each time step, inter-particle interactions occur through local collisions, i.e., the collision process only involves particles at the same site and the same time. The collision rules are designed to conserve particle number, momentum and kinetic energy, locally and exactly. For the HPP model, the collision rules are particularly simple: There are only two-body head-on collisions. When the head-on collision occurs, the relative velocities of the pair of the particles involved in the collision will rotate  $\pi/2$  (or  $-\pi/2$ ), as shown in Fig. (3.1.1). After collision, particles move to adjacent sites in the direction of their momentum.

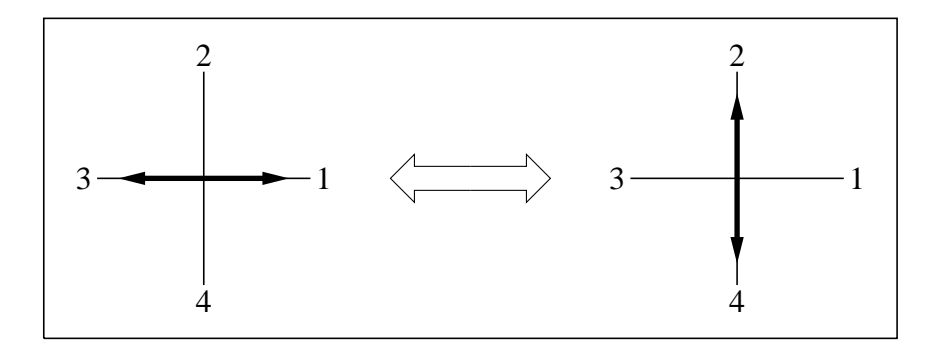


Figure 3.1.1: Two-body (head-on) collision rules of the HPP model.

The HPP model is a completely deterministic one — the evolution is reversible. Also, conservation of kinetic energy is indistinguishable from conservation of particle number (mass conservation), because there is only a single speed of particles. Therefore, the energy conservation does not play any role in the hydrodynamics of the single speed models.

There are immediate drawbacks of the HPP model due to its simplicity. Obviously, the HPP model is not Galilean invariant because of its discrete nature, just as any other discrete models. (The reason is very simple: The collision processes depend on the frame of reference. For instance, a pair of head-on particles in a rest frame of reference is not so in a moving frame of reference with a velocity perpendicular to the velocities of the particles.) In addition, the Navier-Stokes equation derived from the model is anisotropic, because the stress tensor lacks the necessary symmetry (this will be explained in detail later). Also, the collision rule preserves the differences of particle population with opposite momentum along each row and each column of the lattice if a periodic boundary condition is imposed. Therefore, all together, these differences introduce many spurious conserved quantities.

By observing the fact that the triangular lattice possesses the sufficient symmetry, Uriel Frisch, Brosl Hasslacher and Yves Pomeau (FHP) proposed a latticegas model, popularly named the FHP model, with triangular lattice structure, in 1986 [44]. The invention of the FHP model has stimulated research of lattice-gas

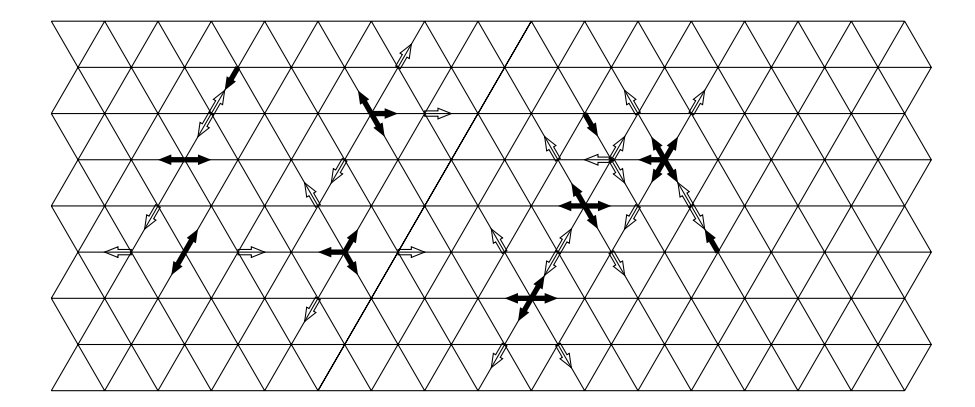


Figure 3.2.1: Triangular-lattice space for FHP models. In this Figure, two successive microscopic configurations of the FHP lattice-gas automaton are shown. Each arrow represents a discrete particle with the momentum directing as the arrow. The solid arrows are particles at time t; and the hollow arrows are those at time t+1, after a collision and an advection process.

automata, and has offered a realistic promise of simulating real physical problems using lattice-gas automata methods [48–50,104].

## 3.2 Evolution, Microscopic Equation and Conservation Laws

The essence of the FHP lattice-gas automaton is not much different from that of the HPP lattice-gas automaton, in the sense that they all possess the exact conservation laws, and have the same evolution processes — collision and advection. The only difference between the HPP and the FHP lattice-gas automaton is the symmetry dictated by the underlying lattice space structure, which in turn determines the symmetry of tensor structure of the models.

The FHP lattice-gas automata live on a two-dimensional triangular-lattice space with unit lattice constant, as shown in Fig. (3.2.1). Each site on the lattice is connected to its six neighbors by links corresponding to the unit vector  $\hat{\boldsymbol{e}}_1$  through  $\hat{\boldsymbol{e}}_6$  given by

$$\hat{\boldsymbol{e}}_{\alpha} = (\cos(2\pi(\alpha - 1)/6), \sin(2\pi(\alpha - 1)/6)) \qquad \alpha \in \{1, 2, \dots, 6\}.$$
 (3.2.1)

(Greek indices  $\alpha$ ,  $\beta$ ,  $\cdots$  always run from 1 to 6, or 0 to 6 for models with one rest particle; whereas Roman indices  $i, j, \cdots$  run between x and y in two-dimensional space and between x, y and z in three-dimensional space, unless otherwise specified.) There can be only one or zero particles lying on each directed link at any time (exclusion principle). Assuming unit particle masses and unit time steps, the momentum and velocity of each particle is simply given by the vector,  $\hat{e}_{\alpha}$ . The evolution of the system consists of two steps: Collision and advection. At each time step, particles on each site collide and then scatter according to a set of rules which conserve mass, momentum and energy exactly and locally. The collisions are elastic and instantaneous, with zero interaction range. Therefore, all particles have equal kinetic energy and zero potential energy. After collision, particles move in the direction of their new velocities to adjacent sites.

Fig. (3.2.2) illustrates the collision rules of the FHP lattice-gas automata. In the left column are the incoming states, and in the right column are outgoing states. In the first row is the two-body head-on collision; in the second row is the symmetric three-body collision; in the third row is the asymmetric three-body collision; and in the fourth row is the four-body collision. In Fig. (3.2.2), all possible configurations for a collision to occur have been illustrated, except for degeneracies by sixfold rotational symmetry of the triangular lattice space or by mirror reflections. Those input states equal to their output states are also omitted in Fig. (3.2.2). Two particles on the same site would collide only if they have opposite momentum, then they will undergo a head-on collision and scatter by rotating  $\pi/3$  randomly either clockwise or counter-clockwise. Three particles on the same site always collide: A triple of particles  $2\pi/3$  apart (symmetric) scatters by rotating  $\pi/3$ ; a pair of head-on particles with a spectator rotates  $\pi/3$  to the only possible configuration dictated by the exclusion principle. Four particles on the same site will collide only if they are two pairs of head-on particles, then one of the pairs is randomly chosen to rotate  $\pi/3$ either clockwise or counter-clockwise. Therefore, the two-body head-on collision rule

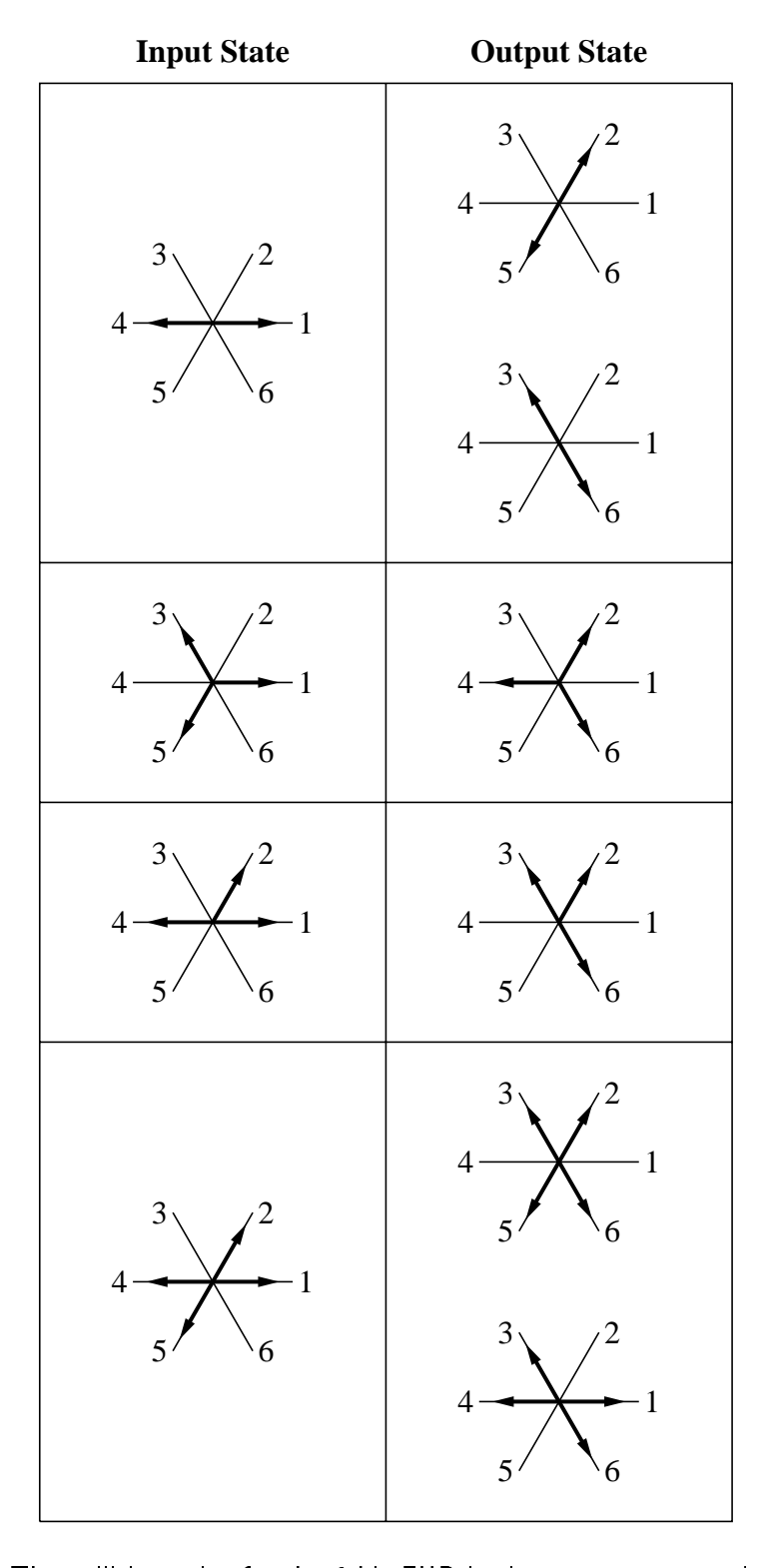


Figure 3.2.2: The collision rules for the 6-bit FHP lattice-gas automata. In the left column are input states, and in the right are output states.

is undeterministic, and so is the four-body collision rule. Whereas the symmetric and asymmetric three-body collision rules are deterministic. The symmetric three-body collisions destroy the spurious conserved quantities along each lattice line. Notice that in the model there may be a particle-hole duality, if two- and four-body collisions are included in the model. In this case, one can view the collision of four particles as the collision of two holes, and *vice versa*. In Fig. (3.2.1), two successive configurations of a FHP lattice-gas automaton, which evolves according to the rules prescribed in Fig. (3.2.2), are illustrated.

Because of the exclusion principle, the occupation number of the particles at site,  $\boldsymbol{x}$ , time, t, with velocity,  $\hat{\boldsymbol{e}}_{\alpha}$ , is a Boolean number. We can therefore use a 6-bit binary number to denote the occupation number of the particles at site,  $\boldsymbol{x}$ , and time, t. For instance, a configuration with one particle with momentum,  $\hat{\boldsymbol{e}}_1$ , and the other one with momentum,  $\hat{\boldsymbol{e}}_4$ , on a site can be represented by a binary number 001001. Therefore, the FHP models without rest particles are also referred as to the 6-bit FHP models. We can therefore construct a table of the collision rules in binary form, which is equivalent to Fig. (3.2.2):

INPUT STATE	OUTPUT STATE
001001	010010
	100100
010101	101010
001011	100110
011011	110110
	101101

Table 3.2.1: The collision table for the 6-bit FHP models.

Because of this binary representation, we can use either Boolean logic operations or table-lookup when implementing the FHP lattice-gas models.

The evolution of the FHP lattice-gas automaton on a two-dimensional triangularlattice space,  $\{x\}$ , with a unit lattice constant and with discrete time,  $t \in \{0, 1, 2, \dots\}$ , is governed by the following equation

$$n_{\alpha}(\boldsymbol{x} + \hat{\boldsymbol{e}}_{\alpha}, t+1) = n_{\alpha}(\boldsymbol{x}, t) + \mathcal{C}_{\alpha}(\{n_{\alpha}\}), \qquad (3.2.2)$$

where  $n_{\alpha}(\boldsymbol{x}, t)$  is the occupation number of the particle at site,  $\boldsymbol{x}$ , time, t, with velocity,  $\hat{\boldsymbol{e}}_{\alpha}$ ;  $\{n_{\alpha}\}$  denotes the set of all  $n_{\alpha}(\boldsymbol{x}, t)$ ,  $\{n_{\alpha}(\boldsymbol{x}, t) \mid \alpha = 1, 2 \cdots, 6\}$ , and  $\mathcal{C}_{\alpha}(\{n_{\alpha}\})$  is the collision operator which represents creation or annihilation of  $n_{\alpha}(\boldsymbol{x}, t)$  due to collisions. Since  $n_{\alpha}(\boldsymbol{x}, t)$  is Boolean, consequently  $\mathcal{C}_{\alpha}(\{n_{\alpha}\}) \in \{-1, 0, 1\}$ .

The collision rules of the FHP lattice-gas models conserve the particle number, momentum and kinetic energy at each individual collision. The conservation laws are satisfied exactly and locally. The conservation laws can be expressed mathematically, similar to Eq. (2.3.16) for the continuum case, as the following

$$\sum_{\alpha} h \mathcal{C}_{\alpha}(\{n_{\alpha}\}) = 0, \qquad (3.2.3)$$

where

$$h = c_0 + \boldsymbol{c}_1 \cdot \hat{\boldsymbol{e}}_{\alpha} + c_2 (\hat{\boldsymbol{e}}_{\alpha} - \boldsymbol{v})^2, \qquad (3.2.4)$$

with  $c_0$  and  $c_2$  as arbitrary constants, and  $c_1$  as an arbitrary D-dimensional constant vector.

For single-speed lattice-gas models, the energy conservation law is equivalent to the mass conservation law. Therefore it is redundant and it does not play any role in the dynamics of the system.

## 3.3 The Collision Operator, $\mathcal{C}_{lpha}$

The collision operator,  $C_{\alpha}(\{n_{\alpha}\})$ , can be written out in detail. Consider the term due to the two-body collisions,  $C_{\alpha}^{(2)}(\{n_{\alpha}\})$ , which represents the scattering of a single pair

of head-on colliding particles with momenta  $\hat{\boldsymbol{e}}_{\alpha}$  and  $-\hat{\boldsymbol{e}}_{\alpha}$  in any directions  $\hat{\boldsymbol{e}}_{\beta}$  and  $-\hat{\boldsymbol{e}}_{\beta}$  with  $\beta \neq \alpha$ . Obviously,

$$\mathcal{C}_{\alpha}^{(2)} = \xi_{R}^{(2)} n_{\alpha+1} n_{\alpha+4} \bar{n}_{\alpha} \bar{n}_{\alpha+2} \bar{n}_{\alpha+3} \bar{n}_{\alpha+5} + \xi_{L}^{(2)} n_{\alpha+2} n_{\alpha+5} \bar{n}_{\alpha} \bar{n}_{\alpha+1} \bar{n}_{\alpha+3} \bar{n}_{\alpha+4} - (\xi_{R}^{(2)} + \xi_{L}^{(2)}) n_{\alpha} n_{\alpha+3} \bar{n}_{\alpha+1} \bar{n}_{\alpha+2} \bar{n}_{\alpha+4} \bar{n}_{\alpha+5} ,$$
(3.3.1)

where

$$\bar{n}_{\alpha} \equiv 1 - n_{\alpha} \tag{3.3.2}$$

is the complement of  $n_{\alpha}$ ;  $\xi_{R}^{(2)}$  and  $\xi_{L}^{(2)}$  are Boolean random numbers which determine the outcome of head-on two-body collisions. Boolean random number  $\xi_{R}^{(2)}$  and  $\xi_{L}^{(2)}$ reflect the randomness of the outcomes of the two-body collision: When  $\xi_{R}^{(2)} = 1$ ( $\xi_{L}^{(2)} = 1$ ), velocities of the scattered pair of particles choose to rotate  $\pi/3$  ( $-\pi/3$ ). The first two terms in  $\mathcal{C}_{\alpha}^{(2)}$  represent the possible creation of  $n_{\alpha}$ , and the last term the possible annihilation, due to the two-body collisions.

Similarly, we can write the collision term due to the symmetric three-body collisions:

$$C_{\alpha}^{(3S)} = \xi^{(3S)} (n_{\alpha+1} n_{\alpha+3} n_{\alpha+5} \bar{n}_{\alpha} \bar{n}_{\alpha+2} \bar{n}_{\alpha+4} - n_{\alpha} n_{\alpha+2} n_{\alpha+4} \bar{n}_{\alpha+1} \bar{n}_{\alpha+3} \bar{n}_{\alpha+5}), \qquad (3.3.3)$$

the collision term due to the asymmetric three-body collisions:

$$\mathcal{C}_{\alpha}^{(3A)} = \xi^{(3A)} \left( n_{\alpha+1} n_{\alpha+2} n_{\alpha+4} \bar{n}_{\alpha} \bar{n}_{\alpha+3} \bar{n}_{\alpha+5} + n_{\alpha+1} n_{\alpha+4} n_{\alpha+5} \bar{n}_{\alpha} \bar{n}_{\alpha+2} \bar{n}_{\alpha+3} + n_{\alpha+1} n_{\alpha+4} n_{\alpha+5} \bar{n}_{\alpha} \bar{n}_{\alpha+2} \bar{n}_{\alpha+3} + n_{\alpha+1} n_{\alpha+2} n_{\alpha+5} \bar{n}_{\alpha} \bar{n}_{\alpha+1} \bar{n}_{\alpha+3} - n_{\alpha+1} n_{\alpha+3} \bar{n}_{\alpha+2} \bar{n}_{\alpha+4} \bar{n}_{\alpha+5} - n_{\alpha} n_{\alpha+2} n_{\alpha+3} \bar{n}_{\alpha+1} \bar{n}_{\alpha+4} \bar{n}_{\alpha+5} - n_{\alpha} n_{\alpha+2} n_{\alpha+3} \bar{n}_{\alpha+1} \bar{n}_{\alpha+4} \bar{n}_{\alpha+5} - n_{\alpha} n_{\alpha+3} n_{\alpha+4} \bar{n}_{\alpha+5} - n_{\alpha} n_{\alpha+3} n_{\alpha+5} \bar{n}_{\alpha+1} \bar{n}_{\alpha+2} \bar{n}_{\alpha+4} \right), \tag{3.3.4}$$

and the collision term due to the four-body collisions:

$$\mathcal{C}_{\alpha}^{(4)} = \xi_{R}^{(4)} n_{\alpha+1} n_{\alpha+2} n_{\alpha+4} n_{\alpha+5} \bar{n}_{\alpha} \bar{n}_{\alpha+3} + \xi_{L}^{(4)} n_{\alpha+1} n_{\alpha+2} n_{\alpha+4} n_{\alpha+5} \bar{n}_{\alpha} \bar{n}_{\alpha+3} - \xi_{R}^{(4)} n_{\alpha} n_{\alpha+1} n_{\alpha+3} n_{\alpha+4} \bar{n}_{\alpha+2} \bar{n}_{\alpha+5} - \xi_{L}^{(4)} n_{\alpha} n_{\alpha+2} n_{\alpha+3} n_{\alpha+5} \bar{n}_{\alpha+1} \bar{n}_{\alpha+4} ,$$
(3.3.5)

where Boolean random number  $\xi^{(3S)}$ ,  $\xi^{(3A)}$ ,  $\xi^{(4)}_R$  and  $\xi^{(4)}_L$  are similar to  $\xi^{(2)}_R$  and  $\xi^{(2)}_L$ .

By observing the form of the collision terms, we can write the collision operator in a general form

$$C_{\alpha}(\lbrace n_{\alpha}\rbrace) = \sum_{\boldsymbol{s},\boldsymbol{s}'} (s'_{\alpha} - s_{\alpha}) \xi_{\boldsymbol{s}\boldsymbol{s}'} \prod_{\beta} n_{\beta}^{S_{\beta}}(\boldsymbol{x}, t) (1 - n_{\beta}(\boldsymbol{x}, t))^{(1 - S_{\beta})}, \qquad (3.3.6)$$

where  $\mathbf{s} \equiv \{s_1, s_2, \dots, s_6\}$  and  $\mathbf{s}' \equiv \{s'_1, s'_2, \dots, s'_6\}$  are all possible incoming and outgoing configurations at a given site,  $\mathbf{x}$ , and time, t, the quantity,  $\xi_{\mathbf{s}\mathbf{s}'}$ , is a Boolean random number in space and time which determines the transition between states  $\mathbf{s}$  and  $\mathbf{s}'$ . In the collision operator, the factor,  $(s_{\alpha}' - s_{\alpha})$ , accounts for the sign of a particular collision term: When  $s_{\alpha}' - s_{\alpha} = +1$  (i.e.,  $s'_{\alpha} = 1$  and  $s_{\alpha} = 0$ ), the collision is a creation process; when  $s'_{\alpha} - s_{\alpha} = -1$  (i.e.,  $s'_{\alpha} = 0$  and  $s_{\alpha} = 1$ ), the collision is an annihilation process; when  $s'_{\alpha} = s_{\alpha}$ , nothing happens in collision process. The Boolean random number,  $\xi_{\mathbf{s}\mathbf{s}'}$ , must satisfy the normalization condition

$$\sum_{\mathbf{s}'} \xi_{\mathbf{s}\mathbf{s}'} = 1, \qquad \forall \mathbf{s} . \tag{3.3.7}$$

 $\xi_{ss'}$  must also have rotational symmetry, *i.e.*, for any states s and s',  $\xi_{ss'}$  is invariant if states s and s' are both subjected to simultaneous proper or improper rotations. Particular examples of  $\xi_{ss'}$  are  $\xi_R^{(2)}$ ,  $\xi_L^{(2)}$ ,  $\xi_L^{(3S)}$ ,  $\xi_R^{(3A)}$ ,  $\xi_R^{(4)}$  and  $\xi_L^{(4)}$ . For the collision operator to satisfy the complete lattice symmetry group, one must have

$$\langle \xi_L^{(2)} \rangle = \langle \xi_R^{(2)} \rangle,$$
 (3.3.8a)

$$\langle \xi_L^{(4)} \rangle = \langle \xi_R^{(4)} \rangle, \tag{3.3.8b}$$

where  $\langle \cdot \rangle$  denotes the ensemble average. Note that

$$n_{\beta}^{S_{\beta}} (1 - n_{\beta})^{(1 - S_{\beta})} = \delta_{n_{\beta}S_{\beta}},$$
 (3.3.9)

where  $\delta n_{\beta} s_{\beta}$  is the Kronecker delta symbol with two indices. Thus, the collision operator can be rewritten<sup>1</sup>

$$C_{\alpha}(\{n_{\alpha}\}) = \sum_{\boldsymbol{s},\boldsymbol{s}'} (s'_{\alpha} - s_{\alpha}) \xi_{\boldsymbol{s}\boldsymbol{s}'} \prod_{\beta} \delta_{n_{\beta}s_{\beta}}.$$
 (3.3.10)

With this concise notation, the collision operator can be easily understood.

With the form of the collision operator given by Eq. (3.3.6), mass and momentum conservation laws can rewritten as

$$\sum_{\alpha} (s_{\alpha}' - s_{\alpha}) = 0, \tag{3.3.11a}$$

$$\sum_{\alpha} (s_{\alpha}' - s_{\alpha}) \hat{\boldsymbol{e}}_{\alpha} = 0. \tag{3.3.11b}$$

#### 3.4 The FHP Model with Rest Particles

In the original paper by Frisch, Hasslacher and Pomeau [44], only the two-body and symmetric three-body collisions were included in the model, which is referred to as the FHP-I model [46]. In a subsequent paper [46], the FHP-II model, which is a 7-bit variation of the FHP-I model including zero-velocity rest particles, was proposed. The FHP-III model is the collision-saturated version of the FHP-II model, *i.e.*, all possible collisions are considered in the model.

<sup>&</sup>lt;sup>1</sup>This notation is due to Ms. Shuling Hou.

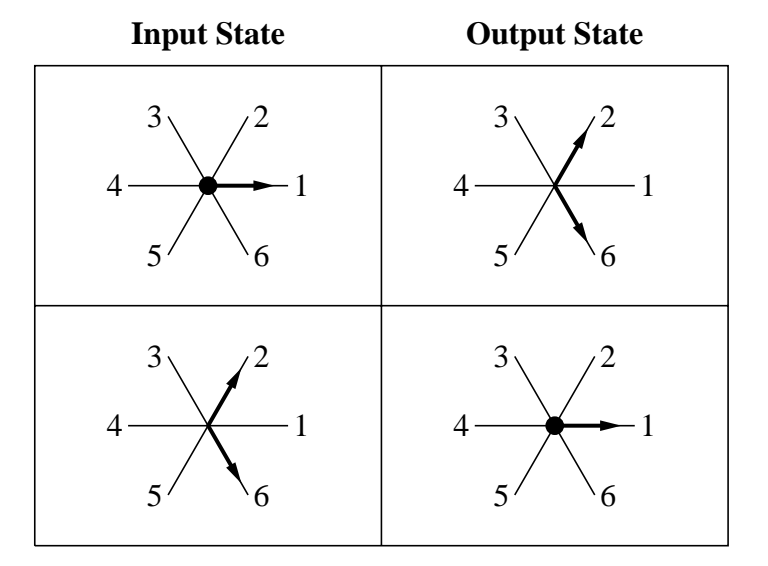


Figure 3.4.1: The two-body collision rules including rest particle for the 7-bit FHP lattice-gas automata. In the left column are incoming states, and in the right are outgoing states. The solid circle represents the presence of a rest particle.

In the FHP-II model, the new collision mechanisms with a zero-velocity rest particle are shown in Fig. (3.4.1). Similar to the 6-bit models, Table (3.4.1) is the binary collision table for the collision rules involving a rest particle. In the binary notation, we use the seventh bit of a binary number to represent the occupation number of the rest particle. The collision operator for the above collisions can be

INPUT STATE	OUTPUT STATE
1000001	0100010
0100010	1000001

Table 3.4.1: The collision table for the 7-bit FHP models. Shown here are only the binary collision rules involving a rest particle. The seventh bit of a binary number represents the occupation number of the rest particle.

easily written down:

$$\mathcal{C}_{\alpha}^{(2R)} = \begin{cases}
\xi_{o}^{(2)} \sum_{\alpha=1}^{6} (n_{\alpha+1} n_{\alpha+5} \bar{n}_{\alpha} \bar{n}_{0} - n_{0} n_{\alpha} \bar{n}_{\alpha+1} \bar{n}_{\alpha+5}), & \alpha = 0, \\
\xi_{o}^{(2R)} = \begin{cases}
\xi_{o}^{(2)} \sum_{\alpha=1}^{6} (n_{\alpha+1} n_{\alpha+5} \bar{n}_{\alpha} \bar{n}_{0} - n_{0} n_{\alpha} \bar{n}_{\alpha+1} \bar{n}_{\alpha+5}), & \alpha \neq 0,
\end{cases} (3.4.1)$$

where the presence of other spectators has not been excluded. Besides the binary collisions, there can be triple collisions with rest particles, Fig. (3.4.2) lists some possible triple collision configurations.

Notice that, like the symmetric triple collisions, the binary collisions involving a rest particle also destroy the spurious conserved quantities along each lattice line. The rationale of introducing binary collisions with rest particles is that, when particle density is low, the probability of triple collisions is much lower than that of binary collisions. Thus, introducing rest particles effectively enhances the probability of the collisions removing the aforementioned spurious conserved quantities along lattice lines. Besides, the enhancement of collision probability reduces the kinematic viscosity,  $\nu$ , and thus enhances the Reynolds number,  $R_e$ . It should also be noticed that the kinetic energy is not conserved in the collisions involving rest particles, whereas mass and momentum are. If each rest particle is considered to carry an amount of potential energy equal to that of the kinetic energy of a moving particle, then the total energy is conserved exactly and locally in the collision processes.

### 3.5 Spurious Conserved Quantities

We have mentioned spurious conserved quantities in the HPP model previously, in §3.1. In this section, we shall discuss spurious conserved quantities with sufficient rigor and details.

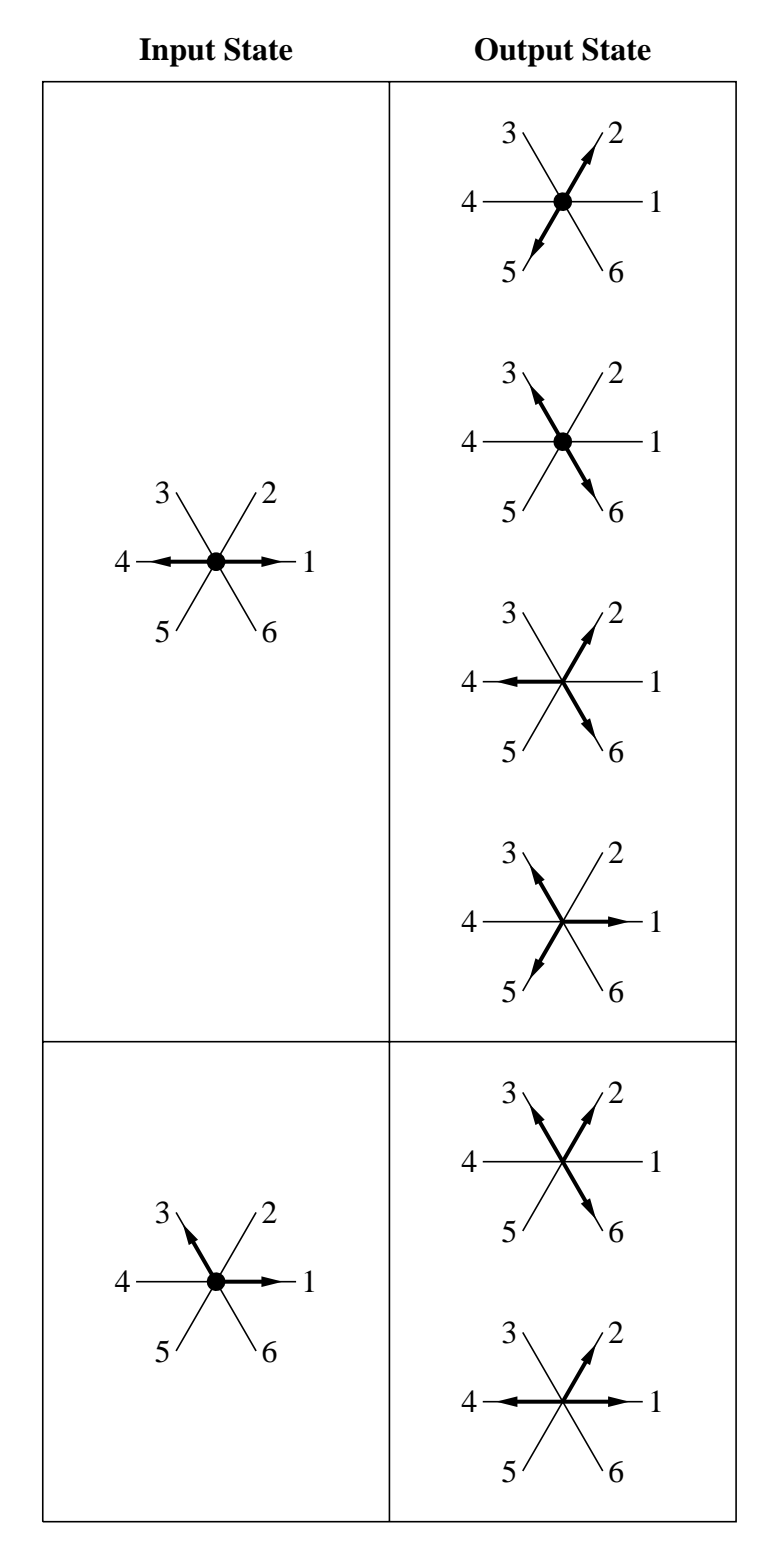


Figure 3.4.2: The three-body collision rules including rest particle for the 7-bit FHP lattice-gas automata. In the left column are incoming states, and in the right are outgoing states. The solid circle represents the presence of a rest particle.

Due to the simplicity of the discrete phase-space structure and updating rules of lattice-gas automata, there exist some extra conserved quantities besides the physical ones (mass, momentum and energy). These unphysical conserved quantities are called spurious conserved quantities. These spurious conserved quantities certainly affect the hydrodynamics of the lattice-gas automata [105–107].

The spurious conserved quantities in the HPP model are total momentum along each lattice line. For periodic boundary conditions, these quantities do not change as the system evolves, therefore, they are static invariants of the system [107]. This kind of spurious conserved quantities are eliminated in FHP models by introducing symmetric three-body collisions. However, there is another kind of spurious conserved quantity found in FHP models, called the staggered invariant [105]. To illustrate the staggered invariant, we start with a trivial example of an one-dimensional cellular automaton with periodic boundary conditions. Suppose the collision rules of this 1-D automaton conserve mass and momentum locally. Then

$$\mathbf{p}_{\text{even}}(t) = \sum_{x=2j} \mathbf{p}(x, t)$$
 (3.5.1a)

$$\boldsymbol{p}_{\text{odd}}(t) = \sum_{x=2j+1} \boldsymbol{p}(x, t)$$
 (3.5.1b)

are the total momentum on even and odd sites, respectively. Because particles can only hop one lattice spacing at each time,  $\boldsymbol{p}_{\text{even}}(t)$  and  $\boldsymbol{p}_{\text{odd}}(t)$  are exchanged at each time step. Therefore, besides the total mass and momentum, an additional conserved quantity,  $(-1)^t(\boldsymbol{p}_{\text{even}}(t)-\boldsymbol{p}_{\text{odd}}(t))$ , exists, which is due to the extremely simple dynamics of the system.

The staggered momentum in the FHP models can be defined as follows

$$\boldsymbol{G}_{\alpha}(t) = (-1)^{t} \sum_{\boldsymbol{r}} (-1)^{\boldsymbol{e}_{\alpha}^{\perp} \cdot \boldsymbol{r}} \, \hat{\boldsymbol{e}}_{\alpha}^{\perp} \cdot \boldsymbol{p}(\boldsymbol{r}, t), \qquad (3.5.2)$$

where the unit vector  $\hat{\boldsymbol{e}}_{\alpha}^{\perp}$  is obtained by rotating  $\hat{\boldsymbol{e}}_{\alpha}$   $\pi/2$  counter-clockwise, and  $\boldsymbol{e}_{\alpha}^{\perp}$  is the reciprocal space vector perpendicular to  $\hat{\boldsymbol{e}}_{\alpha}$ , *i.e.*,  $\boldsymbol{e}_{\alpha}^{\perp} = \frac{2}{\sqrt{3}}\hat{\boldsymbol{e}}_{\alpha}^{\perp}$ . By inspecting Eq. (3.5.2), one can see that the staggered momentum is the difference between the sum of momentum component perpendicular to a lattice line over even lines and that over odd lines. Again, because particles can only move to the nearest neighbors, the sum over even lines and the sum over odd lines alternate at each time step. The factor  $(-1)^t$  accounts for this effect. Due to the spatial symmetry of the underlying lattice structure, *i.e.*,  $\hat{\boldsymbol{e}}_{\alpha} = -\hat{\boldsymbol{e}}_{\alpha+3}$ , there are only three independent staggered-momentum modes, instead of six. The staggered momentum has no physical interpretation or appropriate analogy in real systems.

In addition to the physical conserved quantities, the staggered momentum affects the hydrodynamics of the system. The hydrodynamic equations of the system depend upon the staggered momentum explicitly [105]. Therefore, the lattice-gas automata could produce flow patterns which deviate from solutions of the Navier-Stokes equations. This peculiarity of the lattice-gas automata is completely due to the simplicity and discreteness of the dynamics: Particles can only move between the nearest neighbors with one time step. Thus, one might expect that the staggered-momentum invariants may be eliminated by introducing multi-speed models with the next-nearest neighbor advections, although there is no rigorous proof of this conjecture. In practice, simulation setups commonly used do not seem to have, either in the initial conditions or while running, a significant projection on the staggered-momentum modes, although some pathological initial condition can be found to demonstrate the appreciable effect of the staggered momentum [105].

Because of the spurious conserved quantities in the lattice-gas automata, two remarks are in order. First of all, some additional care should be taken when implementing the algorithm in simulation and analyzing the simulation results by the method. Second, it should be stressed that finding all of the spurious conserved quan-

tities is a nontrivial matter. For further studies on the subject, we refer to the work by d'Humières et al. [107], and Zanetti [108].

### 3.6 Lattice Symmetries and Tensor Structures

The form of macroscopic equations derived from microdynamics depends on the symmetries (*i.e.*, spatial and temporal symmetries) of the underlying dynamics. It can be shown later that the isotropy of the hydrodynamic equations of the LGA systems is completely determined by the symmetries of the tensor,

$$\boldsymbol{E}_{i_1 i_2 \dots i_n}^{(n)} = \sum_{\alpha} \hat{\boldsymbol{e}}_{\alpha, i_1} \hat{\boldsymbol{e}}_{\alpha, i_2} \dots \hat{\boldsymbol{e}}_{\alpha, i_n}, \qquad (3.6.1)$$

where  $\hat{\boldsymbol{e}}_{\alpha,i}$  is the *i*th component of  $\hat{\boldsymbol{e}}_{\alpha}$  in *D*-dimensional Euclidean vector space. In particular, the isotropy of the Navier-Stokes equation depends on the tensor  $\boldsymbol{E}^{(4)}$ , because  $\boldsymbol{E}^{(4)}$  explicitly appears in the leading order approximation of the momentum density flux tensor  $\Pi_{ij}$ . In this section, we briefly discuss symmetries of the tensor,  $\boldsymbol{E}^{(n)}$ , within the context of lattice gas automata.

Tensors that are invariant under continuous rotations and reflections are isotropic tensors. By definition, the tensor,  $\mathbf{E}^{(n)}$ , is symmetric in their space indices. If the symmetric tensor,  $\mathbf{E}^{(n)}$ , obtained with sets of  $\sigma_1$  vectors,  $\{\hat{\mathbf{e}}_{\alpha} | \alpha = 1, 2, \dots, \sigma_1\}$ , uniformly distributed on the unit sphere in D-dimensional space, is isotropic, it must satisfy

$$\mathbf{E}^{(2n+1)} = 0, (3.6.2a)$$

$$\mathbf{E}^{(2n)} = \frac{\sigma_1}{D(D+2)\cdots(D+2n-2)} \Delta^{(2n)}, \qquad (3.6.2b)$$

where

$$\Delta_{ij}^{(2)} = \delta_{ij} \,, \tag{3.6.3a}$$

$$\Delta_{ijkl}^{(4)} = \delta_{ij}\delta_{kl} + \delta_{ik}\delta_{jl} + \delta_{il}\delta_{jk}. \qquad (3.6.3b)$$

In general,  $\Delta^{(2n)}$  consists of a sum of all the  $(2n-1)!!^2$  possible products of Kronecker delta symbols of pairs of indices, given by the recursion relation

$$\Delta_{i_1 i_2 \dots i_{2n}}^{(2n)} = \sum_{j=2}^{2n} \delta_{i_1 i_j} \Delta_{i_2 i_3 \dots i_{j-1} i_{j+1} \dots i_{2n}}^{(2n-2)} . \tag{3.6.4}$$

For a triangular lattice in two-dimensional space, i.e.,  $\sigma_1 = 6$  and D = 2, it can be shown that the tensor,  $\mathbf{E}^{(n)}$ , is isotropic up to n = 5 [45], i.e.,

$$\mathbf{E}^{(2n+1)} = 0, (3.6.5a)$$

$$\mathbf{E}_{ij}^{(2)} = \frac{6}{2} \delta_{ij} \,, \tag{3.6.5b}$$

$$\mathbf{E}_{ijkl}^{(4)} = \frac{6}{2 \cdot 4} \left( \delta_{ij} \delta_{kl} + \delta_{ik} \delta_{jl} + \delta_{il} \delta_{jk} \right) . \tag{3.6.5c}$$

However, for a square lattice in two-dimensional space, the tensor,  $E^{(n)}$ , is isotropic only up to n = 3. Specifically,

$$\mathbf{E}^{(2n+1)} = 0, \tag{3.6.6a}$$

$$\mathbf{E}_{ij}^{(2)} = \frac{4}{2}\delta_{ij} \,, \tag{3.6.6b}$$

$$\boldsymbol{E}_{ijkl}^{(4)} = 2\delta_{ijkl} \,, \tag{3.6.6c}$$

where  $\delta_{ijkl}$  is the Kronecker delta symbol with four indices, which is not isotropic.

 $<sup>2(2</sup>n-1)!! \equiv 1 \cdot 3 \cdot 5 \cdots (2n-3) \cdot (2n-1).$ 

Therefore, the square lattice does not have sufficient symmetry to produce isotropic hydrodynamic equations (this is one of the major shortcomings of the HPP lattice-gas automaton); whereas the triangular lattice does.

The symmetry of discrete lattice is a rich subject, which we will not discuss in depth here. A more extensive discussion of the symmetry considerations can be found in Ref. [45].

# 3.7 The Equilibrium Distribution Function and Necessary Collisions

For the lattice-gas automata, or other discrete velocity gas models [109, 27], the computation of the equilibrium distribution is the same as that of the most probable distribution of an assembly of N non-interacting particles, quantum or classical. The problem can be formulated [110,111] as how to find the most probable distribution,  $\{n_i^*\}$ , of  $\{n_i\}$ , consistent with the constraints of the total number of particles, N, and the total energy, E:

$$\sum_{i} n_i = N , \qquad (3.7.1a)$$

$$\sum_{i} n_{i} \varepsilon_{i} = E, \qquad (3.7.1b)$$

for a given system with micro-eigenstates of which each can be specified by its corresponding energy eigenvalue,  $\varepsilon_i$ , with multiplicity,  $m_i$ , confined by the volume V. The most probable distribution is the one maximizing the entropy, S, of the system for a given macrostate (N, E, V).

The number of distinct microstates,  $\Delta(N, E, V)$ , accessible to the given system

under the macrostate (N, E, V) is given by

$$\Delta(N, E, V) = \sum_{\{n_i\}} W(\{n_i\}), \qquad (3.7.2)$$

where  $W(\{n_i\})$  is the number of distinct microstates associated with the distribution set,  $\{n_i\}$ , and

$$W(\{n_i\}) = \prod_i w(n_i), \qquad (3.7.3)$$

where  $w(n_i)$  is the number of distinct microstates associated with the *i*th eigenstate with  $n_i$  particles. For a classical system, *i.e.*, the Maxwell-Boltzmann case, particles are distinguishable, and

$$w_{MB}(n_i) = \frac{m_i^{n_i}}{n_i!} \,. \tag{3.7.4}$$

For quantum systems, particles are identical and *indistinguishable*. Also, particles can be either Boson (the Bose-Einstein case) or Fermion (the Fermi-Dirac case). In the Bose-Einstein case,

$$w_{BE}(n_i) = \frac{(m_i + n_i + 1)!}{n_i!(m_i - 1)!},$$
(3.7.5)

and in the Fermi-Dirac case,

$$w_{FD}(n_i) = \frac{m_i!}{n_i!(m_i - n_i)!}. (3.7.6)$$

The entropy of the system S(N, E, V) is

$$S(N, E, V) = k_B \ln \Delta(N, E, V) = k_B \ln \sum_{\{n_i\}} W(\{n_i\}).$$
 (3.7.7)

In the thermodynamical limit, we can use the law of large numbers [112]:

$$S(N, E, V) \approx k_B \ln W(\{n_i^*\}),$$
 (3.7.8)

where  $\{n_i^*\}$  denotes the most probable distribution set. Since  $\{n_i^*\}$  maximizes  $W(\{n_i\})$ 

and consequently maximizes the entropy, it is the equilibrium distribution. With the approximation given by Eq. (3.7.8) and the constraints by Eqs. (3.7.1), the equilibrium distribution is determined by

$$\delta \ln W(\{n_i\}) - \left[a \sum_i \delta n_i + b \sum_i \varepsilon_i \delta n_i\right] = 0, \qquad (3.7.9)$$

where a and b are the Lagrangian multipliers. Here, it has already been assumed that N and E are the only constraints, or the conserved quantities, of the system. When numbers  $m_i$  and  $n_i$  are assumed to be large, the Stirling formula

$$n! \approx n^n e^{-n} \tag{3.7.10}$$

can be applied, thus

$$\ln W(\{n_i\}) = \sum_{i} \ln w(n_i)$$

$$\approx \sum_{i} \left[ n_i \ln \left( \frac{m_i}{n_i} - z \right) - \frac{m_i}{z} \ln \left( 1 - z \frac{n_i}{m_i} \right) \right], \qquad (3.7.11)$$

where z = 0 for the Maxwell-Boltzmann case, +1 for the Fermi-Dirac case and -1 for the Bose-Einstein case. Now, Eq. (3.7.9) becomes

$$\sum_{i} \left[ \ln \left( \frac{m_i}{n_i} - z \right) - a - b\varepsilon_i \right]_{n_i = n_i^*} \delta n_i = 0.$$
 (3.7.12)

Obviously, the most probable distribution is

$$n_i^* = \frac{m_i}{e^{a+b\varepsilon_i} + z} \,, (3.7.13)$$

and the equilibrium probability of finding a particle in ith level is

$$f_i^* = \frac{n_i^*}{m_i} = \frac{1}{e^{a+b\varepsilon_i} + z}.$$
 (3.7.14)

The above results can also be derived more rigorously using the formal theory of an ideal gas in the canonical and grand canonical ensembles [111], which we do not discuss here.

For the FHP lattice-gas models satisfying the exclusion principle, we have the equilibrium distribution

$$f_{\alpha}^{(eq)}(\boldsymbol{x},t) = \frac{1}{1 + \exp\left(a + b\hat{\boldsymbol{e}}_{\alpha} \cdot \boldsymbol{v}\right)} \equiv f_{\alpha}^{(FD)}.$$
 (3.7.15)

The single-particle distribution function,  $f_{\alpha}(\boldsymbol{x}, t)$ , is the ensemble average of  $n_{\alpha}(\boldsymbol{x}, t)$ , i.e.,

$$f_{\alpha}(\boldsymbol{x}, t) \equiv \langle n_{\alpha}(\boldsymbol{x}, t) \rangle$$
 (3.7.16)

Note that the conserved quantities are mass and momentum in the models. The constants a and b are functions of  $\rho$  and  $\|\boldsymbol{v}\|^2$  because of the spatial parity symmetry  $(\boldsymbol{v} \to -\boldsymbol{v}, \hat{\boldsymbol{e}}_{\alpha} \to -\hat{\boldsymbol{e}}_{\alpha})$ . They can be obtained analytically when  $\boldsymbol{v}$  is aligned with  $\hat{\boldsymbol{e}}_{\alpha}$  or  $\boldsymbol{v}$  bifurcates two adjacent  $\hat{\boldsymbol{e}}_{\alpha}$ 's [113,114]. In general, a and b can be expanded as a power series in  $\|\boldsymbol{v}\|^2$  [45,46]. This will be discussed in later sections of this chapter. The mean mass density per node  $\rho(\boldsymbol{x},t)$  and mean momentum density per node  $\boldsymbol{p}(\boldsymbol{x},t)$  are related to  $f_{\alpha}(\boldsymbol{x},t)$  by

$$\rho(\boldsymbol{x}, t) = \sum_{\alpha} f_{\alpha}(\boldsymbol{x}, t), \qquad (3.7.17a)$$

$$p(\boldsymbol{x}, t) \equiv \rho(\boldsymbol{x}, t) v(\boldsymbol{x}, t) = \sum_{\alpha} \hat{\boldsymbol{e}}_{\alpha} f_{\alpha}(\boldsymbol{x}, t),$$
 (3.7.17b)

where we assume that the mass of each particle is unity.

We can also view the most probable distribution from the viewpoint of necessary collisions. The number of distinct microstates with the total number of particles with velocity  $\hat{\boldsymbol{e}}_{\alpha}, N_{\alpha} = \sum_{\boldsymbol{x}} n_{\alpha}$ , is

$$\Delta = \frac{N!}{\prod_{\alpha} N_{\alpha}! (N - N_{\alpha})!}, \qquad (3.7.18)$$

with the mass and momentum conservation constraints

$$\sum_{\alpha} N_{\alpha} = N \,, \tag{3.7.19a}$$

$$\sum_{\alpha} N_{\alpha} \hat{\boldsymbol{e}}_{\alpha} = N \boldsymbol{v} \,, \tag{3.7.19b}$$

which pose (D+1) constraints, where D is the dimension of space. The most probable distribution set  $\{N_{\alpha}^*\}$  should maximize  $\Delta$ , therefore, we must have

$$\left. \frac{\partial \Delta}{\partial N_{\alpha}} \right|_{\{N_{\alpha}\}=\{N_{\alpha}^{*}\}} = 0, \qquad \alpha = 1, 2, \cdots, r - D - 1, \qquad (3.7.20)$$

where r is the number of velocities. The results of the above equation are

$$\bar{f}_1\bar{f}_4 = \bar{f}_2\bar{f}_5$$
, (3.7.21a)

$$\bar{f}_2\bar{f}_5 = \bar{f}_3\bar{f}_6$$
, (3.7.21b)

$$\bar{f}_3\bar{f}_6 = \bar{f}_1\bar{f}_4,$$
 (3.7.21c)

where  $\bar{f}_{\alpha} = \frac{f_{\alpha}}{1 - f_{\alpha}}$ . These results show detailed balancing of a set of two-body collisions which conserve mass and momentum. Furthermore, these collisions are dictated by the equilibrium solution, which suggests that the two-body collisions are necessary for thermalizing the system. Of course, spurious conserved quantities have not been considered here.

The method to obtain the equilibrium distribution and the necessary collisions, as illustrated above, can be a quite general procedure, independent of the underlying

lattice structure, details of collision rules and space dimensions [27]. The equilibrium distribution of the FHP lattice-gas automata can also be obtained by other methods [46].

### 3.8 The Lattice Boltzmann Equation

In this section, we shall discuss the Boltzmann approximation in the context of FHP lattice-gas automata, and derive the lattice Boltzmann equation, which leads to the Navier-Stokes equation for FHP models in §3.10.

The ensemble average of Eq. (3.2.2) with the Boltzmann approximation yields the lattice Boltzmann equation [85]:

$$f_{\alpha}(\boldsymbol{x} + \hat{\boldsymbol{e}}_{\alpha}, t+1) = f_{\alpha}(\boldsymbol{x}, t) + \Omega_{\alpha}(\{f_{\alpha}\}), \qquad (3.8.1)$$

where  $f_{\alpha}(\boldsymbol{x}, t)$  is the single-particle mass density distribution function, and  $\{f_{\alpha}\}$  denotes all of  $f_{\alpha}(\boldsymbol{x}, t)$ . The operator,  $\Omega_{\alpha}$ , is equal to  $\mathcal{C}_{\alpha}$  if  $n_{\beta}$  and  $\xi_{\boldsymbol{s}\boldsymbol{s}'}$  are replaced by  $f_{\beta}$  and  $A_{\boldsymbol{s}\boldsymbol{s}'} = \langle \xi_{\boldsymbol{s}\boldsymbol{s}'} \rangle$ , respectively, in Eq. (3.3.6):

$$\Omega_{\alpha}(\lbrace f_{\alpha}\rbrace) = \sum_{\boldsymbol{s},\boldsymbol{s}'} (s'_{\alpha} - s_{\alpha}) A_{\boldsymbol{s}\boldsymbol{s}'} \prod_{\beta} f_{\beta}^{s_{\beta}}(\boldsymbol{x}, t) \left(1 - f_{\beta}(\boldsymbol{x}, t)\right)^{(1-s_{\beta})}. \tag{3.8.2}$$

The ensemble-averaged value of  $\xi_{ss'}$ ,  $A_{ss'} = \langle \xi_{ss'} \rangle$ , defines a transition probability from state s to s', for any arbitrary s and s'. The transition probability  $A_{ss'}$  must satisfy the normalization condition

$$\sum_{\mathbf{s}'} A_{\mathbf{s}\mathbf{s}'} = 1 \qquad \forall \mathbf{s} \,, \tag{3.8.3}$$

and either semi-detailed balance

$$\sum_{\mathbf{s}} A_{\mathbf{s}\mathbf{s}'} = 1 \qquad \forall \mathbf{s}' \tag{3.8.4}$$

or detailed balance

$$A_{\mathbf{s}\mathbf{s}'} = A_{\mathbf{s}'\mathbf{s}}. \tag{3.8.5}$$

Of course,  $A_{ss'}$  has rotational symmetry, as  $\xi_{ss'}$  does. The meaning of semi-detailed balance is that the collision process does not change the probabilities of states.

For the FHP 6-bit models, the constraints of the six-fold rotational symmetry  $\langle \xi_L^{(2)} \rangle = \langle \xi_R^{(2)} \rangle$  and  $\langle \xi_L^{(4)} \rangle = \langle \xi_R^{(4)} \rangle$  imply detailed balance, and *vice versa*. In other words, the six-fold rational symmetry is equivalent to detailed balance for the FHP 6-bit models.<sup>3</sup>

The crucial approximation used to obtain Eq. (3.8.2) is the random phase approximation (RPA) (or molecular chaos)

$$\langle n_{\alpha} n_{\beta} \cdots n_{\gamma} \rangle = \langle n_{\alpha} \rangle \langle n_{\beta} \rangle \langle \cdots \rangle \langle n_{\gamma} \rangle = f_{\alpha} f_{\beta} \cdots f_{\gamma}. \tag{3.8.6}$$

In this approximation, all correlations have been neglected. The difference between the random phase approximation and the Boltzmann approximation is that the lowdensity limit is not imposed in the random phase approximation, here collision processes still include multi-particle collisions.

The above approximation also leads to result that the Fermi-Dirac distribution is the equilibrium distribution. Indeed, it can be shown that the solution of equation

$$\Omega_{\alpha}(\lbrace f_{\alpha}\rbrace) \equiv \sum_{\boldsymbol{s},\boldsymbol{s}'} (s'_{\alpha} - s_{\alpha}) A_{\boldsymbol{s}\boldsymbol{s}'} \prod_{\beta} f_{\beta}^{s_{\beta}} (1 - f_{\beta})^{(1-s_{\beta})} = 0$$

<sup>&</sup>lt;sup>3</sup>This point was brought to the author's attention by Dr. Hudong Chen.

is the Fermi-Dirac distribution function  $f_{\alpha}^{(\text{FD})}$  [46].

### 3.9 The Local and Global H-Theorem

In this section, we show proofs for both the local and the global *H*-theorem in the context of the lattice Boltzmann equation. These proofs are due to M. Hénon and can be found in Ref. [46].

For a pre-collision state, s, P(s) is the probability associated with it, and

$$\sum_{\mathbf{s}} P(\mathbf{s}) = 1. \tag{3.9.1}$$

The single-particle distribution function,  $f_{\alpha}$ , is related to P(s) by

$$f_{\alpha} = \sum_{\mathbf{s}} s_{\alpha} P(\mathbf{s}). \tag{3.9.2}$$

Similarly, denote P'(s') and  $f'_{\alpha}$  for a post-collision state, s'. The probability of a post-collision state s', P'(s'), is related the transition probability from state s to s' via collision,  $A_{ss'}$ , and P(s) as follows

$$P'(\mathbf{s}') = \sum_{\mathbf{s}} A_{\mathbf{s}\mathbf{s}'} P(\mathbf{s}). \tag{3.9.3}$$

The local H-theorem then can be stated as follows.

Theorem 3.1 (Local *H*-Theorem) If the collision rules satisfy semi-detailed balance, and the Boltzmann approximation is valid, then the following inequality holds:

$$\sum_{\alpha} \left[ f'_{\alpha} \ln f'_{\alpha} + (1 - f'_{\alpha}) \ln(1 - f'_{\alpha}) \right] \le \sum_{\alpha} \left[ f_{\alpha} \ln f_{\alpha} + (1 - f_{\alpha}) \ln(1 - f_{\alpha}) \right]. \tag{3.9.4}$$

The proof of above theorem goes as follows: First of all, the function  $P(s) \ln P(s)$  is convex function<sup>4</sup> (derivative is nondecreasing) and  $A_{ss'}$  satisfies semi-detailed balance. Therefore,

$$\sum_{\mathbf{s}} P(\mathbf{s}) \ln P(\mathbf{s}) = \sum_{\mathbf{s}} \left( \sum_{\mathbf{s}'} A_{\mathbf{s}\mathbf{s}'} \right) P(\mathbf{s}) \ln P(\mathbf{s})$$

$$= \sum_{\mathbf{s}'} \frac{\sum_{\mathbf{s}} A_{\mathbf{s}\mathbf{s}'} P(\mathbf{s}) \ln P(\mathbf{s})}{\sum_{\mathbf{s}} A_{\mathbf{s}\mathbf{s}'}}$$

$$\geq \sum_{\mathbf{s}'} \frac{\left( \sum_{\mathbf{s}} A_{\mathbf{s}\mathbf{s}'} P(\mathbf{s}) \right) \ln \left( \sum_{\mathbf{s}} A_{\mathbf{s}\mathbf{s}'} P(\mathbf{s}) \right)}{\sum_{\mathbf{s}} A_{\mathbf{s}\mathbf{s}'}}$$

$$= \sum_{\mathbf{s}'} P'(\mathbf{s}') \ln P'(\mathbf{s}') .$$

$$(3.9.6)$$

Next, using the fact that, for any x,  $\ln x \le x - 1$ , where the equality holds when x = 1, then,

$$\ln\left(\frac{\prod_{\alpha} f_{\alpha}^{S_{\alpha}} (1 - f_{\alpha})^{1 - S_{\alpha}}}{P(s)}\right) \le \frac{\prod_{\alpha} f_{\alpha}^{S_{\alpha}} (1 - f_{\alpha})^{1 - S_{\alpha}}}{P(s)} - 1.$$
(3.9.7)

Multiplying above inequality by P(s) and summing over s, the result obtained is<sup>5</sup>

$$\sum_{\mathbf{s}} P(\mathbf{s}) \ln \left( \frac{\prod_{\alpha} f_{\alpha}^{S_{\alpha}} (1 - f_{\alpha})^{1 - S_{\alpha}}}{P(\mathbf{s})} \right) \le 0.$$
 (3.9.8)

$$f(\lambda x + (1 - \lambda)y) \le \lambda f(x) + (1 - \lambda)f(y) \qquad x, y \in (a, b),$$

the equality holds when  $\lambda = 0$ , 1. For further details about convex functions, see Ref. [115]. <sup>5</sup>Note that, with the Boltzmann approximation,

$$\sum_{\mathbf{s}} \prod_{\alpha} f_{\alpha}^{s_{\alpha}} (1 - f_{\alpha})^{1 - s_{\alpha}} = \sum_{\mathbf{s}} P(\mathbf{s}) = 1.$$

<sup>&</sup>lt;sup>4</sup>If function f(x) is a convex function on an open interval (a, b), then  $\frac{d^2f}{dx^2} \ge 0$  on the interval, or alternatively, for each  $\lambda$ ,  $0 \le \lambda \le 1$ ,

Now, rewrite the above inequality as

$$\sum_{\mathbf{s}} P(\mathbf{s}) \ln P(\mathbf{s}) \geq \sum_{\mathbf{s}} P(\mathbf{s}) \ln \left( \prod_{\alpha} f_{\alpha}^{S_{\alpha}} (1 - f_{\alpha})^{1 - S_{\alpha}} \right)$$

$$= \sum_{\alpha} \sum_{\mathbf{s}} \left[ s_{\alpha} P(\mathbf{s}) \ln f_{\alpha} + (1 - s_{\alpha}) P(\mathbf{s}) \ln (1 - f_{\alpha}) \right]$$

$$= \sum_{\alpha} f_{\alpha} \ln f_{\alpha} + (1 - f_{\alpha}) \ln (1 - f_{\alpha}) ,$$
(3.9.9)

where we have used the result from Eq. (3.9.2). Therefore,

$$\sum_{\mathbf{s}} P(\mathbf{s}) \ln P(\mathbf{s}) \ge \sum_{\alpha} \left[ f_{\alpha} \ln f_{\alpha} + (1 - f_{\alpha}) \ln(1 - f_{\alpha}) \right], \qquad (3.9.10)$$

where the equality holds if and only if

$$P(\mathbf{s}) = \prod_{\alpha} f_{\alpha}^{s_{\alpha}} (1 - f_{\alpha})^{1 - s_{\alpha}}. \tag{3.9.11}$$

Eq. (3.9.11) is an exact statement of the Boltzmann approximation, that is, the probability P(s) for any state s is independent of its previous states. In other word, the fact that the *joint* probability P(s) is a product of individual probabilities,  $f_{\alpha}$ 's, and  $(1 - f_{\alpha})$ 's, implies that  $f_{\alpha}$ 's are independent of each other. Finally, combining the results of inequality (3.9.7) and the equality in (3.9.10) (the Boltzmann approximation), the local H-theorem is obtained.

As a direct consequence of the local H-theorem, the global H-theorem can be obtained by summing inequality (3.9.4) over all lattice sites.

#### Theorem 3.2 (Global H-Theorem) The function

$$\sum_{x} \sum_{\alpha} \left[ f_{\alpha} \ln f_{\alpha} + (1 - f_{\alpha}) \ln(1 - f_{\alpha}) \right]$$
 (3.9.12)

of time t is non-increasing as time t increases.

The H-theorems ensure that systems, with the validity of the Boltzmann approximation, irreversibly approach equilibrium.

### 3.10 The Solution of the Lattice Boltzmann Equation, the Chapman-Enskog Procedure and Hydrodynamic Equations

In what follows, we shall apply the Chapman-Enskog procedure to the lattice Boltzmann equation, and obtain the corresponding macroscopic equations. Because of the special features of the lattice-gas automata, we shall briefly review the Chapman-Enskog procedure within the context of LGA.

## 3.10.1 The Chapman-Enskog Procedure and the Perturbative Solution of the Lattice Boltzmann Equation

Instead of assuming both the lattice constant and the time step size equal to unity, we designate  $\delta_x$  as the lattice constant and  $\delta_t$  as the time step size. Then, the lattice Boltzmann equation becomes

$$f_{\alpha}(\boldsymbol{x} + \delta_{x}\hat{\boldsymbol{e}}_{\alpha}, t + \delta_{t}) - f_{\alpha}(\boldsymbol{x}, t) = \Omega_{\alpha}.$$
(3.10.1)

Expand  $f_{\alpha}(\mathbf{x} + \delta_x \hat{\mathbf{e}}_{\alpha}, t + \delta_t)$  in its Taylor series

$$f_{\alpha}(\boldsymbol{x} + \delta_{x}\hat{\boldsymbol{e}}_{\alpha}, t + \delta_{t}) = \sum_{n=0}^{\infty} \frac{\delta^{n}}{n!} \left( \frac{\partial}{\partial t} + (\hat{\boldsymbol{e}}_{\alpha} \cdot \nabla) \right)^{n} f_{\alpha}(\boldsymbol{x}, t), \qquad (3.10.2)$$

where  $\delta = \delta_x = \delta_t$ . Furthermore,  $f_{\alpha}$  can be expanded as a series of  $\delta$ , around the local equilibrium distribution function  $f_{\alpha}^{(0)} = f_{\alpha}^{(\text{FD})}$ :

$$f_{\alpha} = \sum_{n=0}^{\infty} \delta^n f_{\alpha}^{(n)}, \tag{3.10.3}$$

with the same constraints as those in Eq. (2.4.6)

$$\sum_{\alpha} f_{\alpha}^{(0)} \begin{bmatrix} 1 \\ \hat{\boldsymbol{e}}_{\alpha} \end{bmatrix} = \begin{bmatrix} \rho \\ \rho \boldsymbol{v} \end{bmatrix}, \qquad (3.10.4a)$$

$$\sum_{\alpha} f_{\alpha}^{(n)} \begin{bmatrix} 1 \\ \hat{\boldsymbol{e}}_{\alpha} \end{bmatrix} = 0, \qquad n \ge 1.$$
 (3.10.4b)

Consequently, the collision operator can also be written as a series of  $\delta$ :

$$\Omega_{\alpha} = \sum_{n=0}^{\infty} \delta^n \Omega_{\alpha}^{(n)}. \tag{3.10.5}$$

Here, the parameter,  $\delta$ , is used to obtain a set of equations according to the order of  $\delta$ . Eventually,  $\delta$  should be set to unity.

With the expansions (3.10.2), (3.10.3) and (3.10.5), the lattice Boltzmann equation becomes

$$\sum_{n=0}^{\infty} \delta^n \sum_{m=1}^{n+1} \frac{1}{m!} \left( \frac{D}{Dt} \right)^m f_{\alpha}^{(n+1-m)} = \frac{1}{\delta} \sum_{n=0}^{\infty} \delta^n \Omega_{\alpha}^{(n)}, \qquad (3.10.6)$$

where  $\frac{D}{Dt} \equiv \frac{\partial}{\partial t} + (\hat{\mathbf{e}}_{\alpha} \cdot \nabla)$ . The above equation is obviously different from its continuous counterpart, Eq. (2.4.3). Because of the discrete nature, higher derivatives are important in the equation, as higher order corrections.

As discussed previously, the time scales in Euler's equation and the Navier-Stokes equation are different. To incorporate these different time scales with the proper ordering of spatial derivatives, the multiple time scale formalism should be

explicitly employed. Thus, we write

$$\frac{\partial}{\partial t} = \frac{\partial}{\partial t_0} + \delta \frac{\partial}{\partial t_1} + \delta^2 \frac{\partial}{\partial t_2} + \dots = \sum_{n=0}^{\infty} \delta^n \frac{\partial}{\partial t_n}$$
 (3.10.7)

to separate the different time scales. Eventually, we have to set  $\delta = 1$  in both expansions (3.10.2) and (3.10.7).

To obtain the Euler and the Navier-Stokes equations, only the first two terms are kept in the expansion (3.10.7). Substituting expansion (3.10.7) into Eq. (3.10.6), and equating terms of like order in  $\delta$ , then a set of (infinite many) hierarchical equations can be obtained simultaneously. The first three consecutive (order  $\mathcal{O}(\delta^{-1})$ ,  $\mathcal{O}(1)$  and  $\mathcal{O}(\delta)$ ) equations are

$$\Omega_{\alpha}^{(0)}(\{f_{\alpha}^{(0)}\}) = 0,$$
(3.10.8a)

$$\frac{\partial f_{\alpha}^{(0)}}{\partial t_0} + (\hat{\boldsymbol{e}}_{\alpha} \cdot \nabla) f_{\alpha}^{(0)} = \mathbb{J}_{\alpha\beta} f_{\beta}^{(1)}, \tag{3.10.8b}$$

$$\frac{\partial f_{\alpha}^{(0)}}{\partial t_{1}} + \frac{1}{2} \left( \frac{\partial}{\partial t_{0}} + (\hat{\boldsymbol{e}}_{\alpha} \cdot \nabla) \right)^{2} f_{\alpha}^{(0)} + \left( \frac{\partial}{\partial t_{0}} + (\hat{\boldsymbol{e}}_{\alpha} \cdot \nabla) \right) f_{\alpha}^{(1)} = \Omega_{\alpha}^{(2)}, \ (3.10.8c)$$

where  $J_{\alpha\beta}$  is the Jacobian matrix of the Boltzmann collision operator  $\Omega_{\alpha}$ ,  $\frac{\partial \Omega_{\alpha}}{\partial f_{\beta}}$ , evaluated at  $f_{\alpha} = f_{\alpha}^{(0)}$ ;  $J_{\alpha\beta}f_{\beta}^{(1)} \equiv \Omega_{\alpha}^{(1)}$ ; and  $\Omega_{\alpha}^{(2)}$  depends on  $\{f_{\alpha}^{(0)}\}$ ,  $\{f_{\alpha}^{(1)}\}$  and  $\{f_{\alpha}^{(2)}\}$ . The above three equations are sufficient to obtain the desired macroscopic equations, *i.e.*, the continuity, Euler's, and the Navier-Stokes equation.

Once the lattice Boltzmann equation is solved (up to order of  $\mathcal{O}(\delta)$  in the expansion (3.10.3)), the macroscopic equations can be derived simply by computing the moments of Eqs. (3.10.8). The moments of  $f_{\alpha}$  needed are

$$\rho = \sum_{\alpha} f_{\alpha} \,, \tag{3.10.9a}$$

$$\rho \mathbf{v} = \delta_x \sum_{\alpha} \hat{\mathbf{e}}_{\alpha} f_{\alpha} , \qquad (3.10.9b)$$

$$\Pi_{ij} = \delta_x^2 \sum_{\alpha} \hat{\boldsymbol{e}}_{\alpha,i} \hat{\boldsymbol{e}}_{\alpha,j} f_{\alpha} , \qquad (3.10.9c)$$

where  $\Pi_{ij}$  is the momentum density flux tensor, and  $\delta_x$  accounts for a non-unity lattice constant.

#### 3.10.2 The First Order Solution and the Euler Equations

The solution of the first order equation is the local equilibrium distribution given by the Fermi-Dirac distribution function

$$f_{\alpha}^{(0)} = \frac{1}{1 + \exp(a + b\delta_x \hat{\boldsymbol{e}}_{\alpha} \cdot \boldsymbol{v})}, \qquad (3.10.10)$$

where constant a and b are functions of  $\rho$  and  $v^2$ , and in general they cannot be obtained analytically, except for some special cases [113,114]. Usually, they are evaluated in the small-velocity limit using the series expansions:

$$a = a_0 + a_1 \mathbf{v}^2 + \cdots, (3.10.11a)$$

$$b = b_0 + b_1 v^2 + \cdots {3.10.11b}$$

Denote

$$f_{\text{FD}}(y) = \frac{1}{1 + e^y} \tag{3.10.12}$$

where  $y = a + b\delta_x \hat{\boldsymbol{e}}_{\alpha} \cdot \boldsymbol{v}$ . Then expand  $f_{\alpha}^{(0)}$  at  $\boldsymbol{v} = 0$ :

$$f_{\alpha}^{(0)} = f_{\text{FD}} + f_{\text{FD}}' \frac{\partial y}{\partial \boldsymbol{v}} \cdot \boldsymbol{v} + \frac{1}{2} \left( f_{\text{FD}}'' \left( \frac{\partial y}{\partial \boldsymbol{v}} \right)^2 + f_{\text{FD}}' \frac{\partial^2 y}{\partial \boldsymbol{v}^2} \right) \boldsymbol{v} \boldsymbol{v} + \mathcal{O}(\boldsymbol{v}^3)$$

$$= f_{\text{FD}} + f_{\text{FD}}' (b_0 \delta_x \hat{\boldsymbol{e}}_\alpha \cdot \boldsymbol{v}) + \frac{1}{2} \left( f_{\text{FD}}'' b_0^2 \delta_x^2 (\hat{\boldsymbol{e}}_\alpha \cdot \boldsymbol{v})^2 + f_{\text{FD}}' 2a_1 \boldsymbol{v}^2 \right) + \mathcal{O}(\boldsymbol{v}^3) ,$$
(3.10.13)

where  $f_{\text{FD}}$ ,  $f'_{\text{FD}}$  and  $f''_{\text{FD}}$  are all evaluated at v = 0, i.e.,

$$f_{\text{FD}} = \frac{1}{1 + e^{a_0}} = d,$$
 (3.10.14a)

$$f'_{\text{FD}} = -\frac{e^{a_0}}{(1 + e^{a_0})^2} = d(d - 1),$$
 (3.10.14b)

$$f_{\text{FD}}^{"} = -\frac{e^{a_0}(1 - e^{a_0})}{(1 + e^{a_0})^3} = d(1 - d)(1 - 2d), \qquad (3.10.14c)$$

and  $d \equiv \frac{\rho}{\sigma_1}$  is the mass density in each direction. The first equation above determines the value of  $a_0$ . Consequently, the small-velocity expansion for the equilibrium distribution function is

$$f_{\alpha}^{(0)} = d\left(1 - (1-d)\delta_x b_0(\hat{\boldsymbol{e}}_{\alpha} \cdot \boldsymbol{v}) + \frac{1}{2}(1-d)\left((1-2d)\delta_x^2 b_0^2(\hat{\boldsymbol{e}}_{\alpha} \cdot \boldsymbol{v})^2 - 2a_1\boldsymbol{v}^2\right) + \mathcal{O}(\boldsymbol{v}^3)\right),$$
(3.10.15)

The remaining two coefficients,  $b_0$  and  $a_1$ , can be determined using conservation laws. The mass conservation leads to

$$(1 - 2d)\delta_x^2 b_0^2 \frac{\sigma_1}{D} v^2 - 2\sigma_1 a_1 v^2 = 0,$$

and the momentum conservation leads to

$$-d(1-d)\delta_x^2b_0\frac{\sigma_1}{D}\boldsymbol{v}=\rho\boldsymbol{v}.$$

In above equations, the symmetry properties of the underlying lattice structure, *i.e.*,  $\mathbf{E}^{(2n+1)} = 0$  and  $\mathbf{E}_{ij}^{(2)} = \frac{\sigma_1}{D} \delta_{ij}$ , have been used. The results for  $b_0$  and  $a_1$  are

$$b_0 = -\frac{D}{\delta_x^2 (1 - d)}, \qquad (3.10.16a)$$

$$a_1 = \frac{D}{2\delta_{\pi}^2} \frac{(1-2d)}{(1-d)^2}.$$
 (3.10.16b)

Substituting  $a_1$  and  $b_0$  into  $f_{\alpha}^{(0)}$ , we have

$$f_{\alpha}^{(0)} = \frac{\rho}{\sigma_1} \left( 1 + \frac{D}{\delta_x} \hat{\boldsymbol{e}}_{\alpha,i} v_i + \frac{G(\rho)}{\delta_x^2} \left( \hat{\boldsymbol{e}}_{\alpha,i} \hat{\boldsymbol{e}}_{\alpha,j} - \frac{1}{D} \delta_{ij} \right) v_i v_j + \mathcal{O}(\boldsymbol{v}^3) \right), \qquad (3.10.17)$$

where

$$G(\rho) = \frac{D^2}{2} \frac{(1-2d)}{(1-d)}.$$
 (3.10.18)

As shall be seen later, in the expansion for  $f_{\alpha}^{(0)}$ , Eq. (3.10.17), the constant term only contributes to  $\rho$ ; the linear term (in  $\boldsymbol{v}$ ) only to  $\rho \boldsymbol{v}$ ; the quadratic term to the nonlinear convective term  $\rho \boldsymbol{v} \boldsymbol{v}$  and a velocity dependence of the pressure. Because of the structure of  $f_{\alpha}^{(0)}$  in Eq. (3.10.17), it is useful to define the tensor

$$Q_{\alpha,ij} \equiv \begin{cases} 0, & \alpha = 0, \\ \\ \hat{\boldsymbol{e}}_{\alpha,i} \hat{\boldsymbol{e}}_{\alpha,j} - \frac{1}{D} \delta_{ij}, & \alpha \neq 0, \end{cases}$$
(3.10.19)

which has the property  $\sum_{\alpha} Q_{\alpha,ij} = 0$ , and the tensor

$$T_{ijkl} \equiv \sum_{\alpha} \hat{\boldsymbol{e}}_{\alpha,i} \hat{\boldsymbol{e}}_{\alpha,j} Q_{\alpha,kl}$$

$$= \sum_{\alpha} \hat{\boldsymbol{e}}_{\alpha,i} \hat{\boldsymbol{e}}_{\alpha,j} \left( \hat{\boldsymbol{e}}_{\alpha,k} \hat{\boldsymbol{e}}_{\alpha,l} - \frac{1}{D} \delta_{kl} \right) = \boldsymbol{E}_{ijkl}^{(4)} - \frac{1}{D} \boldsymbol{E}_{ij}^{(2)} \delta_{kl}$$

$$= \frac{\sigma_1}{D(D+2)} \left( \delta_{ik} \delta_{jl} + \delta_{il} \delta_{jk} - \frac{2}{D} \delta_{ij} \delta_{kl} \right)$$

$$= \frac{\sigma_1}{D(D+2)} S_{ijkl},$$
(3.10.20)

both of which will be frequently encountered in what follows.

The zeroth order moment of the second order equation in the Chapman-Enskog procedure, Eq. (3.10.8b), with the approximation  $f_{\alpha} = f_{\alpha}^{(0)}$  given by the low-velocity

expansion (3.10.17), yields the continuity equation

$$\frac{\partial \rho}{\partial t_0} + \nabla' \cdot (\rho \mathbf{v}) = 0, \tag{3.10.21}$$

where  $\nabla' = \frac{\partial}{\partial x'}$ , and  $x' = \delta_x x$ .

With the same approximation, the momentum density flux tensor, in the leading order approximation of the Chapman-Enskog procedure, is

$$\Pi_{ij} \equiv \delta_x^2 \sum_{\alpha} \hat{\boldsymbol{e}}_{\alpha,i} \hat{\boldsymbol{e}}_{\alpha,j} f_{\alpha}^{(0)} = \delta_x^2 \rho \left( \frac{1}{D} \delta_{ij} + \frac{G(\rho)}{\sigma_1} T_{ijkl} v_k v_l \right) 
= g(\rho) \rho v_i v_j + \frac{\delta_x^2}{D} \rho \left( 1 - \frac{g(\rho)}{\delta_x^2} \boldsymbol{v}^2 \right) \delta_{ij} 
= g(\rho) \rho v_i v_j + P \delta_{ij} 
= g(\rho) \rho v_i v_j - \sigma_{ij}^{(0)},$$
(3.10.22)

where the factor

$$g(\rho) = \frac{2}{D(D+2)}G(\rho) = \frac{D}{(D+2)}\frac{(1-2d)}{(1-d)},$$
 (3.10.23)

and

$$\sigma_{ij}^{(0)} = -P\delta_{ij} = -\frac{\delta_x^2}{D}\rho \left(1 - \frac{g(\rho)}{\delta_x^2}\boldsymbol{v}^2\right)\delta_{ij}$$
(3.10.24)

is the leading-order approximation of the stress tensor. The term

$$P = \frac{\delta_x^2}{D} \rho \left( 1 - \frac{g(\rho)}{\delta_x^2} \mathbf{v}^2 \right) = c_s^2 \rho \left( 1 - \frac{g(\rho)}{\delta_x^2} \mathbf{v}^2 \right)$$
(3.10.25)

has been identified as the hydrodynamic pressure. The above equation is the isother-

mal equation of state of the system, where

$$c_s = \frac{\delta_x}{\sqrt{D}} \tag{3.10.26}$$

is the sound speed. Then, the first order moment Eq. (3.10.8b) yields an equation of momentum conservation:

$$\frac{\partial}{\partial t_0}(\rho v_i) = -\frac{\partial \Pi_{ij}}{\partial x_j'} = -\frac{\partial}{\partial x_j'} \left( g(\rho) \rho v_i v_j \right) - \frac{\partial P}{\partial x_i'}. \tag{3.10.27}$$

Eq. (3.10.27) resembles Euler's equation except in two aspects. First, the pressure has a velocity dependent term. Second, Galilean invariance is destroyed by the lead factor in the nonlinear convective term,  $g(\rho)$ , which is not unity in general. Both of these defects can be corrected by properly introducing rest particles and alternating the equilibrium distribution function in the lattice Boltzmann equation, which shall be discussed in a later chapter. However, near the incompressible limit where density,  $\rho$ , is approximately a constant in the system,  $g(\rho)$  can be approximated as a constant, and can be scaled out by changing the variable  $t \to g(\rho)t$ , or equivalently, by  $x \to \frac{x}{g(\rho)}$ .

It should be noticed that  $g(\rho)$  vanishes when  $d=\frac{1}{2}$ , i.e., when particles and holes equally populate in the system. This fact reflects the particle-hole duality:  $f_{\alpha}^{(0)}$  and  $\boldsymbol{v}$  are exactly equivalent to  $(1-f_{\alpha}^{(0)})$  and  $-\boldsymbol{v}$  at  $\rho=\frac{1}{2}$ . This duality holds independent of the collision rules, so long as the semi-detailed balance is satisfied, because the equilibrium distribution function is universal (e.g., Fermi-Dirac distribution, etc.). The duality has no physical reality, it is only an artifact of the model.

## 3.10.3 The Second Order Solution and the Incompressible Navier-Stokes Equations

Since  $f_{\alpha}^{(0)}$  is given by the solution of the first order equation, the left-hand side of the second order equation

$$\frac{Df_{\alpha}^{(0)}}{Dt_{0}} \equiv \left(\frac{\partial}{\partial t_{0}} + \hat{\boldsymbol{e}}_{\alpha} \cdot \nabla\right) f_{\alpha}^{(0)} = J_{\alpha\beta} f_{\beta}^{(1)}$$
(3.10.28)

can be computed explicitly. Thus the above equation can be solved by inverting the matrix  $\mathbb{J}_{\alpha\beta}$ .

The form of  $f_{\alpha}^{(1)}$  is known, as discussed in §2.4 — the *n*th order solution is proportional to the *n*th order spatial derivatives of the hydrodynamic variables  $\rho$ ,  $\boldsymbol{v}$  and  $\varepsilon$ . The first order solution  $f_{\alpha}^{(0)}$  is a local equilibrium which is not an explicit function of time. The Chapman-Enskog ansatz should be assumed, *i.e.*, the dependence of  $f_{\alpha}^{(0)}$  on time is through the macroscopic variables  $\rho$  and  $\boldsymbol{v}$ . Then the term  $\frac{\partial f_{\alpha}^{(0)}}{\partial t_0} = \frac{\partial f_{\alpha}^{(0)}}{\partial \rho} \frac{\partial \rho}{\partial t_0} + \frac{\partial f_{\alpha}^{(0)}}{\partial \boldsymbol{v}} \cdot \frac{\partial \boldsymbol{v}}{\partial t_0}$  depends only on  $\nabla \rho$  and  $\frac{\partial v_j}{\partial x_i}$  (or  $\frac{\partial (\rho v_j)}{\partial x_i}$ ), because of the hydrodynamic equations previously obtained from the first order solution. Therefore, it is natural to assume that

$$f_{\alpha}^{(1)} = -c_{1}^{(1)}(\hat{\boldsymbol{e}}_{\alpha} \cdot \nabla \rho) - (c_{2}^{(1)}\hat{\boldsymbol{e}}_{\alpha,i}\hat{\boldsymbol{e}}_{\alpha,j} + c_{3}^{(1)}\delta_{ij}) \frac{\partial(\rho v_{i})}{\partial x_{i}}, \qquad (3.10.29)$$

where constants,  $c_1^{(1)}$ ,  $c_2^{(1)}$  and  $c_3^{(1)}$ , depend on  $\rho$ , but not on  $\boldsymbol{v}$ , because they are evaluated at  $\boldsymbol{v}=0$ . Because  $f_{\alpha}^{(1)}$  has no contribution to  $\rho$  and  $\rho\boldsymbol{v}$  due to constraints given by Eq. (3.10.4), it is straightforward to show that  $c_2^{(1)}+Dc_3^{(1)}=0$ , (from  $\sum_{\alpha}f_{\alpha}^{(1)}=0$ ), and  $c_1^{(1)}=0$ , (from  $\sum_{\alpha}\hat{\boldsymbol{e}}_{\alpha}f_{\alpha}^{(1)}=0$ ). Thus

$$f_{\alpha}^{(1)} = -c_2^{(1)} Q_{\alpha,ij} \frac{\partial (\rho v_i)}{\partial x_j} = -c_2^{(1)} \left( \hat{\boldsymbol{e}}_{\alpha,i} \hat{\boldsymbol{e}}_{\alpha,j} - \frac{1}{D} \delta_{ij} \right) \frac{\partial (\rho v_i)}{\partial x_j}, \tag{3.10.30}$$

and the stress tensor in the second order approximation is

$$\sigma_{ij}^{(1)} \equiv \delta_x^2 \sum_{\alpha} \hat{\boldsymbol{e}}_{\alpha,i} \hat{\boldsymbol{e}}_{\alpha,j} f_{\alpha}^{(1)} = -c_2^{(1)} \delta_x^2 T_{ijkl} \frac{\partial (\rho v_l)}{\partial x_k}$$

$$= -c_2^{(1)} \delta_x^2 \frac{\sigma_1}{D(D+2)} \left( \left( \frac{\partial (\rho v_i)}{\partial x_j} + \frac{\partial (\rho v_j)}{\partial x_i} \right) - \frac{2}{D} \delta_{ij} (\nabla \cdot \rho \boldsymbol{v}) \right) . \quad (3.10.31)$$

Note that the coefficient in the above equation is directly related to the viscosity.

Now, the zeroth-order moment of the third-order equation in the Chapman-Enskog procedure, Eq. (3.10.8c), is

$$\frac{\partial}{\partial t_{1}} \sum_{\alpha} f_{\alpha}^{(0)} + \frac{1}{2} \frac{\partial}{\partial t_{0}} \left( \frac{\partial}{\partial t_{0}} \sum_{\alpha} f_{\alpha}^{(0)} + \nabla \cdot \sum_{\alpha} \hat{\boldsymbol{e}}_{\alpha} f_{\alpha}^{(0)} \right) + 
\frac{1}{2} \nabla \cdot \left( \frac{\partial}{\partial t_{0}} \sum_{\alpha} \hat{\boldsymbol{e}}_{\alpha} f_{\alpha}^{(0)} + \nabla \cdot \sum_{\alpha} \hat{\boldsymbol{e}}_{\alpha} \hat{\boldsymbol{e}}_{\alpha} f_{\alpha}^{(0)} \right) + 
\frac{\partial}{\partial t_{1}} \sum_{\alpha} f_{\alpha}^{(1)} + \nabla \cdot \sum_{\alpha} \hat{\boldsymbol{e}}_{\alpha} f_{\alpha}^{(1)} = 0.$$
(3.10.32)

The second and third term of the left-hand side of the above equation are identical to zero because of the the continuity equation (3.10.21) and Euler's equation (3.10.27). The last two terms are zero because  $f_{\alpha}^{(1)}$  has no contribution to mass and momentum, due to the constraints given by Eqs. (3.10.4). Therefore, the above equation reduces to

$$\frac{\partial \rho}{\partial t_1} = 0. \tag{3.10.33}$$

The equation for the first order moment of Eq. (3.10.8c) is

$$\frac{\partial}{\partial t_1} \sum_{\alpha} \hat{\boldsymbol{e}}_{\alpha} f_{\alpha}^{(0)} + \frac{1}{2} \frac{\partial}{\partial t_0} \left( \frac{\partial}{\partial t_0} \sum_{\alpha} \hat{\boldsymbol{e}}_{\alpha} f_{\alpha}^{(0)} + \nabla \cdot \sum_{\alpha} \hat{\boldsymbol{e}}_{\alpha} \hat{\boldsymbol{e}}_{\alpha} f_{\alpha}^{(0)} \right) + \\
\frac{1}{2} \nabla \cdot \left( \frac{\partial}{\partial t_0} \sum_{\alpha} \hat{\boldsymbol{e}}_{\alpha} \hat{\boldsymbol{e}}_{\alpha} f_{\alpha}^{(0)} + \nabla \cdot \sum_{\alpha} \hat{\boldsymbol{e}}_{\alpha} \hat{\boldsymbol{e}}_{\alpha} \hat{\boldsymbol{e}}_{\alpha} f_{\alpha}^{(0)} \right) + \\$$

$$\frac{\partial}{\partial t_1} \sum_{\alpha} \hat{\boldsymbol{e}}_{\alpha} f_{\alpha}^{(1)} + \nabla \cdot \sum_{\alpha} \hat{\boldsymbol{e}}_{\alpha} \hat{\boldsymbol{e}}_{\alpha} f_{\alpha}^{(1)} = 0. \tag{3.10.34}$$

In above equation, the first term is  $\frac{1}{\delta_x} \frac{\partial (\rho \mathbf{v})}{\partial t_1}$ ; the second term is equal to zero due to Euler's equation; and the fourth term is equal to zero because  $f_{\alpha}^{(1)}$  has no contribution to momentum; the last term is  $\frac{1}{\delta_x^2} \frac{\partial \sigma_{ij}^{(1)}}{\partial x_j}$ , where  $\sigma_{ij}^{(1)}$  is given by Eq. (3.10.31). Because

$$\sum_{lpha} \hat{m{e}}_{lpha,i} \hat{m{e}}_{lpha,j} f_{lpha}^{(0)} = rac{1}{D} 
ho \delta_{ij} + rac{G(
ho)}{\sigma_1} T_{ijkl} (
ho v_k v_l),$$

and

$$\sum_{\alpha} \hat{\boldsymbol{e}}_{\alpha,i} \hat{\boldsymbol{e}}_{\alpha,j} \hat{\boldsymbol{e}}_{\alpha,k} f_{\alpha}^{(0)} = \frac{D}{\delta_{x} \sigma_{1}} \sum_{\alpha} \hat{\boldsymbol{e}}_{\alpha,i} \hat{\boldsymbol{e}}_{\alpha,j} \hat{\boldsymbol{e}}_{\alpha,k} \hat{\boldsymbol{e}}_{\alpha,l} (\rho v_{l})$$

$$= \frac{D}{\delta_{x} \sigma_{1}} \left( T_{ijkl} + \frac{\sigma_{1}}{D^{2}} \delta_{ij} \delta_{kl} \right) (\rho v_{l}), \qquad (3.10.35)$$

therefore,

$$\frac{1}{2} \frac{\partial}{\partial x_{j}} \left( \frac{\partial}{\partial t_{0}} \sum_{\alpha} \hat{\boldsymbol{e}}_{\alpha,i} \hat{\boldsymbol{e}}_{\alpha,j} f_{\alpha}^{(0)} + \frac{\partial}{\partial x_{k}} \sum_{\alpha} \hat{\boldsymbol{e}}_{\alpha,i} \hat{\boldsymbol{e}}_{\alpha,j} \hat{\boldsymbol{e}}_{\alpha,k} f_{\alpha}^{(0)} \right) \\
= \frac{1}{2D} \frac{\partial}{\partial x_{j}} \left( \frac{\partial \rho}{\partial t_{0}} + \nabla' \cdot (\rho \boldsymbol{v}) \right) \delta_{ij} + \frac{1}{2} \frac{\partial^{2}}{\partial t_{0} \partial x_{j}} \left( \frac{G(\rho)}{\sigma_{1}} T_{ijkl} \left( \rho v_{k} v_{l} \right) \right) + \\
+ \frac{D}{2\delta_{x} \sigma_{1}} T_{ijkl} \frac{\partial^{2}(\rho v_{l})}{\partial x_{j} \partial x_{k}}, \tag{3.10.36}$$

where the first term in the right-hand side of the above equation is zero because of Euler's equation — Eq. (3.10.27); the second term is usually neglected because it is of order  $\mathcal{O}(\mathbf{v}^2)$ , whereas the remaining terms are of order  $\mathcal{O}(\mathbf{v})$ , and the low-velocity approximation is still in consideration. Now, Eq. (3.10.34) reduces to

$$\frac{1}{\delta_x} \frac{\partial}{\partial t_1} (\rho v_i) - \frac{\partial}{\partial x_i} \left( \left( c_2^{(1)} - \frac{D}{2\delta_x \sigma_1} \right) T_{ijkl} \frac{\partial (\rho v_l)}{\partial x_k} \right) = 0. \tag{3.10.37}$$

To obtain Navier-Stokes equations, setting  $\delta = 1$ , substituting

$$\frac{\partial}{\partial t} = \frac{\partial}{\partial t_0} + \frac{\partial}{\partial t_1},\tag{3.10.38a}$$

$$\sigma_{ij} = \sigma_{ij}^{(0)} + \sigma_{ij}^{(1)}, \tag{3.10.38b}$$

and combining Eqs. (3.10.21) and (3.10.33), we obtain the usual continuity equation:

$$\frac{\partial \rho}{\partial t} + \nabla' \cdot (\rho \mathbf{v}) = 0. \tag{3.10.39}$$

Eqs. (3.10.27) and (3.10.37) lead to

$$\frac{\partial}{\partial t}(\rho v_i) = -\frac{\partial}{\partial x_j'}(g(\rho)\rho v_i v_j) - \frac{\partial P}{\partial x_i'} + \frac{\partial}{\partial x_j'} \left( \left( c_2^{(1)} \delta_x^3 - \frac{D\delta_x^2}{2\sigma_1} \right) \frac{\sigma_1}{D(D+2)} S_{ijkl} \frac{\partial(\rho v_l)}{\partial x_k'} \right), \tag{3.10.40}$$

where the substitution  $T_{ijkl} = \frac{\sigma_1}{D(D+2)} S_{ijkl}$  has been made. The above equation does bear strong resemblance to the Navier-Stokes equation. In contrast with the standard Navier-Stokes equation, it can be immediately recognized that the term

$$\nu = \left(\frac{\delta_x^3 \sigma_1}{D(D+2)} c_2^{(1)} - \frac{\delta_x^2}{2(D+2)}\right) = \nu_c + \nu_p \tag{3.10.41}$$

is effectively the kinematic shear viscosity, which consists of two parts:

$$\nu_c = \frac{\delta_x^3 \sigma_1}{D(D+2)} c_2^{(1)}, \tag{3.10.42a}$$

$$\nu_p = -\frac{\delta_x^2}{2(D+2)}. (3.10.42b)$$

The first part,  $\nu_c$ , is due the collision processes, and is called the collision viscosity. The second part,  $\nu_p$ , is purely due to the discrete nature of the model, which directly comes from the second order spatial derivative in the Taylor expansion of  $f_{\alpha}(\mathbf{x} + \delta_x \hat{\mathbf{e}}_{\alpha}, t + \delta_t)$ , and  $\nu_p$  is usually called propagation viscosity. Note that  $\nu_p$  is

negative, and consequently it reduces the kinematic viscosity.

In the approximation of homogeneity, i.e.,  $\rho = \rho_0 + \delta \rho$ , where  $\rho_0$  is constant and the density fluctuation  $\delta \rho \ll \rho_0$ , the continuity equation (3.10.39) becomes

$$\nabla' \cdot \boldsymbol{v} = 0, \tag{3.10.43}$$

where the term involved  $\delta \rho$  has been neglected because it is a higher order term in the homogeneity approximation. Similarly, Eq. (3.10.40) becomes

$$\frac{\partial \mathbf{v}}{\partial t'} + \mathbf{v} \cdot \nabla' \mathbf{v} = -\nabla' P' + \nu' \nabla'^2 \mathbf{v}, \qquad (3.10.44)$$

where

$$t' = g(\rho_0)t,$$
 (3.10.45a)

$$\nabla' = \frac{1}{\delta_r} \nabla, \tag{3.10.45b}$$

$$P' = c_s^2 \left( \delta \rho - \rho_0 \frac{g(\rho_0)}{\delta_x^2} \mathbf{v}^2 \right), \qquad (3.10.45c)$$

$$\nu' = \frac{\nu(\rho_0)}{g(\rho_0)}. (3.10.45d)$$

Eqs. (3.10.43) and (3.10.44) constitute the exact form of the incompressible Navier-Stokes equations.

An alternative representation of the incompressible Navier-Stokes equation is to use the mass density current  $j \equiv \rho v$  instead of the velocity v. Then, we have

$$\nabla' \cdot \boldsymbol{j} = 0, \tag{3.10.46a}$$

$$\frac{\partial \boldsymbol{j}}{\partial t} + \frac{g(\rho_0)}{\rho_0} \boldsymbol{j} \cdot \nabla' \boldsymbol{j} = -\nabla' P' + \nu(\rho_0) \nabla'^2 \boldsymbol{j}.$$
 (3.10.46b)

The advantage of using the j-representation is that it better approximates the steady states of the Navier-Stokes equation, because, the continuity equation at the steady state implies exactly  $\nabla \cdot \boldsymbol{j} = 0$ .

### 3.10.4 The Viscosity due to Collisions

In Eq. (3.10.40), the coefficient  $c_2^{(1)}$  is yet to be determined. This can be done by directly solving Eq. (3.10.8b)

$$rac{\partial f_{lpha}^{(0)}}{\partial t_0} + \hat{m{e}}_{lpha} \cdot 
abla f_{lpha}^{(0)} = \mathbb{J}_{lphaeta} f_{eta}^{(1)}.$$

Now, the Jacobian matrix  $\mathbb{J}_{\alpha\beta}$  is evaluated at the zero-velocity limit, *i.e.*, at  $f_{\alpha}=f_{\alpha}^{(0)}|_{\boldsymbol{v}=0}=d$ 

$$J_{\alpha\beta} = \left. \frac{\partial \Omega_{\alpha}}{\partial f_{\beta}} \right|_{f_{\alpha} = d}.$$
 (3.10.47)

By using the small-velocity expansion and neglecting all terms beyond the linear ones in the velocity  $\boldsymbol{v}$ , one has

$$\frac{\partial f_{\alpha}^{(0)}}{\partial t} = \frac{1}{\sigma_{1}} \frac{\partial \rho}{\partial t} + \frac{D}{\delta_{x} \sigma_{1}} \hat{\boldsymbol{e}}_{\alpha} \cdot \frac{\partial (\rho \boldsymbol{v})}{\partial t} + \mathcal{O}(\boldsymbol{v}^{2})$$

$$= -\frac{1}{\delta_{x} \sigma_{1}} \nabla \cdot (\rho \boldsymbol{v}) - \frac{1}{\sigma_{1}} \hat{\boldsymbol{e}}_{\alpha} \cdot \nabla \rho + \mathcal{O}(\boldsymbol{v}^{2}),$$

where the Euler equations have been substituted, and the terms neglected are  $g(\rho)v_iv_j$  and  $\frac{g(\rho)}{\delta^2}\mathbf{v}^2$ . One also has

$$\hat{\boldsymbol{e}}_{\alpha} \cdot \nabla f_{\alpha}^{(0)} = \frac{1}{\sigma_{1}} \hat{\boldsymbol{e}}_{\alpha} \cdot \nabla \rho + \frac{D}{\delta_{x} \sigma_{1}} (\hat{\boldsymbol{e}}_{\alpha} \cdot \nabla) (\hat{\boldsymbol{e}}_{\alpha} \cdot (\rho \boldsymbol{v})) + \mathcal{O}(\boldsymbol{v}^{2}). \tag{3.10.48}$$

Then

$$\frac{\partial f_{\alpha}^{(0)}}{\partial t} + \hat{\boldsymbol{e}}_{\alpha} \cdot \nabla f_{\alpha}^{(0)} = \frac{D}{\delta_{x} \sigma_{1}} \left( \hat{\boldsymbol{e}}_{\alpha,i} \hat{\boldsymbol{e}}_{\alpha,j} - \frac{1}{D} \delta_{ij} \right) \frac{\partial (\rho v_{i})}{\partial x_{i}} + \mathcal{O}(\boldsymbol{v}^{2})$$

$$= \frac{D}{\delta_x \sigma_1} Q_{\alpha,ij} \frac{\partial (\rho v_i)}{\partial x_j} + \mathcal{O}(\mathbf{v}^2)$$
 (3.10.49)

and, with Eq. (3.10.30), Eq. (3.10.8b) becomes

$$\frac{D}{\delta_x \sigma_1} Q_{\alpha,ij} \frac{\partial (\rho v_i)}{\partial x_j} = -c_2^{(1)} J_{\alpha\beta} Q_{\beta,ij} \frac{\partial (\rho v_i)}{\partial x_j}, \qquad (3.10.50)$$

or

$$\left(\mathbb{J}_{\alpha\beta} + \frac{D}{c_2^{(1)}\delta_x \sigma_1} \delta_{\alpha\beta}\right) Q_{\beta,ij} \frac{\partial (\rho v_i)}{\partial x_j} = 0.$$
(3.10.51)

This equation is true for arbitrary  $\frac{\partial(\rho v_i)}{\partial x_j}$ , hence

$$\left(J_{\alpha\beta} + \frac{D}{c_2^{(1)}\delta_x\sigma_1}\delta_{\alpha\beta}\right)Q_{\beta,ij} = 0.$$
(3.10.52)

This means that, for any pair of indices (i, j),  $Q_{\alpha,ij}$  is the  $\alpha$ -th component of an eigenvector of the matrix  $J_{\alpha\beta}$ , with the eigenvalue  $-\frac{D}{c_2^{(1)}\delta_x\sigma_1}$ . Therefore,

$$c_2^{(1)} = -\frac{D}{\delta_x \sigma_1} \frac{Q_{\alpha,ij} Q_{\alpha,ij}}{Q_{\alpha,ij} J_{\alpha\beta} Q_{\beta,ij}},$$
(3.10.53)

and the collision viscosity is

$$\nu_c = -\frac{\delta_x^2}{(D+2)} \frac{Q_{\alpha,ij} Q_{\alpha,ij}}{Q_{\alpha,ij} J_{\alpha\beta} Q_{\beta,ij}}.$$
(3.10.54)

Note that the sum has been taken over all of the repeated indices:  $\alpha$ ,  $\beta$ , i and j.

The eigenvectors of J, which are also relate to tensor  $Q_{\alpha,ij}$ , can be computed in a straightforward manner. Denote these eigenvectors as  $|Q_{\alpha,ij}\rangle$ . Then, it is easy to

show that

$$|Q_{\alpha,xx}\rangle = -|Q_{\alpha,yy}\rangle = \frac{1}{4} \begin{pmatrix} 2\\-1\\-1\\2\\-1\\-1 \end{pmatrix}, \qquad |Q_{\alpha,xy}\rangle = |Q_{\alpha,yx}\rangle = \frac{\sqrt{3}}{4} \begin{pmatrix} 0\\1\\-1\\0\\1\\-1 \end{pmatrix}.$$

It turns out, as we shall see in Chapter 4, these eigenvectors are degenerate ones with the same eigenvalue  $\lambda$ . Therefore, the viscosity is

$$\nu = -\frac{\delta_x^2}{(D+2)} \left( \frac{1}{\lambda} + \frac{1}{2} \right). \tag{3.10.55}$$

### 3.11 Rest Particles and the Compressible Navier-Stokes Equations

The derivation of the Navier-Stokes equation from the 6-bit FHP model in §3.10 indicates that the bulk viscosity is zero for the 6-bit models. However, this is changed with the presence of rest particles in the model. As mentioned previously, non-vanishing bulk viscosity may be due to two causes: The correlations among  $f_{\alpha}$ 's and the internal degrees of freedom of particles. The collision processes involving both the rest and the moving particles imitate the latter cause. Intuitively, this can be understood as follows: The compressibility of a gas system is represented by  $\zeta \nabla \cdot \boldsymbol{v}$ . This implies that there are sources or sinks of the velocity field, or the kinetic energy. In other words, there must be a mechanism of energy transfer between kinetic energy and other forms of energy. The inclusion of rest particles in lattice-gas automata provides such a mechanism.

In this section, the 7-bit model will be considered. The compressible Navier-Stokes equation with the corresponding transport coefficients (e.g., the bulk viscosity) arising from the model will be derived by the same technique — the Chapman-Enskog procedure.

### 3.11.1 The Euler Equations

Let  $f_0$  be the distribution function for zero-velocity particles (rest particles). Because rest particle also satisfies the exclusion principle, its equilibrium distribution function must also obey the same Fermi-Dirac statistics, with  $\hat{e}_0 = 0$ , *i.e.*,

$$f_0 = \frac{1}{1 + e^a} \,, \tag{3.11.1}$$

where  $a = a_0 + a_1 \mathbf{v}^2 + \cdots$ . Therefore, the small-velocity expansion (up to  $\mathcal{O}(\mathbf{v}^2)$ ) for the equilibrium distribution functions is

$$f_{\alpha}^{(0)} = \begin{cases} f_{\text{FD}} + \frac{1}{2} \left( f'_{\text{FD}} 2a_{1} \boldsymbol{v}^{2} \right) & \alpha = 0, \\ \\ f_{\text{FD}} + f'_{\text{FD}} (b_{0} \delta_{x} \hat{\boldsymbol{e}}_{\alpha} \cdot \boldsymbol{v}) + \frac{1}{2} \left( f''_{\text{FD}} b_{0}^{2} \delta_{x}^{2} (\hat{\boldsymbol{e}}_{\alpha} \cdot \boldsymbol{v})^{2} + f'_{\text{FD}} 2a_{1} \boldsymbol{v}^{2} \right) & \alpha \neq 0. \end{cases}$$
(3.11.2)

As consequences of conservation laws, we have

$$b_0 = -\left(\frac{\sigma}{\sigma_1}\right) \frac{D}{\delta_x^2 (1-d)}, \qquad (3.11.3a)$$

$$a_1 = \left(\frac{\sigma}{\sigma_1}\right) \frac{D}{2\delta_x^2} \frac{(1-2d)}{(1-d)^2},$$
 (3.11.3b)

where  $\sigma$  is the total number of particles allowed per site, i.e.,  $\sigma = \sigma_0 + \sigma_1$ ,  $\sigma_0$  is maximum number the rest particles per site,  $\sigma_0 = 1$  for the 7-bit FHP models. Then

$$f_{\alpha}^{(0)} = \begin{cases} d\left(1 + \frac{G(\rho)}{\delta_x^2} c_s^2 \delta_{ij} v_i v_j\right) & \alpha = 0, \\ d\left(1 + \frac{\sigma}{\sigma_1} \frac{D}{\delta_x} \hat{\boldsymbol{e}}_{\alpha,i} v_i + \frac{G(\rho)}{\delta_x^2} \left(Q_{\alpha,ij} + \left(\frac{1}{D} - \frac{c_s^2}{\delta_x^2}\right) \delta_{ij}\right) v_i v_j \right) & \alpha \neq 0, \end{cases}$$

$$(3.11.4)$$

where

$$c_s = \delta_x \sqrt{\frac{\sigma_1}{\sigma D}} \tag{3.11.5}$$

is sound speed, and

$$G(\rho) = \left(\frac{\sigma}{\sigma_1}\right)^2 \frac{D^2}{2} \frac{(1-2d)}{(1-d)}.$$
 (3.11.6)

The factor  $G(\rho)$  here is consistent with the previous definition, Eq. (3.10.18), for the 6-bit models, as  $\frac{\sigma}{\sigma_1} = 1$  for the 6-bit models. Also note that  $d = \frac{\rho}{\sigma}$  here.

The leading order approximation of the momentum density flux tensor is

$$\Pi_{ij} \equiv \delta_x^2 \sum_{\alpha} \hat{\boldsymbol{e}}_{\alpha,i} \hat{\boldsymbol{e}}_{\alpha,j} f_{\alpha}^{(0)}$$

$$= \delta_x^2 d \left( \frac{\sigma_1}{D} \delta_{ij} + \frac{G(\rho)}{\delta_x^2} \left( \frac{\sigma_1}{D(D+2)} S_{ijkl} + \frac{\sigma_0 \sigma_1}{D^2 \sigma} \delta_{ij} \delta_{kl} \right) v_k v_l \right)$$

$$= g(\rho) \rho v_i v_j + c_s^2 \rho \delta_{ij} + g(\rho) \left( \frac{\sigma_0 (D+2) - 2\sigma}{2\sigma D} \right) \rho \boldsymbol{v}^2 \delta_{ij}$$

$$= g(\rho) \rho v_i v_j + P \delta_{ij} ,$$
(3.11.7)

where the pressure

$$P = c_s^2 \rho \left( 1 - \frac{g(\rho)}{2\delta_x^2} \left( (D+2) - \frac{\delta_x^2}{c_s^2} \right) \mathbf{v}^2 \right) , \qquad (3.11.8)$$

and the factor

$$g(\rho) = \frac{\sigma_1}{\sigma} \frac{2}{D(D+2)} G(\rho) = \frac{\sigma}{\sigma_1} \frac{D}{(D+2)} \frac{(1-2d)}{(1-d)}.$$
 (3.11.9)

Then one can obtain the Euler equations as before (with a different sound speed and a different velocity dependence of the pressure term)

$$\frac{\partial \rho}{\partial t_0} + \nabla' \cdot (\rho \mathbf{v}) = 0, \qquad (3.11.10a)$$

$$\frac{\partial}{\partial t_0}(\rho v_i) = -\frac{\partial}{\partial x_j'}(g(\rho)\rho v_i v_j) + \frac{\partial P}{\partial x_i'}.$$
 (3.11.10b)

### 3.11.2 The Compressible Navier-Stokes Equations

Next, by the virtue of the conservation laws, we can immediately write

$$f_{\alpha}^{(1)} = \begin{cases} c_1^{(1)} \sigma_1 \delta_{ij} \frac{\partial (\rho v_i)}{\partial x_j} & \alpha = 0, \\ \\ -(c_2^{(1)} Q_{\alpha,ij} + c_1^{(1)} \delta_{ij}) \frac{\partial (\rho v_i)}{\partial x_j} & \alpha \neq 0, \end{cases}$$
(3.11.11)

where the constants,  $c_1^{(1)}$  and  $c_2^{(1)}$ , are yet to be determined. The stress tensor in the second order approximation can be evaluated:

$$\sigma_{ij}^{(1)} = -\delta_x^2 \sum_{\alpha} \hat{\mathbf{e}}_{\alpha,i} \hat{\mathbf{e}}_{\alpha,j} f_{\alpha}^{(1)} 
= \delta_x^2 \left( \frac{\sigma_1 c_2^{(1)}}{D(D+2)} S_{ijkl} + \frac{\sigma_1 c_1^{(1)}}{D} \delta_{ij} \delta_{kl} \right) \frac{\partial (\rho v_l)}{\partial x_k} 
= \delta_x^3 \left( \frac{\sigma_1 c_2^{(1)}}{D(D+2)} S_{ijkl} + \frac{\sigma_1 c_1^{(1)}}{D} \delta_{ij} \delta_{kl} \right) \frac{\partial (\rho v_l)}{\partial x_k'}.$$
(3.11.12)

Then, it is obvious that

$$\nu_c = \frac{\delta_x^3 \sigma_1}{D(D+2)} c_2^{(1)}, \qquad (3.11.13a)$$

$$\zeta_c = \frac{\delta_x^3 \sigma_1}{D} c_1^{(1)} \,, \tag{3.11.13b}$$

where  $\zeta_c$  is the bulk viscosity due to collisions, and  $\zeta = \frac{\eta_2}{\rho}$ .

Similar to that in the previous section, the zeroth order moment of the thirdorder equation gives

$$\frac{\partial \rho}{\partial t_1} = 0. \tag{3.11.14}$$

There is a slight difference in evaluating the first order moment, because

$$\frac{1}{2} \frac{\partial}{\partial x_{j}} \left( \frac{\partial}{\partial t_{0}} \sum_{\alpha} \hat{\boldsymbol{e}}_{\alpha,i} \hat{\boldsymbol{e}}_{\alpha,j} f_{\alpha}^{(0)} + \frac{\partial}{\partial x_{k}} \sum_{\alpha} \hat{\boldsymbol{e}}_{\alpha,i} \hat{\boldsymbol{e}}_{\alpha,j} \hat{\boldsymbol{e}}_{\alpha,k} f_{\alpha}^{(0)} \right) \\
= \frac{1}{2D} \frac{\partial}{\partial x_{j}} \left( \frac{\sigma_{1}}{\sigma} \frac{\partial \rho}{\partial t_{0}} + \nabla' \cdot (\rho \boldsymbol{v}) \right) \delta_{ij} + \frac{D}{2\delta_{x} \sigma_{1}} T_{ijkl} \frac{\partial^{2}(\rho v_{l})}{\partial x_{j} \partial x_{k}} \\
= \frac{\delta_{x}}{2D} \frac{\sigma_{0}}{\sigma} \frac{\partial^{2}(\rho v_{j})}{\partial x_{i}' \partial x_{j}'} + \frac{\delta_{x}}{2(D+2)} S_{ijkl} \frac{\partial^{2}(\rho v_{l})}{\partial x_{i}' \partial x_{k}'}, \qquad (3.11.15)$$

where we have omitted the terms of order  $\mathcal{O}(\mathbf{v}^2)$  or higher. Moreover,

$$\nabla \cdot \sum_{\alpha} \hat{\boldsymbol{e}}_{\alpha,i} \hat{\boldsymbol{e}}_{\alpha,j} f_{\alpha}^{(1)} = -\frac{1}{\delta_x^2} \frac{\partial}{\partial x_j} \left( \nu_c S_{ijkl} + \zeta_c \delta_{ij} \delta_{kl} \right) \frac{\partial (\rho v_l)}{\partial x_k}. \tag{3.11.16}$$

Then, the macroscopic equation of the first-order moment is

$$\frac{\partial(\rho v_i)}{\partial t_1} = \frac{\partial}{\partial x_j'} \left( (\nu S_{ijkl} + \zeta \delta_{ij} \delta_{kl}) \frac{\partial(\rho v_l)}{\partial x_k'} \right) , \qquad (3.11.17)$$

where

$$\nu = \nu_c + \nu_p \,, \tag{3.11.18a}$$

$$\zeta = \zeta_c + \zeta_p \,, \tag{3.11.18b}$$

and

$$\nu_p = -\frac{\delta_x^2}{2(D+2)},\tag{3.11.19a}$$

$$\zeta_p = -\frac{\delta_x^2 \sigma_0}{2D\sigma} \,. \tag{3.11.19b}$$

Combining the results from the first and the second order solution, we obtain the final macroscopic equations

$$\frac{\partial \rho}{\partial t} + \nabla' \cdot (\rho \mathbf{v}) = 0, \qquad (3.11.20a)$$

$$\frac{\partial(\rho v_i)}{\partial t} = -\frac{\partial}{\partial x_j'}(g(\rho)\rho v_i v_j) - \frac{\partial P}{\partial x_j'} + \frac{\partial}{\partial x_j'}\left((\nu S_{ijkl} + \zeta \delta_{ij}\delta_{kl})\frac{\partial(\rho v_l)}{\partial x_k'}\right). \quad (3.11.20b)$$

The above equations are the compressible Navier-Stokes equations derived for the 7-bit FHP model.

### 3.11.3 Evaluation of the Coefficients of Viscosity

The coefficients of viscosity for the 7-bit models can be evaluated in the same way as for the 6-bit models in the previous section. First,

$$\frac{\partial f_{\alpha}^{(0)}}{\partial t} + \hat{\boldsymbol{e}}_{\alpha} \cdot \nabla f_{\alpha}^{(0)} = \begin{cases}
-\frac{1}{\delta_{x}\sigma} \delta_{ij} \frac{\partial (\rho v_{i})}{\partial x_{j}} & \alpha = 0, \\
\left(\frac{D}{\delta_{x}\sigma_{1}} Q_{\alpha,ij} + \frac{1}{\delta_{x}\sigma\sigma_{1}} \delta_{ij}\right) \frac{\partial (\rho v_{i})}{\partial x_{j}} & \alpha \neq 0.
\end{cases} (3.11.21)$$

Because of isotropy, the linearized collision matrix,  $\mathbb{J}_{\alpha\beta}$ , has the property that  $\mathbb{J}_{0\alpha} = \mathbb{J}_{0\beta}$ , for all  $\alpha, \beta \neq 0$ ; and of course,  $\mathbb{J}_{\alpha\beta} = \mathbb{J}_{\beta\alpha}$ . The kinetic equation, (3.10.8b),

becomes

$$\frac{\partial f_0^{(0)}}{\partial t_0} = \mathbb{J}_{00} f_0^{(1)} + \mathbb{J}_{01} \sum_{\alpha=1}^{\sigma_1} f_{\alpha}^{(1)}, \qquad (3.11.22a)$$

$$\frac{\partial f_{\alpha}^{(0)}}{\partial t_{0}} + \hat{\boldsymbol{e}}_{\alpha} \cdot \nabla f_{\alpha}^{(0)} = \mathbb{J}_{01} f_{0}^{(1)} + \sum_{\beta=1}^{\sigma_{1}} \mathbb{J}_{\alpha\beta} f_{\beta}^{(1)}, \qquad \alpha \neq 0.$$
 (3.11.22b)

Because J conserves mass, *i.e.*,

$$J_{00} + \sigma_1 J_{01} = 0, \qquad (3.11.23a)$$

$$J_{01} + \sum_{\beta=1}^{\sigma_1} J_{\alpha\beta} = 0.$$
 (3.11.23b)

Also

$$\sum_{\alpha=1}^{\sigma_1} f_{\alpha}^{(1)} = -f_0^{(1)}. \tag{3.11.24}$$

Then,

$$c_1^{(1)} = \frac{1}{\delta_x \sigma^2 \sigma_1 J_{01}}. (3.11.25)$$

The right-hand side of Eq. (3.11.22b) is

$$\begin{split} & \mathbb{J}_{01} f_{0}^{(1)} + \sum_{\beta=1}^{\sigma_{1}} \mathbb{J}_{\alpha\beta} f_{\beta}^{(1)} = \mathbb{J}_{01} f_{0}^{(1)} - \sum_{\beta=1}^{\sigma_{1}} \mathbb{J}_{\alpha\beta} \left( c_{2}^{(1)} Q_{\beta,ij} + c_{1}^{(1)} \delta_{ij} \right) \frac{\partial (\rho v_{i})}{\partial x_{j}} \\ & = \left( -c_{2}^{(1)} \sum_{\beta=1}^{\sigma_{1}} \mathbb{J}_{\alpha\beta} Q_{\beta,ij} + c_{1}^{(1)} \mathbb{J}_{01} (\sigma_{1} + 1) \delta_{ij} \right) \frac{\partial (\rho v_{i})}{\partial x_{j}} \\ & = \left( -c_{2}^{(1)} \sum_{\beta=1}^{\sigma_{1}} \mathbb{J}_{\alpha\beta} Q_{\beta,ij} + \frac{1}{\delta_{x} \sigma \sigma_{1}} \delta_{ij} \right) \frac{\partial (\rho v_{i})}{\partial x_{j}} , \end{split}$$

where Eq. (3.11.23b) and the result of  $c_1^{(1)}$  given by Eq. (3.11.25) have been substituted.

Hence, Eq. (3.11.22b) becomes

$$\frac{D}{\delta_x \sigma_1} Q_{\alpha,ij} = -c_2^{(1)} \sum_{\beta=1}^{\sigma_1} J_{\alpha\beta} Q_{\beta,ij} , \qquad (3.11.26)$$

and it follows immediately that

$$c_2^{(1)} = -\frac{D}{\delta_x \sigma_1} \frac{Q_{\alpha,ij} Q_{\alpha,ij}}{Q_{\alpha,ij} J_{\alpha\beta} Q_{\beta,ij}},$$
(3.11.27)

where the convention  $Q_{\alpha,ij} = 0$  for  $\alpha = 0$  has been used. Note that the above result is identical to the one for the 6-bit models. Now, the coefficients of viscosity due to collisions for the 7-bit FHP model can be given explicitly:

$$\nu_c = -\frac{\delta_x^2}{(D+2)} \frac{Q_{\alpha,ij} Q_{\alpha,ij}}{Q_{\alpha,ij} J_{\alpha\beta} Q_{\beta,ij}}, \qquad (3.11.28a)$$

$$\zeta_c = -\frac{\delta_x^2}{D\sigma^2 J_{01}}.$$
(3.11.28b)

## 3.12 Normal Mode Frequencies of the LGA Hydrodynamics

In the linear regime, the momentum  $\boldsymbol{p} \approx \rho_0 \boldsymbol{v}$ , and the Navier-Stokes equations can be rewritten as

$$\frac{\partial \rho}{\partial t} + \rho_0 \nabla \cdot \boldsymbol{v} = 0, \tag{3.12.1a}$$

$$\rho_0 \frac{\partial \mathbf{v}}{\partial t} = -c_s^2 \nabla \rho + \rho_0 \nu \nabla^2 \mathbf{v} + \rho_0 \left( \zeta + \frac{D-2}{D} \nu \right) \nabla \nabla \cdot \mathbf{v}, \qquad (3.12.1b)$$

where the nonlinear term  $g(\rho)\rho vv$  has been neglected. Define

$$\tilde{\boldsymbol{v}}(\boldsymbol{k},\,\omega) = \frac{1}{\sqrt{2\pi}^{(D+1)}} \int d\boldsymbol{x} dt \ e^{-i(\boldsymbol{k}\cdot\boldsymbol{x}+\omega t)} \boldsymbol{v}(\boldsymbol{x},\,t) , \qquad (3.12.2a)$$

$$\tilde{\rho}(\boldsymbol{k},\,\omega) = \frac{1}{\sqrt{2\pi^{(D+1)}}} \int d\boldsymbol{x} dt \,\, e^{-i(\boldsymbol{k}\cdot\boldsymbol{x}+\omega t)} \rho(\boldsymbol{x},\,t) \,. \tag{3.12.2b}$$

Then the Fourier transform of the linearized Navier-Stokes equation is

$$i\omega\tilde{\rho} + i\rho_0 \mathbf{k} \cdot \tilde{\mathbf{v}} = 0, \qquad (3.12.3a)$$

$$i\omega\rho_0\tilde{\boldsymbol{v}} = -i\boldsymbol{k}c_s^2\tilde{\rho} - k^2\rho_0\nu\tilde{\boldsymbol{v}} - \boldsymbol{k}\rho_0\left(\zeta + \frac{D-2}{D}\nu\right)(\boldsymbol{k}\cdot\boldsymbol{v}). \tag{3.12.3b}$$

The velocity v can be divided into two parts, the transverse and the longitudinal component with respect to the wave vector k:

$$v = v_{\perp} + v_{\parallel}$$

where

$$\boldsymbol{v}_{\perp} \cdot \boldsymbol{k} = 0$$
 .

Then, we have

$$\omega \tilde{\rho} + i \rho_0 k \tilde{v}_{\parallel} = 0, \qquad (3.12.4a)$$

$$i\omega\rho_0\tilde{v}_{\parallel} = -kc_s^2\tilde{\rho} - k^2\rho_0\left(\zeta + \frac{2(D-1)}{D}\nu\right)\tilde{v}_{\parallel}, \qquad (3.12.4b)$$

$$i\omega\rho_0\tilde{\mathbf{v}}_\perp = k^2\rho_0\nu\tilde{\mathbf{v}}_\perp. \tag{3.12.4c}$$

In order for the solutions of  $\tilde{\rho}$ ,  $\tilde{v}_{\parallel}$  and  $\tilde{\boldsymbol{v}}_{\perp}$  to exist, the determinant of the coefficients of  $\tilde{\rho}$ ,  $\tilde{v}_{\parallel}$  and  $\tilde{\boldsymbol{v}}_{\perp}$  must be zero. This leads to three solutions of  $\omega$ :

$$\omega_{\perp} = ik^2\nu \,, \tag{3.12.5a}$$

$$\omega_{\pm} = \frac{1}{2}ik^{2}\left(\zeta + \frac{2(D-1)}{D}\nu\right) \pm \frac{1}{2}\sqrt{4k^{2}c_{s}^{2} - k^{4}\left(\zeta + \frac{2(D-1)}{D}\nu\right)^{2}}$$

$$\approx \pm kc_s + \frac{1}{2}ik^2\left(\zeta + \frac{2(D-1)}{D}\nu\right). \tag{3.12.5b}$$

The above results suggest that the transverse-momentum mode decays like  $e^{-k^2\nu t}$ , and the modes which couple the longitudinal momentum and the density (or the pressure) modes propagate with a speed  $c_s$ , and decay like  $e^{-\frac{k^2}{2}(\zeta + \frac{2(D-1)}{D}\nu)t}$ . The modes coupling the longitudinal momentum and the density are called the sound modes.

### 3.13 Epilogue

In this chapter, the macroscopic equations have been derived from the FHP latticegas automata. In obtaining the hydrodynamic equations, two crucial approximations have been employed: The first is the Boltzmann approximation (molecular chaos) which neglects the correlations between molecules involved in a collision process; and the second is the zero-velocity limit or the small March number limit.

The Boltzmann approximation is justified if one is interested in the Navier-Stokes systems, where the correlations are unimportant. There has been a numerical test which confirms that the Boltzmann approximation is indeed valid for FHP models: In Ref. [116], D. d'Humières and P. Lallemand numerically compared  $f_{\alpha}$  with the Fermi-Dirac distribution function, and they found the error is less than 1%. However, there are other systems where the correlations do play an important role. Examples are systems with shock waves, *i.e.*, Burgers' equation [76], or chemical reactive systems capable of spontaneous self-organization [59–65]. Also, it is a well known result that in two dimensions the transport coefficients, such as the kinematic viscosity,  $\nu$ , diverge logarithmically in ||L|| (L is the system size) [117]. This result can be theoretically obtained only by including correlations [118].

It should be stressed that the Boltzmann equation for the lattice-gas automata is different from that for continuous systems in two aspects. First of all, for lattice-

gas automata, the lattice Boltzmann equation keeps not just two-body collisions, it includes all possible many-body collisions, while the original Boltzmann equation only considers two-body collision. This difference arises because of the difference in the dynamics. The dynamics of lattice-gas automata is completely local, as opposed to non-local in other systems. The other difference is in the expansion parameter in the Chapman-Enskog procedure. In the case of lattice-gas automata, not only the mean free path, but also the lattice constant have to be considered. There is an interplay between them. In the continuum case, only the mean free path needs to be considered.

The small Mach number limit poses a severe limitation on the maximum obtainable Reynolds number. It, in turn, affects the efficiency of using the LGA algorithms to simulate hydrodynamical systems [119]. Despite this disadvantage, one can still use LGA as an alternative for problems which are very difficult (if not impossible) for traditional methods to deal with, such as multi-phase/multi-component flow through porous media. Therefore, LGA can be viewed as a complement to traditional methods.

Besides viewing the lattice-gas automata as practical algorithms for simulations, more importantly, one may also view them as simple, but powerful, models for appropriate physical systems, just as the Ising model is for ferromagnetism, which captures the physical essence of the phase transition in the system. In this view, the importance of the lattice-gas automata then becomes self-evident, the model might eventually provide insight and prove to be useful in studying nonequilibrium systems.

In summary, the lattice-gas automata can be characterized as follows. The model mimics the Newtonian dynamics at the microscopic level in a most simplistic way. However, at the macroscopic level, it leads to the correct hydrodynamics equations because it satisfies the minimum requirements of conservation laws and symmetries. This is possible precisely because of the universality of the Navier-Stokes equations (or other macroscopic equations). That is, the Navier-Stokes equations are valid for either

gases or liquids despite the drastic difference between the molecular constituents of, and the inter-molecular interactions in these systems. These differences only affect the numerical value of the transport coefficients, but not the form of the macroscopic equations, provided that the symmetry criteria are fulfilled. This heuristic point of view, although somewhat ad hoc, is very intuitive. This argument is most eloquently presented by the late Richard P. Feynman, when he tried to explain the reason why the FHP lattice-gas automaton works for hydrodynamical systems. We would like to conclude this chapter by an inspiring quotation from Feynman [120]:

We have noticed in nature that the behavior of a fluid depends very little on the nature of the individual particles in that fluid. For example, that flow of sand is very similar to the flow of water or the flow of a pile of ball bearings. We have therefore taken advantage of this fact to invent a type of imaginary particle that is especially simple for us to simulate. This particle is a perfect ball bearing that can move at a single speed in one of six directions. The flow of these particles on a large enough scale is very similar to the flow of natural fluids.

### CHAPTER FOUR

# THE LINEARIZED LATTICE BOLTZMANN EQUATION

The full lattice Boltzmann equation is a nonlinear equation for the distribution function,  $f_{\alpha}$ . Analytic solutions are difficult to obtain in general for this equation. As a common practice in dealing with nonlinear equations, the linearized approximate equations are studied. In this chapter, we discuss the solution of the linearized lattice Boltzmann equation. The linearized lattice Boltzmann equation will be used to provide two main results: One is the generalized hydrodynamics of LGA; the other is analytic solutions for some simple flows.

Ordinary hydrodynamics is valid in the hydrodynamic limit, i.e., the limit of long wavelength ( $\mathbf{k} \to 0$ ) and slow time variation ( $\omega \to 0$ ). Ordinary hydrodynamics studies macroscopic spatial-temporal behavior of fluids. The objective of generalized hydrodynamics is to go beyond the macroscopic scale to the microscopic scale. This extension is needed because the usual hydrodynamics requires significant modification when the characteristic length scale is the same order as the mean free path. Usually (as is done here), a generalization is made to include wavenumber dependence of the transport coefficients in such a way that the constitutive relation is preserved [121]. This generalization produces a nonlocal hydrodynamic response to fluctuations. Generalized hydrodynamics has been studied previously in the context of a hard sphere fluid [122,123,121]. The study of generalized hydrodynamics in the context of LGA

models is motivated by the fact that the LGA method has been successfully used to solve difficult physical problems such as flow through porous media [124, 125], a situation where generalized hydrodynamics can be important.

There are a few pedagogic examples in hydrodynamics for which analytic solutions can be obtained. Such examples are forced flow between two parallel plates (Poiseuille flow [106]) and Couette flow [1]. These problems have been used as tests for LGA simulations. Here, analytic solutions of the linearized lattice Boltzmann equation for these flows are obtained. Differences between the ordinary hydrodynamics and generalized hydrodynamics will be discussed. The method developed in this chapter can be used for other discrete velocity models.

This chapter is organized as follows: §4.1 derives the linearized lattice Boltzmann equation as an approximation to the full lattice Boltzmann equation, and studies the properties of the linearized collision operator. Because the linearized collision operator is related to the circulant matrix, §4.2 gives a quick review of the circulant matrix. §4.3 solves the eigenvalue problem of the linearized collision operator. This is the solution for the linearized lattice Boltzmann equation in the limit of  $k \to 0$ . §4.4 solves the linearized lattice Boltzmann equation through a perturbative scheme. Closedform solutions are found along some special directions of k. Also, the k-dependent dispersion relations of the transport coefficients, the kinematic viscosity,  $\nu$ , the bulk viscosity,  $\zeta$ , and the sound speed,  $c_s$ , are calculated. §4.5 compares the results from a simulation of the dispersion relation of  $c_s$  by computing the power spectrum of the density-density correlation function and that from the solution of the linearized lattice Boltzmann equation. Finally, §4.6 analytically computes velocity profiles of Poiseuille flow and plane Couette flow. The analytic results are also compared with the results of LGA simulations. Also, boundary effects due to a finite mean free path (Knudsen layer effects) are analyzed.

## 4.1 The Linearized Lattice Boltzmann Equation and the Linearized Collision Operator

Assuming that  $f_{\alpha}(\boldsymbol{x}, t) = d(1 + \phi_{\alpha}(\boldsymbol{x}, t))$  with  $|\phi_{\alpha}| \ll 1$ , where d is the equilibrium density per direction at zero mean velocity, we can linearize Eq. (3.8.1) to obtain

$$\phi_{\alpha}(\boldsymbol{x} + \hat{\boldsymbol{e}}_{\alpha}, t+1) = \phi_{\alpha}(\boldsymbol{x}, t) + \mathbb{J}_{\alpha\beta}\phi_{\beta}(\boldsymbol{x}, t). \tag{4.1.1}$$

Because

$$\frac{\partial \Omega_{\alpha}}{\partial f_{\beta}} = \sum_{\boldsymbol{s},\boldsymbol{s}'} (s'_{\alpha} - s_{\alpha}) A_{\boldsymbol{s}\boldsymbol{s}'} \frac{(s_{\beta} - f_{\beta})}{f_{\beta}(1 - f_{\beta})} \prod_{\gamma} f_{\gamma}^{s_{\gamma}} (1 - f_{\gamma})^{1 - s_{\gamma}}, \qquad (4.1.2)$$

then

$$\mathbb{J}_{\alpha\beta} = \sum_{\mathbf{s},\mathbf{s}'} (s'_{\alpha} - s_{\alpha})(s_{\beta} - d) A_{\mathbf{s}\mathbf{s}'} d^{S-1} (1 - d)^{\sigma - S - 1}, \qquad (4.1.3)$$

where  $s = \sum_{\alpha} s_{\alpha} = s^2 = ||s||$  is the number of particles in a configuration s. For any states, s and s', with finite transition probability,  $A_{ss'}$ , s = s' because of mass conservation. Assuming semi-detailed balance, it is easy to show that

$$\sum_{\mathbf{s},\mathbf{s}'} (s'_{\alpha} - s_{\alpha}) A_{\mathbf{s}\mathbf{s}'} d^{S-1} (1 - d)^{\sigma - S - 1} = 0.$$
 (4.1.4)

Therefore,

$$\mathbb{J}_{\alpha\beta} = \sum_{\mathbf{s},\mathbf{s}'} (s'_{\alpha} - s_{\alpha}) s_{\beta} A_{\mathbf{s}\mathbf{s}'} d^{S-1} (1 - d)^{\sigma - S - 1} . \tag{4.1.5}$$

If we further impose the condition of detailed balance, *i.e.*,  $A_{ss'} = A_{s's}$ , which is true for all 6-bit models with isotropy, then we can exchange s and s' in the above equation:

$$\mathbb{J}_{\alpha\beta} = \sum_{\mathbf{s}.\mathbf{s}'} (s_{\alpha} - s'_{\alpha}) s'_{\beta} A_{\mathbf{s}\mathbf{s}'} d^{S-1} (1 - d)^{\sigma - S - 1}, \qquad (4.1.6)$$

where the conservation of mass,  $s = \sum_{\alpha} s_{\alpha} = \sum_{\alpha} s'_{\alpha} = s'$ , has been used. The average of the above two equations leads to a symmetric expression for  $J_{\alpha\beta}$ :

$$J_{\alpha\beta} = -\frac{1}{2} \sum_{\mathbf{s},\mathbf{s}'} (s'_{\alpha} - s_{\alpha})(s'_{\beta} - s_{\beta}) A_{\mathbf{s}\mathbf{s}'} d^{S-1} (1 - d)^{\sigma - S - 1}. \tag{4.1.7}$$

Note that  $J_{\alpha\beta}$  depends only the equilibrium density, d, for a given set of collision rules. Because of the six-fold rotational symmetry,  $J_{\alpha\beta}$  is not only a  $6 \times 6$  symmetric matrix, it is also a circulant matrix for the 6-bit models.

For the 7-bit models, the lower-right  $6 \times 6$  block is circulant because of the isotropy. However, the linearized collision operator is symmetric if and only if  $J_{0\alpha} = J_{\alpha 0}$  for  $\alpha \neq 0$ , that is, if detailed balance is satisfied.

### 4.2 The Circulant Matrix

In this section, we shall only briefly discuss the circulant matrix for what is necessary for the subsequent sections. The following material is extracted from Ref. [126]. For more extended details, one should refer to Ref. [126].

An  $n \times n$  matrix, C, is a circulant matrix of order n, if

$$C = \begin{pmatrix} c_1 & c_2 & c_3 & \cdots & c_m & \cdots & c_n \\ c_n & c_1 & c_2 & \cdots & c_{m-1} & \cdots & c_{n-1} \\ c_{n-1} & c_n & c_1 & \cdots & c_{m-2} & \cdots & c_{n-2} \\ \vdots & \vdots & \vdots & \ddots & \vdots & \ddots & \vdots \\ c_{n-l+1} & c_{n-l+2} & c_{n-l+3} & \cdots & c_{m-l} & \cdots & c_{n-l} \\ \vdots & \vdots & \vdots & \ddots & \vdots & \ddots & \vdots \\ c_2 & c_3 & c_4 & \cdots & c_{m+1} & \cdots & c_1 \end{pmatrix} . \tag{4.2.1}$$

The above circulant matrix is denoted by

$$\mathbb{C} \equiv \operatorname{circ}(c_1, c_2, c_3, \cdots, c_m, \cdots, c_n). \tag{4.2.2}$$

Obviously, we can also write

$$C_{ij} = c_{j-i+1} , \qquad (4.2.3)$$

where the subscripts of  $c_{j-i+1}$  are  $(j-i+1) \mod n$ .

Associated with the *n*-tuple

$$\gamma = (c_1, c_2, c_3, \dots, c_m, \dots, c_n), \qquad (4.2.4)$$

the polynomial,

$$P_{\gamma}(z) = c_1 + c_2 z + c_3 z^2 + \dots + c_m z^{m-1} + \dots + c_n z^{n-1}, \qquad (4.2.5)$$

is called the representer of the circulant.

Let  $w = e^{2\pi i/n}$ . By Fourier matrix of order n, we mean the matrix,  $\mathbb{F}$ , such that

$$\mathbb{F}^{\dagger} = \frac{1}{\sqrt{n}} \begin{pmatrix} 1 & 1 & 1 & \cdots & 1 \\ 1 & w & w^{2} & \cdots & w^{n-1} \\ 1 & w^{2} & w^{4} & \cdots & w^{2(n-1)} \\ \vdots & \vdots & \vdots & \ddots & \vdots \\ 1 & w^{n-1} & w^{2(n-1)} & \cdots & w^{(n-1)(n-1)} \end{pmatrix}, \tag{4.2.6}$$

that is  $\mathbb{F}_{ij}^{\dagger} = \frac{1}{\sqrt{n}} w^{(i-1)(j-1)}$ , where  $\mathbb{F}^{\dagger}$  is the conjugate transpose of  $\mathbb{F}$ .

Now, we can state the following theorem:

Theorem 4.1 If  $\mathbb{C}$  is a circulant, it is diagonalized by  $\mathbb{F}$ ,

$$C = \mathbb{F}^{\dagger} \mathbb{L} \mathbb{F} \,, \tag{4.2.7}$$

where ∟ is the diagonal matrix:

$$\mathbb{L} = \mathbf{diag}(P_{\gamma}(1), P_{\gamma}(w), P_{\gamma}(w^{2}), \cdots, P_{\gamma}(w^{m}), \cdots, P_{\gamma}(w^{n-1})). \tag{4.2.8}$$

Therefore, the eigenvalues of  $\mathbb{C}$  are

$$\lambda_j = P_\gamma(w^{j-1}). \tag{4.2.9}$$

Note that the eigenvalues need not be distinct. Furthermore, the columns of  $\mathbb{F}^{\dagger}$  are a universal set of (right) eigenvectors for the circulant matrix.

### 4.3 The Eigenvalues and Eigenvectors of the Linearized Collision Operator

Before solving the linearized lattice Boltzmann equation, it is useful to study the linearized collision operator, J. In what follows, the calculations will be done for the case of the FHP 6-bit collision saturated model. For the model,  $J_{\alpha\beta}$  is a circulant matrix of order 6, which can be diagonalized by  $\mathbb{F}$ . Also, because of the conservation laws, we do know that  $J_{\alpha\beta}$  has a zero eigenvalue with (D+1)-fold degeneracy, where D is the dimension of the space. The eigenvectors with zero eigenvalue are the modes associated with conservation of mass and components of momentum.

The matrix,  $J_{\alpha\beta}$ , is not only circulant, it is also symmetric, therefore  $J_{\alpha\beta}$  has

only four independent matrix elements (instead of six):

$$\mathbb{J}_{\alpha\beta} = \mathbf{circ}(J_1, J_2, J_3, J_4, J_3, J_2), \tag{4.3.1}$$

where the  $J_{\alpha}$ 's can be computed directly from the collision operator,  $\Omega_{\alpha}$ . For the 6-bit collision saturated model,

$$J_1 = \mathbb{J}_{\alpha\alpha} = -d(1-d)\left(\xi^{(2)}(1-d)^2 + (4\xi^{(3A)} + \xi^{(3S)})d(1-d) + \xi^{(4)}d^2\right), \quad (4.3.2a)$$

$$J_2 = \mathbb{J}_{\alpha\alpha+1} = d(1-d) \left( \xi_R^{(2)} (1-d)^2 + (2\xi^{(3A)} + \xi^{(3S)}) d(1-d) + \xi_L^{(4)} d^2 \right) , \quad (4.3.2b)$$

$$J_3 = J_{\alpha\alpha+2} = d(1-d) \left( \xi_L^{(2)} (1-d)^2 + (2\xi^{(3A)} - \xi^{(3S)}) d(1-d) + \xi_R^{(4)} d^2 \right), \quad (4.3.2c)$$

$$J_4 = \mathbb{J}_{\alpha\alpha+3} = -d(1-d)\left(\xi^{(2)}(1-d)^2 + (4\xi^{(3A)} - \xi^{(3S)})d(1-d) + \xi^{(4)}d^2\right). (4.3.2d)$$

Assuming that  $\xi_R^{(2)} = \xi_L^{(2)} = \frac{1}{2}\xi^{(2)}$  and  $\xi_R^{(4)} = \xi_L^{(4)} = \frac{1}{2}\xi^{(4)}$  (as required by isotropy), then the eigenvalues of the linearized collision operator are:

$$\lambda_1 = P_{\gamma}(1) = 0, \qquad (4.3.3a)$$

$$\lambda_2 = P_{\gamma}(w) = 0,$$
(4.3.3b)

$$\lambda_3 = P_{\gamma}(w^2) = -3\tilde{d}\left(\xi^{(2)}(1-d)^2 + 4\xi^{(3A)}\tilde{d} + \xi^{(4)}d^2\right), \qquad (4.3.3c)$$

$$\lambda_4 = P_{\gamma}(w^3) = -6\xi^{(3S)}\tilde{d}^2, \qquad (4.3.3d)$$

$$\lambda_5 = P_\gamma(w^4) = \lambda_3 \,, \tag{4.3.3e}$$

$$\lambda_6 = P_\gamma(w^5) = 0,$$
(4.3.3f)

where  $\tilde{d}=d(1-d)$ . For the collision saturated 6-bit model,  $\xi^{(2)}=\xi^{(3S)}=\xi^{(3A)}=\xi^{$ 

 $\xi^{(4)} = 1$ , then

$$\lambda_{1,2,6} = 0 \,, \tag{4.3.4a}$$

$$\lambda_{3,5} = -3\tilde{d} \left( 1 + 2\tilde{d} \right) , \qquad (4.3.4b)$$

$$\lambda_4 = -6\tilde{d}^2. \tag{4.3.4c}$$

The universal eigenvectors of  $6 \times 6$  circulant matrix are:

$$|\lambda_{1}\rangle = \frac{1}{\sqrt{6}} \begin{pmatrix} 1\\1\\1\\1\\1\\1 \end{pmatrix}, \qquad |\lambda_{2}\rangle = |\lambda_{6}\rangle^{*} = \frac{1}{\sqrt{6}} \begin{pmatrix} 1\\w\\-w^{*}\\-1\\-w\\w^{*} \end{pmatrix}, \qquad (4.3.5a)$$

$$|\lambda_{3}\rangle = |\lambda_{5}\rangle^{*} = \frac{1}{\sqrt{6}} \begin{pmatrix} 1\\ -w^{*}\\ -w\\ 1\\ -w^{*}\\ -w \end{pmatrix}, \qquad |\lambda_{4}\rangle = \frac{1}{\sqrt{6}} \begin{pmatrix} 1\\ -1\\ 1\\ -1\\ 1\\ -1 \end{pmatrix}, \qquad (4.3.5b)$$

where \* means the complex conjugate. These eigenvectors can be reorganized such that their components are real. Let  $|n\rangle = |\lambda_1\rangle$ ,  $|p_x\rangle = \frac{1}{\sqrt{2}}(|\lambda_2\rangle + |\lambda_6\rangle)$ ,  $|p_y\rangle = \frac{1}{i\sqrt{2}}(|\lambda_2\rangle - |\lambda_6\rangle)$ ,  $|K_3\rangle = \frac{1}{\sqrt{2}}(|\lambda_3\rangle + |\lambda_5\rangle)$ , and  $|K_4\rangle = |\lambda_4\rangle$ ,  $|K_5\rangle = \frac{1}{i\sqrt{2}}(|\lambda_3\rangle - |\lambda_5\rangle)$ .

Then,

$$|p_x\rangle = \frac{1}{2\sqrt{3}} \begin{pmatrix} 2\\1\\-1\\-2\\-1\\1 \end{pmatrix}, \qquad |p_y\rangle = \frac{1}{2} \begin{pmatrix} 0\\1\\1\\0\\-1\\-1 \end{pmatrix}, \qquad (4.3.6a)$$

$$|K_{3}\rangle = \frac{1}{2\sqrt{3}} \begin{pmatrix} 2\\ -1\\ -1\\ 2\\ -1\\ -1 \end{pmatrix}, \qquad |K_{5}\rangle = \frac{1}{2} \begin{pmatrix} 0\\ 1\\ -1\\ 0\\ 1\\ -1 \end{pmatrix}. \tag{4.3.6b}$$

The eigenvectors corresponding to zero eigenvalues, namely,  $|n\rangle$ ,  $|p_x\rangle$  and  $|p_y\rangle$ , are called the hydrodynamic modes, and the remaining three are called the kinetic modes. The physical significance of the hydrodynamic modes are obvious:  $|n\rangle$ ,  $|p_x\rangle$  and  $|p_y\rangle$  are the density, x-momentum and y-momentum modes, respectively.

### 4.4 The Solution of the Linearized Lattice Boltzmann Equation and Generalized Hydrodynamics

The Fourier transform of Eq. (4.1.1) is

$$\phi_{\alpha}(\mathbf{k}, t+1) = e^{-i\mathbf{k}\cdot\hat{\mathbf{e}}_{\alpha}} \sum_{\beta} (\delta_{\alpha\beta} + \mathbb{J}_{\alpha\beta}) \phi_{\beta}(\mathbf{k}, t). \tag{4.4.1}$$

This can be written in a vector form as

$$|\phi(\mathbf{k}, t+1)\rangle = \mathbb{H}(\mathbf{k}) |\phi(\mathbf{k}, t)\rangle,$$
 (4.4.2)

where the component of the fluctuation vector  $|\phi(\mathbf{k}, t)\rangle$  is  $\phi_{\alpha}(\mathbf{k}, t)$ , i.e.,  $|\phi(\mathbf{k}, t)\rangle = (\phi_1, \phi_2, \phi_3, \phi_4, \phi_5, \phi_6)^T$ . The matrix

$$\mathbb{H}(\mathbf{k}) = \mathbb{D}(\mathbf{k})\mathbb{H}_0,\tag{4.4.3}$$

where

$$\mathbb{H}_0 = \mathbb{I} + \mathbb{J} \tag{4.4.4}$$

is the evolution operator. The diagonal matrix

$$\mathbb{D}(\mathbf{k}) = \operatorname{diag}(e^{-i\mathbf{k}\cdot\hat{\mathbf{e}}_1}, e^{-i\mathbf{k}\cdot\hat{\mathbf{e}}_2}, \cdots, e^{-i\mathbf{k}\cdot\hat{\mathbf{e}}_6})$$
(4.4.5)

is the displacement operator.

In general, the eigenvalue problem for  $\mathbb{H}(\mathbf{k})$  cannot be solved analytically except for special cases, whereas that for  $\mathbb{H}_0 \equiv \mathbb{H}(0)$  can be trivially solved because  $\mathbb{H}_0$  is a circulant matrix. Indeed, the eigenvalues of  $\mathbb{H}_0$  are  $1 + \lambda_{\alpha}$ , where  $\lambda_{\alpha}$ 's are the eigenvalues of  $\mathbb{J}$ , and the eigenvectors of  $\mathbb{H}_0$  are those of  $\mathbb{J}$ . Then, the matrix  $\mathbb{H}_0$  has three unit eigenvalues corresponding to those three hydrodynamic modes, *i.e.*, the corresponding eigenvectors are associated with the conserved quantities of the system.  $\mathbb{H}_0$  also has three non-unity eigenvalues corresponding to those three kinetic modes. In what follows we will show how these modes can be analytically continued to the  $\mathbf{k} \neq 0$  region by a perturbative procedure.

Because the hydrodynamic modes have a three-fold degeneracy, they must be recombined to obtain a new basis for the perturbed system. It can be shown that the new eigenvectors are

$$|u_{\perp}(0)\rangle = \cos\theta |p_{y}\rangle - \sin\theta |p_{x}\rangle = |p_{\perp}\rangle,$$
 (4.4.6a)

$$|u_{\pm}(0)\rangle = \frac{1}{\sqrt{2}}(|n\rangle \pm (\cos\theta |p_x\rangle + \sin\theta |p_y\rangle)) = \frac{1}{\sqrt{2}}(|n\rangle \pm |p_{\parallel}\rangle), \quad (4.4.6b)$$

where  $\theta$  as the angle between  $\mathbf{k}$  and  $\hat{\mathbf{e}}_1$  (=  $\hat{\mathbf{x}}$ );  $|p_{\perp}\rangle$  and  $|p_{\parallel}\rangle$  are the transverse and longitudinal momentum with respect to  $\mathbf{k}$ , respectively. Now,  $|u_{\perp}(\mathbf{k})\rangle$  and  $|u_{\pm}(\mathbf{k})\rangle$  are the generalized hydrodynamic eigenvectors, which represent one transverse and two sound modes, respectively.

Let  $\phi_{\perp}(\mathbf{k}, t) = \langle u_{\perp}(\mathbf{k}) | \phi(\mathbf{k}, t) \rangle$  and  $\phi_{\pm}(\mathbf{k}, t) = \langle u_{\pm}(\mathbf{k}) | \phi(\mathbf{k}, t) \rangle$ , then the linearized hydrodynamic equations for the linearized lattice Boltzmann equation are

$$\phi_{\perp}(\boldsymbol{k}, t+1) = z_{\perp}(\boldsymbol{k})\phi_{\perp}(\boldsymbol{k}, t) = e^{(t+1)\ln z_{\perp}}\phi_{\perp}(\boldsymbol{k}, 0), \tag{4.4.7a}$$

$$\phi_{\pm}(\mathbf{k}, t+1) = z_{\pm}(\mathbf{k})\phi_{\pm}(\mathbf{k}, t) = e^{(t+1)\ln z_{\pm}}\phi_{\pm}(\mathbf{k}, 0),$$
 (4.4.7b)

and the generalized hydrodynamic transport coefficients are defined in analogy to their definitions in hydrodynamics [121]:

$$\nu(\mathbf{k}) = -\frac{\ln(z_{\perp}(\mathbf{k}))}{k^2}, \qquad (4.4.8a)$$

$$\frac{1}{2}(\nu(\boldsymbol{k}) + \zeta(\boldsymbol{k})) = -\frac{\operatorname{Re}(\ln(z_{\pm}(\boldsymbol{k})))}{k^2}, \qquad (4.4.8b)$$

$$c_s(\mathbf{k}) = \pm \frac{\operatorname{Im}(\ln(z_{\pm}(\mathbf{k})))}{k},$$
 (4.4.8c)

where  $\nu$ ,  $\zeta$  and  $c_s$  are the kinematic viscosity, the bulk viscosity and the sound speed, respectively. By expanding  $\mathbb{D}(\mathbf{k})$  in  $\mathbf{k}$ , *i.e.*,

$$\mathbb{D}(\mathbf{k}) = \sum_{n=0}^{\infty} \frac{(-ik)^n}{n!} \mathbb{P}^n(\theta)$$
 (4.4.9)

with

$$\mathbb{P}(\theta) = \operatorname{diag}(\cos \theta, \cos(\theta - \pi/3), \cdots, \cos(\theta + \pi/3)), \tag{4.4.10}$$

the coefficients of perturbation expansions for the eigenvalues of  $\mathbb{H}(\mathbf{k})$ , e.g.,  $z_{\perp}$  and  $z_{\pm}$ , can be calculated. The coefficients in perturbation expansions for the transport coefficients are just the cumulants [127] of the corresponding eigenvalues. As an example, the first few coefficients in perturbation expansions for  $z_{\perp}(\mathbf{k})$  and the kinematic viscosity,  $\nu(\mathbf{k})$ , are given as follows:

$$z_{\perp}(\mathbf{k}) = 1 - z_{\perp}^{(2)} k^2 + z_{\perp}^{(4)} k^4 + \cdots$$

where

$$\begin{split} z_{\perp}^{(2)} &= -\frac{1}{8} \left( 1 + \frac{2}{\lambda_3} \right), \\ z_{\perp}^{(4)} &= \frac{z_{\perp}^{(2)}}{48\lambda_3^2 \lambda_4} \{ 2(6\lambda_3 - 6\lambda_4 + 3\lambda_3^2 - 6\lambda_3\lambda_4 - \lambda_3^2\lambda_4) + \\ &- \cos(6\theta)\lambda_3 (12 + 6\lambda_3 + 6\lambda_4 + \lambda_3\lambda_4) \}. \end{split}$$

Then the kinematic viscosity is

$$\nu(\mathbf{k}) = \nu_0 - \nu_2 k^2 + \cdots,$$

where

$$\begin{split} \nu_{\scriptscriptstyle 0} &= z_{\scriptscriptstyle \perp}^{\scriptscriptstyle (2)}, \\ \nu_{\scriptscriptstyle 2} &= \frac{1}{2} (z_{\scriptscriptstyle \perp}^{\scriptscriptstyle (2)})^2 - z_{\scriptscriptstyle \perp}^{\scriptscriptstyle (4)}. \end{split}$$

The zeroth order (in k) results of the transport coefficients obtained by this perturbative method are identical to the earlier results [44,45].

The above analysis clearly shows that the zeroth order result of the viscosity,  $\nu_0$ , is independent of the angle  $\theta$  (of  $\mathbf{k}$ ), therefore it is isotropic. However, the higher order results depend on  $\theta$ . For instance,  $\nu_2$  depends on  $\cos(6\theta)$ , and the next order result depends on both  $\cos(6\theta)$  and  $\cos(12\theta)$ , so on and so forth. This result is a clear reflection of the fact that the tensor,  $\mathbf{E}^{(2n)}$ , is isotropic only up to n=2 in the triangular lattice space.

In the case of  $\theta = 0$  or  $\theta = \pi/6$ , the eigenvalues of  $\mathbb{H}(\mathbf{k})$  are obtained analytically for arbitrary k. For  $\theta = 0$ ,  $\mathbb{H}(\mathbf{k})$  can be decomposed into the direct sum of a  $2 \times 2$  and a  $4 \times 4$  matrix. For  $\theta = \pi/6$ ,  $\mathbb{H}(\mathbf{k})$  becomes a direct sum of two  $3 \times 3$  matrices. Therefore, the eigenvalues are roots of quadratic, quartic or cubic algebraic polynomials. The decomposition of  $\mathbb{H}(\mathbf{k})$  along the special directions  $\theta = 0$  and  $\theta = \pi/6$  is a consequence of the fact that the collision operator,  $\Omega_{\alpha}$ , is invariant under the complete lattice symmetry group [45]. This decomposition is also applicable to other FHP 2-D models.

For  $\theta = 0$ , the eigenvalue corresponding to the transverse mode can be obtained analytically:

$$z_{\perp}(\mathbf{k}) = \frac{1}{2}(2+\lambda_3)\cos(k/2) + \frac{1}{2}\sqrt{(2+\lambda_3)^2\cos^2(k/2) - 4(1+\lambda_3)}.$$
 (4.4.11)

The kinematic viscosity possesses an imaginary part between the two branch points of  $z_{\perp}$  which satisfy  $(2 + \lambda_3)^2 \cos^2(k/2) - 4(1 + \lambda_3) = 0$ . As k increases from 0 to the first branch point,  $z_{\perp}(\mathbf{k})$  and the eigenvalue of the kinetic mode coupled by the quadratic equation collide with each other. Then both of them become complex conjugate until they collide again at the second branch point. After the second collision they separate along the real axis of the z-plane. The cusps in Figs. (4.4.1) clearly exhibit the coalescence of the eigenvalues. Numerical results indicate that a similar situation occurs when  $0 < \theta < \pi/6$  for the transverse mode. However, when  $\theta = \pi/6$ , the kinematic viscosity has no imaginary part in the physical region (0 < d < 1) of the k-d plane. The fact that  $z_{\perp}(\mathbf{k})$  can be complex indicates that the relaxation of the

transverse momentum can be oscillatory. In the limit  $d \to 0$ ,  $z_{\perp}(\mathbf{k}) \to e^{i\frac{\mathbf{k}}{2}}$ . This suggests that oscillations in relaxations of the transverse momentum are related to the free streaming of particles (a ballistic effect). Indeed, this kind of oscillation has been observed in numerical simulations.

Plots of the wave number dependence of the kinematic viscosity,  $\nu$ , the bulk viscosity,  $\zeta$ , and the sound speed,  $c_s$ , for density d=0.2 and  $\theta=0, \pi/12$  and  $\pi/6$  are shown in Figs. (4.4.1). For  $\theta=\pi/12$ , results are obtained by calculating the eigenvalues of  $\mathbb{H}(\mathbf{k})$  directly. We also calculated  $\nu(\mathbf{k})$  and  $c_s(\mathbf{k})$  by perturbation expansion for  $\theta=\pi/12$ . The 8th order perturbative result of  $\nu(\mathbf{k})$  agrees with the exact result for  $k \leq 0.5$ ; and for  $c_s(\mathbf{k})$ , results agree when  $k \leq 0.2$ . One can clearly see that these transport coefficients are highly anisotropic even for moderate values of k. This fact indicates that in LGA simulations, only very small k results are isotropic. Hence, a large number of cells must be averaged over in order to overcome the anisotropy.

Note that, for  $\theta=0$ ,  $\zeta(\boldsymbol{k})$  is negative for  $\boldsymbol{k}\neq 0$ . Whereas in the case of usual hydrodynamics (i.e., in the limit of  $\boldsymbol{k}\to 0$  and  $\omega\to 0$ ), it can be shown that all the transport coefficients should be positive for the sake of stability [1, §15–16 and §49]. It should be pointed out that, it is not just  $\zeta$ , but the combination of  $\nu$  and  $\zeta$ , i.e.,  $\frac{1}{2}(\nu+\zeta)$ , which determines the stability (or damping) of the sound modes (see detailed analysis in §3.12). Moreover,  $\frac{1}{2}(\nu+\zeta)$  is always positive here for all  $\boldsymbol{k}$ ; and both  $\nu$  and  $\zeta$  are non-negative at the limit of  $\boldsymbol{k}=0$ . The negative  $\zeta(\boldsymbol{k})$  in certain regions of  $\boldsymbol{k}\neq 0$  has been observed in numerical simulations, but there were no correct interpretations given at that time [128, 116, 129]. The negative bulk viscosity  $\zeta(\boldsymbol{k})$  in the context of generalized hydrodynamics has been studied first by the author [114], then by Das et al. [130]. It should also be stressed that the negative  $\zeta(\boldsymbol{k})$  for  $\boldsymbol{k}\neq 0$  does not contradict the H-theorems for the lattice-gas automata shown in §3.9, because the local H-theorem is proven based upon the pointwise collision mechanism on the

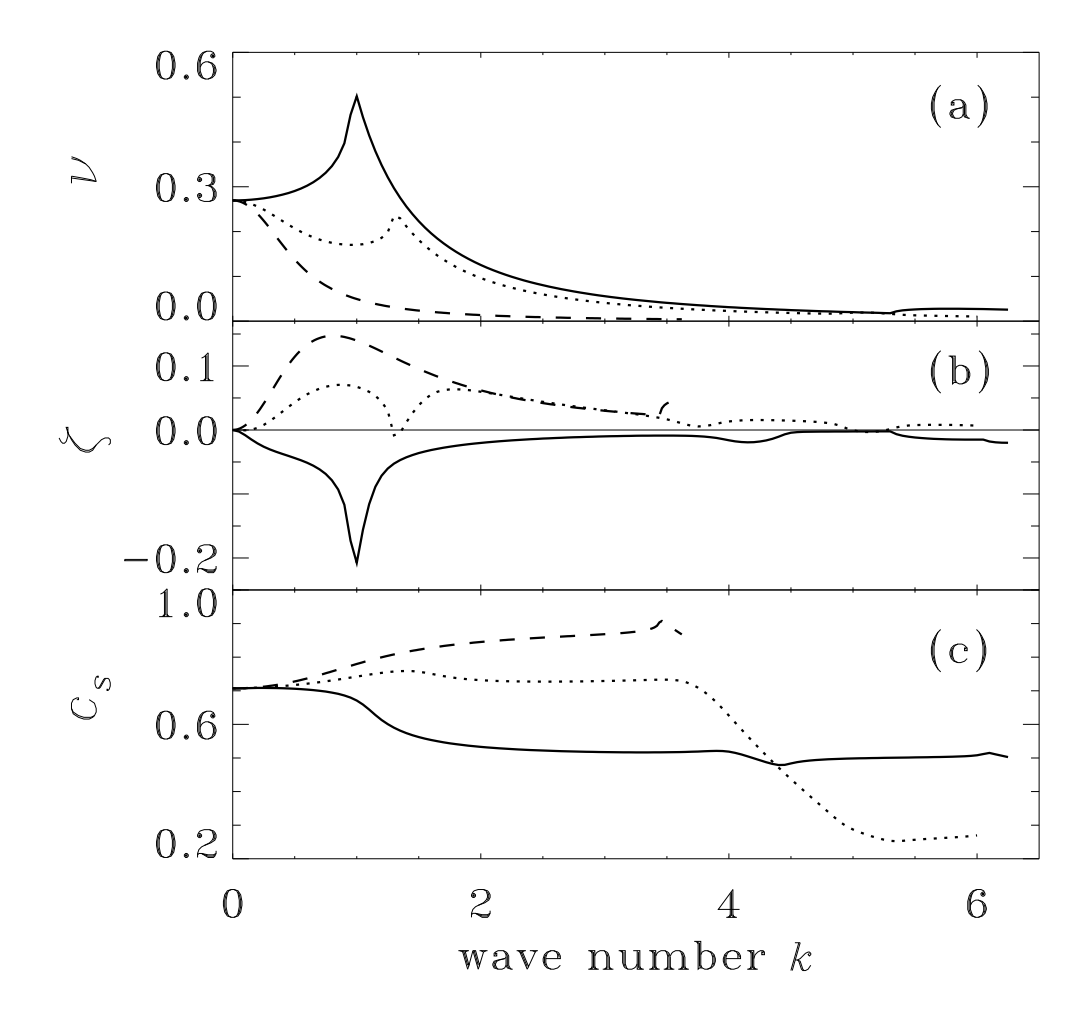


Figure 4.4.1: Kinematic viscosity  $\nu(\boldsymbol{k})$ , bulk viscosity  $\zeta(\boldsymbol{k})$  and sound speed  $c_s(\boldsymbol{k})$  vs.  $\boldsymbol{k}$  for density = 0.2, and  $\theta$  = 0 (solid line),  $\pi/12$  (dotted line) and  $\pi/6$  (dashed line): (a)  $\nu(\boldsymbol{k})$  vs.  $\boldsymbol{k}$ ; (b)  $\zeta(\boldsymbol{k})$  vs.  $\boldsymbol{k}$ ; (c)  $c_s(\boldsymbol{k})$  vs.  $\boldsymbol{k}$ .

lattice, a situation where k is not a relevant quantity.

The anisotropy of the LGA is definitely unphysical. It is an effect due to the small number of allowed velocities. More precisely, the tensor,  $\mathbf{E}^{(2n)}$ , is isotropic only up to the order n=2. That means the transport coefficients are isotropic only at the limit  $\mathbf{k} \to 0$ . The analysis here quantitatively shows the anisotropic effect in the transport coefficients related to the higher order spatial derivatives (or higher order in  $\mathbf{k}$ ). The anisotropy of the transport coefficients is a direct consequence of the anisotropy of the tensor,  $\mathbf{E}^{(2n)}$ , for n > 2.

## 4.5 A Numerical Test of the Dispersion Relation of the Sound Speed

To verify the dispersion relations of transport coefficients discussed in the previous section, we set up a numerical test of the dispersion relation of the sound speed,  $c_s(\mathbf{k})$ . The measurement is made by computing the power spectrum of the density-density correlation function, which is based upon the Green-Kubo formula. In what follows, we will derive the form of the power spectrum from the linearized LGA hydrodynamic equation, and discuss the details of the simulation.

### 4.5.1 The Green-Kubo Formula

Define the Laplace-Fourier transform

$$\tilde{\boldsymbol{v}}(\boldsymbol{k}, s) = \frac{1}{\sqrt{2\pi}^{(D+1)}} \int d\boldsymbol{x} dt \ e^{-(i\boldsymbol{k}\cdot\boldsymbol{x}+st)} \boldsymbol{v}(\boldsymbol{x}, t), \qquad (4.5.1a)$$

$$\tilde{\rho}(\boldsymbol{k}, s) = \frac{1}{\sqrt{2\pi^{(D+1)}}} \int d\boldsymbol{x} dt \ e^{-(i\boldsymbol{k}\cdot\boldsymbol{x}+st)} \rho(\boldsymbol{x}, t), \qquad (4.5.1b)$$

where  $s=\epsilon+i\omega$ , and  $\epsilon>0$ . Then the transformed linearized Navier-Stokes equations are:

$$s\tilde{\rho} + i\rho_0 \mathbf{k} \cdot \tilde{\mathbf{v}} = \tilde{\rho}(\mathbf{k}, 0), \qquad (4.5.2a)$$

$$s\rho_0\tilde{\boldsymbol{v}} = -i\boldsymbol{k}c_s^2\tilde{\rho} - k^2\rho_0\nu\tilde{\boldsymbol{v}} - \boldsymbol{k}\rho_0\left(\zeta + \frac{D-2}{D}\nu\right)(\boldsymbol{k}\cdot\boldsymbol{v}) + \rho_0\tilde{\boldsymbol{v}}(\boldsymbol{k},0). (4.5.2b)$$

From the above equations, it follows almost immediately that

$$\frac{\langle \tilde{\rho}(\boldsymbol{k}, s) \tilde{\rho}^*(\boldsymbol{k}, s) \rangle}{\langle \tilde{\rho}(\boldsymbol{k}, 0) \tilde{\rho}^*(\boldsymbol{k}, s) \rangle} = \frac{\langle \tilde{\rho}(\boldsymbol{k}, s) \tilde{\rho}^*(\boldsymbol{k}, 0) \rangle}{\langle \tilde{\rho}(\boldsymbol{k}, 0) \tilde{\rho}^*(\boldsymbol{k}, 0) \rangle} = \frac{s + k^2(\zeta + \nu)}{s^2 + sk^2(\zeta + \nu) + k^2c_s^2},$$
(4.5.3)

where we have assumed D=2, and  $\langle \tilde{\boldsymbol{v}}(\boldsymbol{k},0)\tilde{\rho}^*(\boldsymbol{k},0)\rangle = \langle \tilde{\boldsymbol{v}}(\boldsymbol{k},0)\tilde{\rho}^*(\boldsymbol{k},s)\rangle = 0$ , because  $\boldsymbol{v}$  and  $\rho$  are statistically independent variables. Taking the limit  $\epsilon \to 0$ , we have the power spectrum of the density-density correlation function:

$$\frac{\langle \tilde{\rho}(\boldsymbol{k}, \omega) \tilde{\rho}^*(\boldsymbol{k}, \omega) \rangle}{\langle \tilde{\rho}(\boldsymbol{k}, 0) \tilde{\rho}^*(\boldsymbol{k}, 0) \rangle} = \frac{\omega^2 + k^4 (\zeta + \nu)^2}{(\omega - kc_s)^2 (\omega + kc_s)^2 + \omega^2 k^4 (\zeta + \nu)^2}$$
(4.5.4)

The quantity  $\frac{\langle \tilde{\rho}(\boldsymbol{k}, \omega) \tilde{\rho}^*(\boldsymbol{k}, \omega) \rangle}{\langle \tilde{\rho}(\boldsymbol{k}, 0) \tilde{\rho}^*(\boldsymbol{k}, 0) \rangle}$  is called the scattering function [101].

In the limit of  $k \to 0$ , which is a part of the hydrodynamic limit (the other requirement is  $\omega \to 0$ ), and for  $\omega \approx \pm c_s k$ , the scattering function can be approximated as

$$\frac{\langle \tilde{\rho}(\boldsymbol{k}, \omega) \tilde{\rho}^*(\boldsymbol{k}, \omega) \rangle}{\langle \tilde{\rho}(\boldsymbol{k}, 0) \tilde{\rho}^*(\boldsymbol{k}, 0) \rangle} \approx \frac{1}{4} \left( \frac{1}{(\omega - c_s k)^2 + (k^2(\zeta + \nu)/2)^2} + \frac{1}{(\omega + c_s k)^2 + (k^2(\zeta + \nu)/2)^2} \right). \tag{4.5.5}$$

This approximation only affects the  $\mathcal{O}(k^4)$  term in the numerator of Eq. (4.5.4). In above equation, the spectrum has two Lorentzian peaks centered at the frequencies  $\omega = \pm c_s k$ . These are the Brillouin peaks, which are related to the propagating sound modes in the fluid. The half-width at half-maximum of the peaks is given by  $\omega = \frac{1}{2}k^2(\zeta + \nu)$ . Note that for homogeneous systems,

$$\langle \tilde{\rho}(\mathbf{k}, \omega) \tilde{\rho}^*(\mathbf{k}, \omega) \rangle = \langle \delta \tilde{\rho}(\mathbf{k}, \omega) \delta \tilde{\rho}^*(\mathbf{k}, \omega) \rangle,$$
 (4.5.6)

where  $\delta \rho = \rho - \rho_0$  is the density fluctuation, and  $\rho_0 = 6d$  for the 6-bit models.

#### 4.5.2 The Simulation

The simulation to compute the dispersion relation of the sound speed will now be described. Assume a 6-bit, collision saturated FHP LGA with a system size  $N_x \times N_y$ , (where  $N_x$  and  $N_y$  are the number of the lattice points along x and y directions,

respectively, and  $N_x$  is along the direction of  $\hat{\boldsymbol{e}}_1$ ) and assume periodic boundary conditions. We first let the system run for a period of time to obtain equilibrium. Then, the density,  $\rho$ , is averaged along the direction of  $N_x$ , so it becomes a function of y and time, t,  $\bar{\rho}(y,t)$ . Next, the spatial Fourier transform of  $\bar{\rho}$  is computed with  $k = \frac{2\pi}{L_y}$ , where  $L_y = \frac{\sqrt{3}}{2}N_y$ . Now, a time series of  $\bar{\rho}_k(t)$  is obtained. We then compute the power spectrum of  $\bar{\rho}_k(t)$  with a period of T time steps. The spatial average has been used to replace the ensemble average.

Fig. (4.5.1) shows the power spectra with  $N_y = 16$ , 32, 64 and 128, respectively. The vertical axis is the intensity of the power spectra and the horizontal axis is  $\frac{\omega T}{2\pi}$ . The Lorentzian form given by Eq. (4.5.5) is used to fit the spectra and locate the center of the peaks,  $\omega_c$ . The sound speed can be determined by  $\omega_c = kc_s$ .

In Figure (4.5.2), the analytic result and LGA simulations of  $c_s$  are compared for the direction  $\theta = \pi/6$ . Simulation results confirm the prediction of the analytic result that  $c_s$  increases as k increases along the direction  $\theta = \pi/6$ . The relative differences between the LGA simulation and the analytic result are less than 1%.

### 4.6 Analytic Solutions for Simple Flows

In this section, we show that the linearized lattice Boltzmann equation with simple boundary conditions can be solved analytically. Although we only examine the equation for the 6-bit models, the following method can be extended to any other LGA models.

Consider the system under the influence of time-independent external force,  $\mathbf{F}(\mathbf{x})$ . Then we have

$$|\phi(\mathbf{k}, t+1)\rangle = \mathbb{H}(\mathbf{k}) |\phi(\mathbf{k}, t)\rangle + |F(\mathbf{k})\rangle,$$
 (4.6.1)

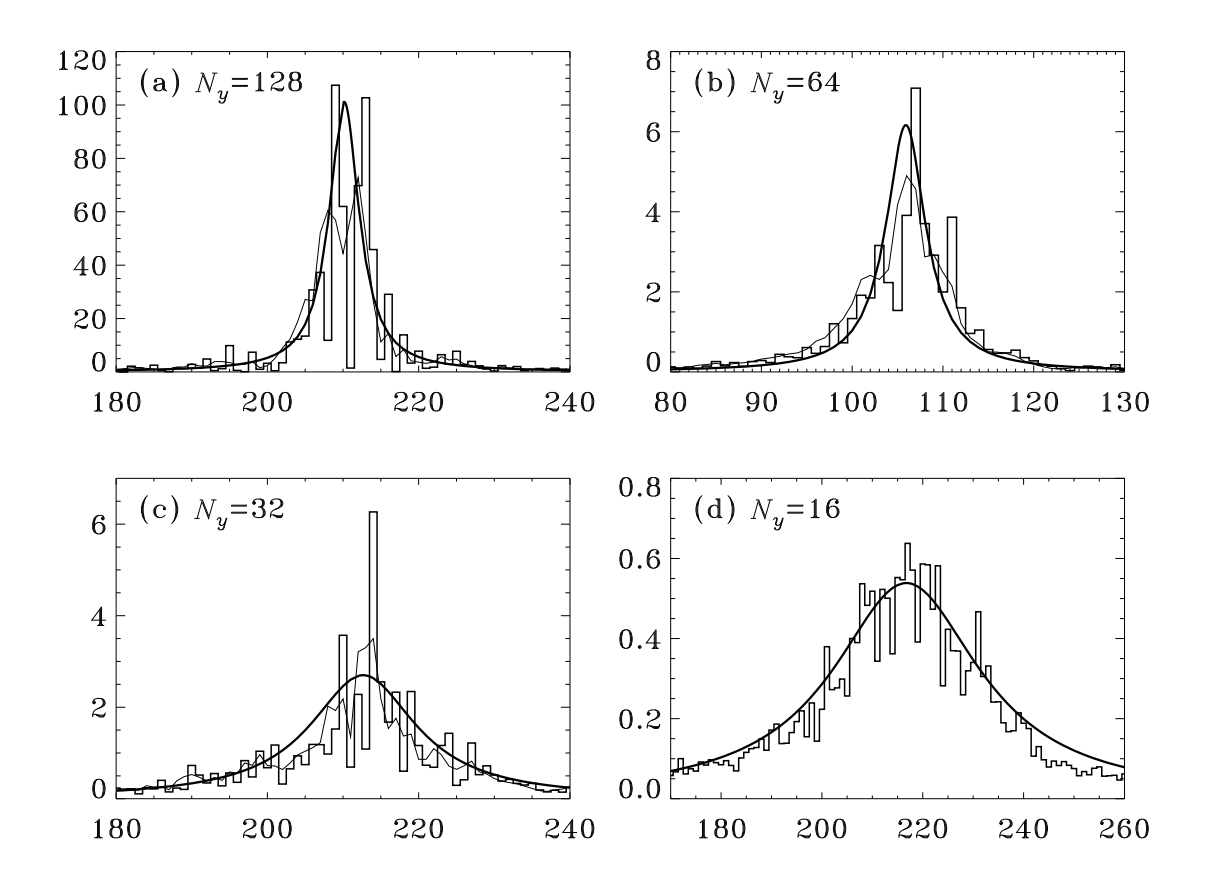


Figure 4.5.1: The power spectra to determine sound speed  $c_s$  with various values of k and  $\theta=\pi/6$ . The histograms represent the data of the power spectra, the thin solid lines are three-point-averaged smoothed results of the spectra, and the thick solid lines are the fitting results of the smoothed ones by the Lorentzian form given by Eq. (4.5.5). (a)  $N_y=128$ ,  $T=2^{15}=32768$ ; (b)  $N_y=64$ ,  $T=2^{15}=32768$ ; (c)  $N_y=32$ ,  $T=2^{13}=8192$ ; (d)  $N_y=16$ ,  $T=2^{12}=4096$ .

where the components of  $|F(\mathbf{k})\rangle$  are the Fourier transform of the projection of  $\mathbf{F}$  on the direction  $\hat{\mathbf{e}}_{\alpha}$ . Here it is assumed that the magnitude of the forcing is of the same order of the fluctuation,  $\phi$ .

Since the force is weak and time-independent, we assume the existence of the steady state, i.e.,  $|\phi(\mathbf{k}, t+1)\rangle = |\phi(\mathbf{k}, t)\rangle = |\phi(\mathbf{k})\rangle$ . Then,

$$|\phi(\mathbf{k})\rangle = [\mathbb{I} - \mathbb{H}(\mathbf{k})]^{-1} |F(\mathbf{k})\rangle.$$
 (4.6.2)

By specifying  $|F(\mathbf{k})\rangle$ ,  $|\phi(\mathbf{k})\rangle$  can be calculated. One should note that even though

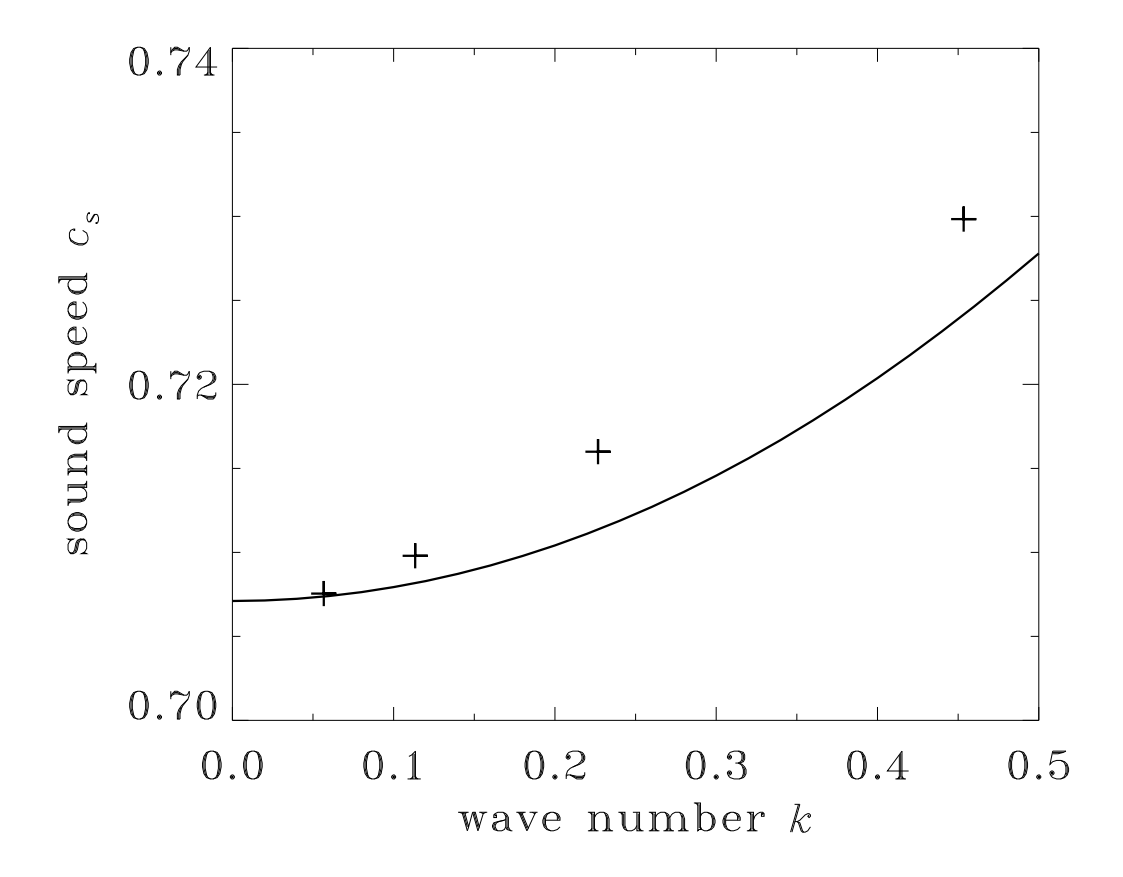


Figure 4.5.2: Sound speed  $c_s(\mathbf{k})$  vs. k for density d=0.2 and  $\theta=\pi/6$ . The analytic result is represented by the solid line and the LGA simulations by +. The relative differences between the LGA simulation and the analytic result are less than 1%. Nonlinear effects must explain the differences.

the eigenvalue problem for  $\mathbb{H}(\mathbf{k})$  cannot be solved analytically in general,  $[\mathbb{I} - \mathbb{H}(\mathbf{k})]^{-1}$  and  $|\phi(\mathbf{k})\rangle$  can always be obtained analytically. Therefore, the flow profile can be calculated for simple forcing functions.

In what follows, two simple flows are analyzed: Poiseuille flow and plane Couette flow. The analytic results shall be compared with results of LGA simulations. In performing the LGA simulation, the microscopic rules of applying uniform body force are described in Fig. (4.6.1). The uniform body force is achieved by assigning a random number r,  $0 \le r \le 1$ , to each site at each time step, after collision and advection process have taken place at each time step, the microscopic forcing rules described in Fig. (4.6.1) are executed if  $r \le r_0$  and if the rule is allowed at the

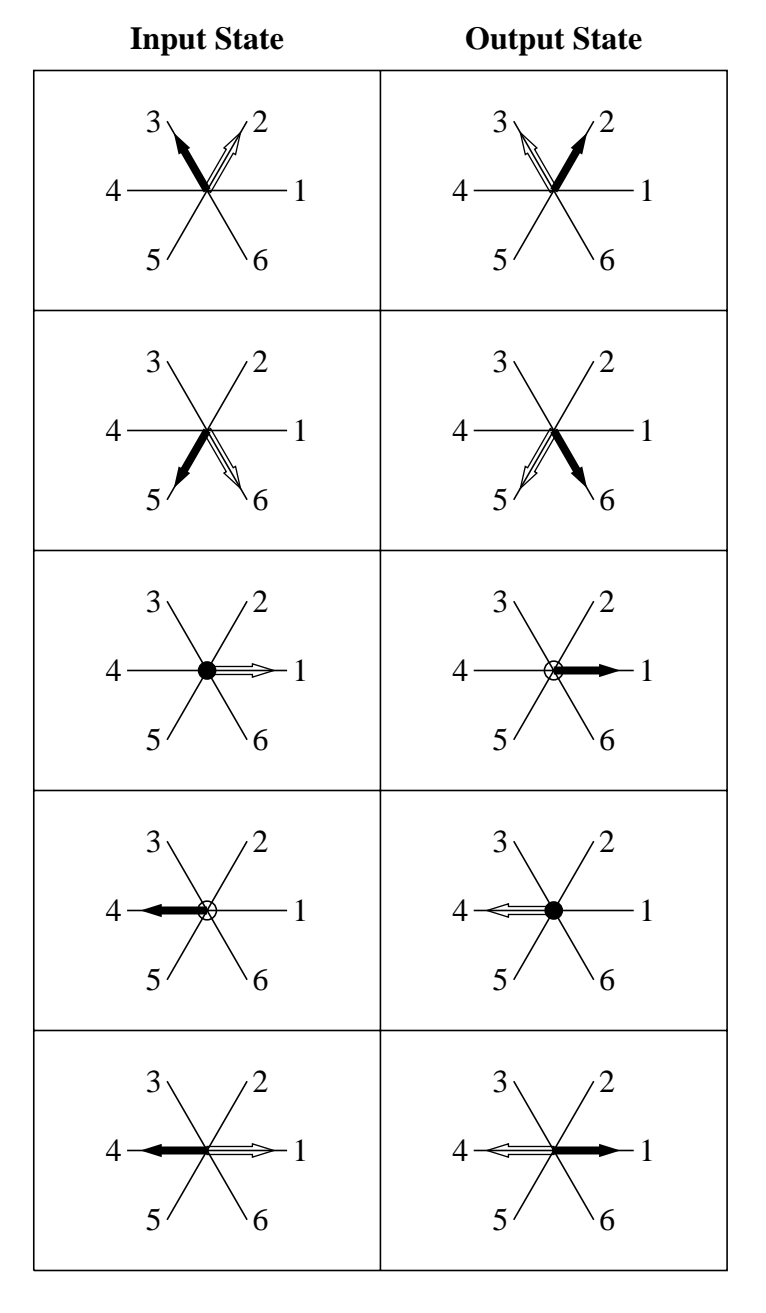


Figure 4.6.1: Forcing rules of FHP 7-bit models. In the left column are states before the forcing. Those in the right column are after forcing. The rules in the first four rows add one unit of momentum to the system, whereas the rule in the fifth row adds two units. The solid arrows indicate occupied states while the hollow ones indicate vacant states. States not indicated may be either occupied or vacant.

particular site. Upon each successful forcing application, the system gains one or two units of momentum in  $\hat{x}$  direction.

#### 4.6.1 Poiseuille Flow

Poiseuille flow is uniformly forced flow between two parallel plates. We use periodic boundary conditions for both x and y directions. The forcing is a square-wave function along x-axis, i.e.,  $\mathbf{F}(\mathbf{x}) = F(y)\hat{\mathbf{x}}$ , where

$$F(y) = \begin{cases} F_0 & 1 \le y < N_y/2, \\ -F_0 & N_y/2 + 1 \le y < N_y, \end{cases}$$
 (4.6.3)

and  $N_y$  is twice the channel width between the two plates. Then,

$$F(k) = \frac{1}{N_u} \frac{4F_0}{\pi (2k-1)}. (4.6.4)$$

The Fourier transform of  $v_x$  is

$$v_x(k) = \langle \hat{\boldsymbol{x}} | \phi(\boldsymbol{k}) \rangle = \langle \hat{\boldsymbol{x}} | (\mathbb{I} - \mathbb{H}(\boldsymbol{k}))^{-1} | \hat{\boldsymbol{x}} \rangle F(k), \tag{4.6.5}$$

where

$$\langle \hat{\boldsymbol{x}} | (\mathbb{I} - \mathbb{H}(\boldsymbol{k}))^{-1} | \hat{\boldsymbol{x}} \rangle = \frac{1}{N_y} \left( a + \frac{6b}{\sin^2 \left( \frac{\sqrt{3}}{2} \frac{\pi(2k-1)}{N_y} \right)} \right), \qquad (4.6.6)$$

and

$$a = \frac{(2 - 3\tilde{d} - 15\tilde{d}^2)}{3\tilde{d}^2(2 - 3\tilde{d} - 6\tilde{d}^2)},\tag{4.6.7a}$$

$$b = \frac{3\tilde{d}(1+2\tilde{d})}{4(2-3\tilde{d}-6\tilde{d}^2)}. (4.6.7b)$$

With the approximation  $k \ll N_y$ ,

$$\langle \hat{\boldsymbol{x}} | (\mathbb{I} - \mathbb{H}(\boldsymbol{k}))^{-1} | \hat{\boldsymbol{x}} \rangle \approx \frac{1}{N_y} \left( a + \frac{8bN_y^2}{\pi^2(2k-1)^2} \right).$$
 (4.6.8)

Therefore,

$$v_{x}(y) = \frac{1}{N_{y}} \sum_{k=1}^{N_{y}/2} v_{x}(k) \sin\left(\frac{2\pi(2k-1)y}{N_{y}}\right), \qquad 1 \le y \le N_{y},$$

$$\approx \begin{cases} \frac{F_{0}}{N_{y}^{2}} (4bN_{y}^{2}(N_{y}/2 - y)y + a) & 1 \le y \le N_{y}/2, \\ \frac{F_{0}}{N_{y}^{2}} (4bN_{y}^{2}(y - N_{y}/2)(y - N_{y}) - a) & N_{y}/2 + 1 \le y \le N_{y}. \end{cases}$$

$$(4.6.9)$$

In the thermodynamic limit  $(N_y \to \infty, d \to 0 \text{ and } N_y^2 d \to d_0 = \text{constant})$ , the following parabolic velocity profile is obtained:

$$\bar{v}_x(\bar{y}) = \lim_{\substack{N \to \infty \\ d \to 0}} \frac{v_x(y)}{N_y^2} = \begin{cases} F_0(4\bar{b}\bar{y}(1-\bar{y}) + \bar{a}) & 0 < \bar{y} < 1 \\ F_0(4\bar{b}(\bar{y}-1)(\bar{y}-2) - \bar{a}) & 1 < \bar{y} < 2 \end{cases},$$
(4.6.10)

where  $\bar{a} = 1/(3d_0^2)$ ,  $\bar{b} = 3d_0/32$ , and  $\bar{y} = y/N_y$ . We can rewrite  $\bar{a} = 2\bar{l}$ , where  $\bar{l}$  is the mean free path in the limit. Therefore, the discontinuity of the momentum profiles, which represents the slip velocity at the walls [131], is proportional to the mean free path in this limit.

We perform a simulation to test the accuracy of the linearized theory. The setup of this simulation will now be described. Plates are placed parallel to the velocity direction  $(\hat{e}_1)$  and periodic boundary conditions are applied. The forcing is a square-wave function between plates. It is of uniform magnitude on sites  $1 \le y \le N_y/2$  and of opposite uniform magnitude on sites  $N_y/2 + 1 \le y \le N_y$ .

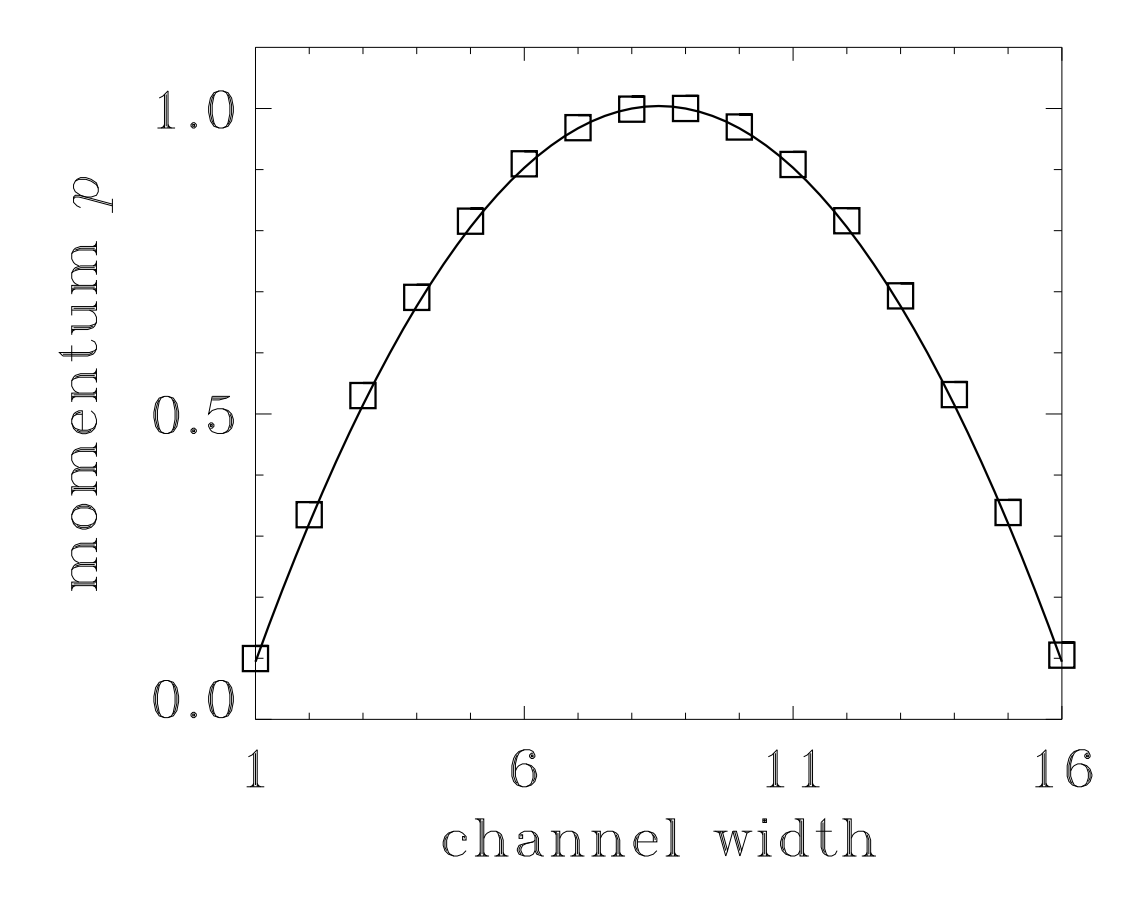


Figure 4.6.2: Momentum profile of Poiseuille flow for density d=0.2 and a channel width of 16 lattice sites. To obtain steady state,  $10^6$  time iterations were run before the average. The momentum  $p_x$  is averaged over  $L_y$  and over  $2\times 10^6$  time iterations. The analytic result (Eq. (4.6.9)) is represented by the solid line and the LGA simulation by  $\Box$ . The graph is rescaled so that  $p_{max}=1$ . Note the agreement for the non-zero momentum at the walls due to finite mean free path. The simulation was run on CRAY Y-MP, with  $F_0=1.0641\times 10^{-3}$ .

In Figure (4.6.2), the velocity profile of forced flow between parallel plates (Poiseuille flow) [132] from our analysis and LGA simulations are compared. Note that, in Figure (4.6.2), the discontinuity of the velocity profiles at the boundaries (the slip velocity) is accurately predicted by the analysis. This phenomenon is a manifestation of existence of a Knudsen layer [131, 133].

### 4.6.2 Plane Couette Flow

Plane Couette flow is the flow between two parallel plates moving in opposite directions. In the case considered here, two plates move in opposite directions, but with the same speed. The forcing term for plane Couette flow is

$$\mathbf{F}(y) = F_0 \hat{\mathbf{x}} \left( \delta(y - 1) - \delta(y - N_y/2 - 1) \right), \tag{4.6.11}$$

with the Fourier transform

$$F(k) = \begin{cases} \frac{2F_0}{N_y} & k = 2n+1, & n = 0, 1, 2, \dots \\ 0 & k = 2n. \end{cases}$$
 (4.6.12)

Then, the Fourier transform of the velocity is

$$v_x(k) = \langle \hat{\boldsymbol{x}} | (\mathbb{I} - \mathbb{H}(\boldsymbol{k}))^{-1} | \hat{\boldsymbol{x}} \rangle F(k)$$

$$\approx \frac{2F_0}{N_y^2} \left( a + \frac{8bN_y^2}{\pi^2(2k-1)^2} \right), \tag{4.6.13}$$

and

$$v_x(y) = \frac{2F_0}{N_y^2} \sum_{k=1}^{N_y/2} v_x(k) \cos\left(\frac{2\pi y(2k-1)}{N_y}\right)$$
$$= \frac{2F_0 a}{N_y^2} \sum_{k=1}^{N_y/2} \cos\left(\frac{2\pi (2k-1)y}{N_y}\right) + F_0 b(N_y/2 - 2y), \qquad (4.6.14)$$

where a and b are given by Eqs. (4.6.7). Because

$$\sum_{k=1}^{N_y/2} \cos\left(\frac{2\pi(2k-1)y}{N_y}\right) = \begin{cases} (-1)^n N_y & \text{if } y = nN_y, \ n = 0, 1, 2, \dots \\ 0 & \text{otherwise,} \end{cases}$$

therefore,

$$v_x(y) = \begin{cases} \frac{2F_0 a}{N_y} + \frac{F_0 b N_y}{2} & y = 1, \\ F_0 b(N_y/2 - 2y) & 1 < y < N_y, \\ -\frac{2F_0 a}{N_y} - \frac{F_0 b N_y}{2} & y = N_y. \end{cases}$$
(4.6.15)

Again, the above equation shows that the velocity profile has a slip (discontinuity) at wall, due to the finite mean free path.

In Figure (4.6.3), the velocity profile of plane Couette flow from our analysis and LGA simulations are compared. The setup of the simulation is the same as for the Poiseuille flow, but the uniform forcing is only applied on two rows: y = 1 and  $y = N_y/2 + 1$ , with the same magnitude and opposite directions.

Our analysis here confirms what have been found in molecular dynamics simulations [117,121]. That is, hydrodynamics does apply quantitatively in very small scales comparable to the mean free path. However, kinetic effects are also visible in the small scales. Furthermore, we have shown that, for both Poiseuille flow and plane Couette flow modeled by lattice-gas automata, the velocity profile consists a part which satisfies the Navier-Stokes equation, and a part which is due to kinetic effect of a finite mean free path and cannot be described by the Navier-Stokes equation.

In conclusion, we have obtained an analytical solution of the linearized lattice Boltzmann equation. We have quantitatively analyzed boundary effects due to a finite

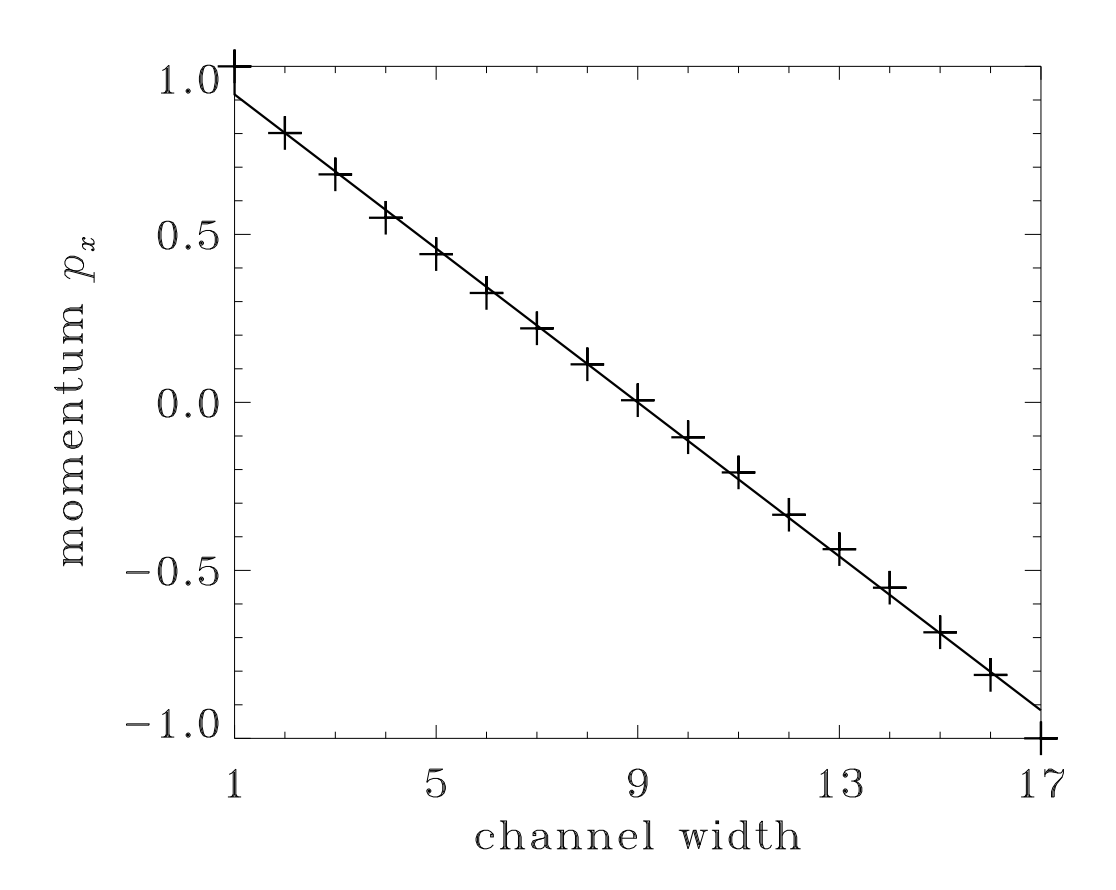


Figure 4.6.3: Velocity profile of plane Couette flow for density per link d=0.2 and a channel width of 16 lattice sites. The system size  $N_x \times N_y = 16384 \times 32$ . The probability of applying forcing is 0.06. To obtain a steady state,  $10^3$  time iterations were run before the average. The velocity,  $v_x$ , is averaged over  $N_x$  and over  $2 \times 10^3$  time iterations. The analytic result of Eq (4.6.15) is represented by the solid line and the LGA simulation by "+". The graph is rescaled so that  $v_{max}=1$ . The simulation was run on a CM-200 computer.

mean free path (Knudsen layer) and anisotropy effects due to the lattice symmetry, and find reasonable agreement with LGA simulations.

### CHAPTER FIVE

# THE LINEAR LATTICE BOLTZMANN EQUATION

The Boltzmann equation has been used as a theoretical tool to connect the microscopic dynamics and the macroscopic equations. In the context of the lattice-gas automata, the lattice Boltzmann equation has also been used as a technique for numerical simulations [85]. More recently, it has become popular to use the linear Boltzmann equations as an alternative simulation technique, for their simplicity of implementation, flexibility of varying the transport coefficients, compatibility in both two and three dimensions, immunity from the statistical noise due to the large fluctuations of particle population, and computational efficiency [134–141, 53, 142, 143, 56].

The first lattice Boltzmann equation technique proposed by McNamara and Zanetti in Ref. [85] is a straightforward floating-point-number counterpart of the FHP lattice-gas automaton. Ignoring the correlations, probabilities, or average populations,  $\{f_{\alpha}\}$ , substitute for discrete particle number,  $\{n_{\alpha}\}$ . The resulting equation is Eq. (3.8.1), in which the collision operator becomes an arithmetic nonlinear operator. The main advantage of this technique is the elimination of statistical noise. Their method is more efficient than lattice-gas automata in simulating flow with low Reynolds number ( $Re \leq 100$ ) [85]. However, this approach is not easily implemented in three dimensions.

An alternative approach is to use a lattice Boltzmann equation with the collision

operator linearized about a chosen local equilibrium. This approach is not only easy to implement in both two and three dimensions, it also possesses several additional virtues. First of all, the collision operator is simplified. Thus the computational efficiency is enhanced. Second, the viscosity can be adjusted quite close to zero, so that high Reynolds numbers can be obtained in simulations. Third, the artifacts due to non-unity factor,  $g(\rho)$ , and velocity dependence of the equation of state can be completely eliminated by choosing an appropriate distribution function [53,143,142].

As has been stressed before, one of the main advantages of the Boltzmann models over the lattice-gas automaton models is the elimination of statistical noise. Freedom from statistical noise is a virtue shared with systems such as the Navier-Stokes equations. However, for systems in which statistical noise plays a crucial role, such as chemical reactive flows or phase transition phenomena, the lattice-gas method should be used, because it contains the fluctuations needed for the systems.

In the next two sections, two models of linear lattice Boltzmann equation are studied. In §5.3, the related *H*-theorems will be proved.

### 5.1 The Linear Collision Operator and the Equilibrium Distribution

There are at least two undesirable features in the Navier-Stokes equation derived from LGA systems which we wish to correct. The first is the lack of Galilean invariance due to non-unity factor,  $g(\rho)$ , and the second is the velocity dependence of the equation of state. These two problems arise because of the form of the Fermi-Dirac distribution function. If the coefficients of the quadratic terms (in  $\mathbf{v}$ ) in the distribution function were altered, then the aforementioned artifacts can be eliminated [54,143,142].

We write the linear lattice Boltzmann equation as follows:

$$f_{\alpha}(\boldsymbol{x} + \hat{\boldsymbol{e}}_{\alpha}, t+1) = f_{\alpha}(\boldsymbol{x}, t) + \mathbb{J}_{\alpha\beta}(f_{\beta} - f_{\beta}^{(eq)}), \qquad (5.1.1)$$

where  $f_{\beta}^{(eq)}$  is an equilibrium distribution yet to be determined. The construction of the above equation consists of two ingredients. First, the collision operator is so constructed that it has the exact symmetry as that of the collision operator linearized about the equilibrium  $\rho = \rho_0$ . However, the matrix elements of J are not determined by the collision rules of LGA models, rather they are adjustable parameters for tuning the system to the desired transport coefficients. The second ingredient is the construction of the equilibrium distribution function,  $f_{\alpha}^{(eq)}$ , so that the factor,  $g(\rho)$ , is set to unity, and the velocity dependence of the equation of state is eliminated.

From the analysis presented in Chapter 3, it can be clearly identified the sources where the unphysical effects of  $g(\rho)$  and velocity dependence of the equation of state come from. The factor,  $g(\rho)$ , is due to the lead coefficient in the  $\mathcal{O}(\mathbf{v}^2)$  term in the small velocity expansion of the distribution function. The velocity dependence of the equation of state is due the diagonal term in  $S_{ijkl}v_kv_l$ . Therefore, the unphysical effects can be eliminated if the aforementioned two terms were adjusted properly. We can set  $g(\rho) = 1$  for  $f_{\alpha}$  being a polynomial in  $\mathbf{v}$  up to second order, and adjust the lead coefficient of  $\delta_{ij}\mathbf{v}^2$  to correct the velocity dependence of the equation of state. The degree of freedom provided by rest particles can be used to satisfy the mass and momentum conservation constraints. In particular, the following distribution function has the desired features:

$$f_{\alpha}^{(eq)} = \begin{cases} \frac{\rho}{\sigma} \left( \sigma_0 - \frac{\sigma_1}{Dc_s^2} \delta_{ij} v_i v_j \right) & \alpha = 0, \\ \\ \frac{\rho}{\sigma} \left( 1 + \frac{\delta_x}{c_s^2} \hat{\boldsymbol{e}}_{\alpha,i} v_i + \frac{(D+2)}{2c_s^2} \left( Q_{\alpha,ij} + \frac{2}{D(D+2)} \delta_{ij} \right) v_i v_j \right) & \alpha \neq 0, \end{cases}$$

$$(5.1.2)$$

where  $\sigma_0$  and  $\sigma_1$  are the maximum number of rest and moving particles with speed one per site, respectively;  $\sigma = \sigma_0 + \sigma_1$  is the maximum number of particles per site; and

$$c_s = \delta_x \sqrt{\frac{\sigma_1}{\sigma D}} \tag{5.1.3}$$

is the sound speed. Therefore, the sound speed can be adjusted by varying  $\sigma_0$  (with  $\sigma_1$  fixed), that is, by varying the fraction of rest particles in the system. The more rest particles, the smaller the sound speed. It is easy to verify that  $\sum_{\alpha} f_{\alpha}^{(eq)} = \rho$ ,  $\delta_x \sum_{\alpha} \hat{\boldsymbol{e}}_{\alpha} f_{\alpha}^{(eq)} = \rho \boldsymbol{v}$ , and

$$\Pi_{ij} = \delta_x^2 \sum_{\alpha} \hat{\boldsymbol{e}}_{\alpha,i} \hat{\boldsymbol{e}}_{\alpha,j} f_{\alpha}^{(\mathrm{eq})} = c_s^2 \rho \delta_{ij} + \rho v_i v_j.$$

Thus, both aforementioned artifacts have been eliminated.

The linear collision operator, J, is constructed as follows. To preserve the rotational invariance of J, the transition probabilities among moving particles must form a symmetric circulant matrix. Also, the transition probabilities between rest particles and moving particles with momentum  $\hat{\boldsymbol{e}}_{\alpha}$ ,  $\alpha=1,\,2,\,\cdots,\,6$ , must be the same. Then,

$$J = \begin{pmatrix} c & \boldsymbol{b}^T \\ \boldsymbol{b} & \boldsymbol{A} \end{pmatrix} , \tag{5.1.4}$$

where  $\mathbf{b} = b(1, 1, 1, 1, 1, 1)^T$ , and  $\mathbf{A} = \mathbf{circ}(A_1, A_2, A_3, A_4, A_3, A_2)$ . Assuming that the maximum number of rest particles is  $\sigma_0$ , and that of the moving particles with velocity  $\hat{\mathbf{e}}_{\alpha}$  is one, the matrix J must have a zero eigenvalue with (D+1)-fold degeneracy, which corresponds to mass and momentum conservation constraints. The conservation constraints lead to

$$\sigma_0 c + 6b = 0, (5.1.5a)$$

$$A_1 + 2A_2 + 2A_3 + A_4 + \sigma_0 b = 0, (5.1.5b)$$

$$A_1 + A_2 - A_3 - A_4 = 0. (5.1.5c)$$

There are also three additional non-zero eigenvalues

$$\gamma_1 = 6(A_1 + A_2) + 2\sigma_0 b, \qquad (5.1.6a)$$

$$\gamma_2 = -6(A_1 + 2A_2) - 3\sigma_0 b, \qquad (5.1.6b)$$

$$\gamma_3 = -\left(\frac{6}{\sigma_0} + \sigma_0\right)b, \qquad (5.1.6c)$$

where  $\gamma_1$  has a two-fold degeneracy. Among the nonzero eigenvalues,  $\gamma_1$  is the most important one, because the viscosity is related to  $\gamma_1$  by

$$\nu = -\frac{1}{(D+2)} \left( \frac{1}{2} + \frac{1}{\gamma_1} \right) . \tag{5.1.7}$$

Thus, the range of  $\gamma_1$  must be between -2 and 0 for  $\nu$  to be positive. It should be noted that by choosing  $\gamma_1$  close to -2 from above, the viscosity,  $\nu$ , can be arbitrarily close to zero and the Reynolds number can be enhanced. Of course, care must be taken to ensure that the smallest scale of the simulated flow is greater than the lattice scale, or numerical inaccuracies will occur and instabilities are observed. Of course, this problem is not unique to LGA or LBE methods. It is a common problem for any numerical methods for solving the Navier-Stokes equation. By specifying the  $\gamma$ 's, the matrix elements of J can be completely determined. Usually,  $\gamma_1$  is chosen according to the desired  $\nu$ ;  $\gamma_2$  and  $\gamma_3$  are chosen to be -1 so that the corresponding kinetic modes decay to zero as quickly as possible (in one time step), as these modes decay like  $1+\gamma_2$  and  $1+\gamma_3$ . It should be pointed out that the matrix elements,  $J_{\alpha\beta}$ 's, determined by choosing  $\gamma_{\alpha}$ 's may have no LGA equivalent. That is, no collision mechanism leads to the values of  $J_{\alpha\beta}$ 's for certain values of  $\gamma_{\alpha}$ 's.

Now, the linear lattice Boltzmann equation, which approximates the incompress-

ible Navier-Stokes equations, is

$$f_{\alpha}(\boldsymbol{x} + \hat{\boldsymbol{e}}_{\alpha}, t+1) = f_{\alpha}(\boldsymbol{x}, t) + J_{\alpha\beta} f_{\beta}^{(\text{neq})}, \qquad (5.1.8)$$

where  $f_{\alpha}^{(\text{neq})}$  is the nonequilibrium part of the distribution function:

$$f_{\alpha}^{(\text{neq})} = f_{\alpha} - f_{\alpha}^{(\text{eq})}. \tag{5.1.9}$$

The Navier-Stokes equation derived from above system does not have the artifacts due to unphysical  $g(\rho)$  factor and the velocity dependence of the equation of state found in the lattice-gas method.

### 5.2 Lattice BGK Model

The collision operator, J, can be further simplified by the single relaxation time approximation. In what follows, the single relaxation time approximation and the related equation are discussed.

### 5.2.1 The Single Relaxation Time Approximation

Recall the Boltzmann equation,

$$\frac{\partial f}{\partial t} + \boldsymbol{\xi} \cdot \nabla f = \mathcal{C}(f, f),$$

where the collision operator

$$C(f, f) = \int dS d\boldsymbol{\xi}_1 (f'f'_1 - ff_1).$$

Near equilibrium, the system is close to a local Maxwell-Boltzmann state. Moreover, the post-collision distribution functions, f''s, should be closer to equilibrium than the pre-collision f's, because of the H-theorem. Therefore, we can apply the following approximation:

$$\int dS d\xi_1 f' f'_1 \approx \int dS d\xi_1 f'^{(0)} f'^{(0)}_1. \tag{5.2.1}$$

Because  $f^{(0)}$  is the solution of  $\mathcal{C}(f^{(0)}, f^{(0)}) = 0$ , then,

$$\int dS d\boldsymbol{\xi}_1 f'^{(0)} f_1^{\prime(0)} = \int dS d\boldsymbol{\xi}_1 f^{(0)} f_1^{(0)} = f^{(0)} \int dS d\boldsymbol{\xi}_1 f_1^{(0)}, \qquad (5.2.2)$$

where we have used the fact that  $f^{(0)}$  is independent of  $\xi_1$ . Consequently, from the above two equations, we have

$$\int dS d\xi_1 f' f'_1 \approx f^{(0)} \int dS d\xi_1 f_1^{(0)}. \tag{5.2.3}$$

Also, because of the constraints of the Chapman-Enskog expansion, that is, the hydrodynamic moments of f are equal to that of  $f^{(0)}$ , therefore,

$$\int dS d\xi_1 f f_1 = f \int dS d\xi_1 f_1 = f \int dS d\xi_1 f_1^{(0)}.$$
 (5.2.4)

Now, the collision term in the Boltzmann equation can be approximated by

$$C(f, f) = -\frac{1}{\tau}(f - f^{(0)}), \tag{5.2.5}$$

where

$$\frac{1}{\tau} = \int dS d\xi_1 f_1^{(0)}, \tag{5.2.6}$$

 $\tau$  is the characteristic relaxation time of collision processes, and  $\omega = 1/\tau$  is the characteristic frequency. Then the Boltzmann equation becomes the BGK equation

$$\frac{\partial f}{\partial t} + \boldsymbol{\xi} \cdot \nabla f = -\frac{1}{\tau} (f - f^{(0)}). \tag{5.2.7}$$

The above equation is called BGK equation, after P. L. Bhatnager, E. F. Gross and M. Krook [144]. In the literature, the operator

$$C(f, f) = -\frac{1}{\tau}(f - f^{(0)})$$

is some times referred to as the Krook operator.

The simple BGK equation still retains some important properties of the Boltzmann equation: H-theorem, and the correct prediction of the thermo-fluid conservation equations. However, the simplification also leads to some shortcomings. One of its most noticeable defects is that it gives the wrong Prandtl number  $\nu/\kappa$ . Therefore, discretion must be taken when using the model.

#### 5.2.2 Lattice BGK model

Application of the single relaxation time approximation to the lattice Boltzmann equation leads to the lattice BGK equation:

$$f_{\alpha}(\boldsymbol{x} + \hat{\boldsymbol{e}}_{\alpha}, t+1) = f_{\alpha}(\boldsymbol{x}, t) - \frac{1}{\tau} (f_{\alpha}(\boldsymbol{x}, t) - f_{\alpha}^{(eq)}), \tag{5.2.8}$$

where  $f_{\alpha}^{(eq)}$  is given by Eq. (5.1.2) in the previous section. The viscosity of the lattice BGK model is related to the collision time,  $\tau$ , by

$$\nu = \frac{2\tau - 1}{2(D+2)}.\tag{5.2.9}$$

This result is obtained by recognizing that  $\gamma_1 = -\frac{1}{\tau}$  here. Because of the above equation, we must set  $\tau > \frac{1}{2}$  to keep  $\nu$  positive so that the system is stable.

The lattice BGK equation has great computational advantage when it is implemented on parallel computers, because it does not require memory to store the collision matrix in each processor.

An important virtue of the linear Boltzmann equation technique is that one has the freedom to choose the equilibrium distribution function,  $f_{\alpha}^{(eq)}$ . By properly choosing  $f_{\alpha}^{(eq)}$ , the linear Boltzmann equation can be used to simulated various kinds of physical systems, such as multi-phase or multi-component fluids [58]. Also, with the freedom, one is not restricted to the triangle lattice now. Indeed, the square lattice (with speed 0, 1 and  $\sqrt{2}$ ) can be used by choosing an appropriate equilibrium distribution function,  $f_{\alpha}^{(eq)}$ , to satisfy the symmetry criteria [137,142].

# 5.3 The H-Theorem for Linear Lattice Boltzmann Equations

In this section, we will study how the linear lattice Boltzmann models approach equilibrium. For the sake of simplicity, we shall prove the *H*-theorem for the following system:

$$\frac{\partial f_{\alpha}}{\partial t} + \hat{\boldsymbol{e}}_{\alpha} \cdot \nabla f_{\alpha} = -\frac{1}{\tau} (f_{\alpha} - f_{\alpha}^{(eq)}). \tag{5.3.1}$$

## 5.3.1 The Local H-Theorem for Spatially Homogeneous Systems

We first prove the local H-theorem for spatially homogeneous systems:

$$\frac{\partial f_{\alpha}}{\partial t} = -\frac{1}{\tau} (f_{\alpha} - f_{\alpha}^{(e_{q})}), \tag{5.3.2}$$

where  $f_{\alpha}^{(eq)}$  is a constant.

Define

$$H = \sum_{\alpha} f_{\alpha} \ln(f_{\alpha}/f_{\alpha}^{(eq)}), \qquad (5.3.3)$$

then we can show that  $\frac{dH}{dt} \leq 0$ . The proof goes as follows.

$$\frac{dH}{dt} = \sum_{\alpha} \frac{\partial f_{\alpha}}{\partial t} \ln(f_{\alpha}/f_{\alpha}^{(eq)}) + \sum_{\alpha} \frac{\partial f_{\alpha}}{\partial t}$$

$$= -\frac{1}{\tau} \sum_{\alpha} (f_{\alpha} - f_{\alpha}^{(eq)}) \ln(f_{\alpha}/f_{\alpha}^{(eq)}) + \frac{\partial}{\partial t} \sum_{\alpha} f_{\alpha}.$$

The second term in the above equation is zero because of the homogeneity ( $f_{\alpha}^{(eq)} = \text{constant}$ ):

$$\frac{\partial}{\partial t} \sum_{\alpha} f_{\alpha} = \frac{\partial}{\partial t} \sum_{\alpha} f_{\alpha}^{(eq)} = 0.$$

Furthermore,  $(f_{\alpha} - f_{\alpha}^{(eq)}) \ln(f_{\alpha}/f_{\alpha}^{(eq)}) \ge 0$  for positive  $f_{\alpha}$  and  $f_{\alpha}^{(eq)}$ . Thus, it follows immediately that

$$\frac{dH}{dt} \le 0. (5.3.4)$$

Next, we can show that H, as a function of  $f_{\alpha}$ , is bounded from below, and has a minimum at  $f_{\alpha} = f_{\alpha}^{(eq)}$ . Since the system has the following conservation constraints:

$$\begin{split} & \rho = \sum_{\alpha} f_{\alpha} = \sum_{\alpha} f_{\alpha}^{(\text{eq})}, \\ & p_{x} = \sum_{\alpha} \hat{\boldsymbol{e}}_{\alpha,x} f_{\alpha} = \sum_{\alpha} \hat{\boldsymbol{e}}_{\alpha,x} f_{\alpha}^{(\text{eq})}, \\ & p_{y} = \sum_{\alpha} \hat{\boldsymbol{e}}_{\alpha,y} f_{\alpha} = \sum_{\alpha} \hat{\boldsymbol{e}}_{\alpha,y} f_{\alpha}^{(\text{eq})}, \end{split}$$

the system at minimum  $\{f_{\alpha}^*\}$  should satisfy

$$\frac{\delta H}{\delta f_{\alpha}} + c_1 \frac{\delta \rho}{\delta f_{\alpha}} + c_2 \frac{\delta p_x}{\delta f_{\alpha}} + c_3 \frac{\delta p_y}{\delta f_{\alpha}} = 0,$$

where the constant c's are the Lagrangian multipliers. This leads to

$$\ln(f_{\alpha}^*/f_{\alpha}^{(eq)}) + (c_1 + 1) + c_2 \hat{\boldsymbol{e}}_{\alpha,x} + c_3 \hat{\boldsymbol{e}}_{\alpha,y} = 0,$$

or,

$$f_{\alpha}^* = f_{\alpha}^{(eq)} \exp\left(-(c_1+1) - c_2 \hat{\boldsymbol{e}}_{\alpha,x} - c_3 \hat{\boldsymbol{e}}_{\alpha,y}\right),$$

where the constant c's are to be determined by solving the following equations from the conservation constraints:

$$\begin{split} &\sum_{\alpha} f_{\alpha}^{(\text{eq})} = e^{-(c_1+1)} \sum_{\alpha} f_{\alpha}^{(\text{eq})} \exp\left(-c_2 \hat{\boldsymbol{e}}_{\alpha,x} - c_3 \hat{\boldsymbol{e}}_{\alpha,y}\right), \\ &\sum_{\alpha} \hat{\boldsymbol{e}}_{\alpha,x} f_{\alpha}^{(\text{eq})} = e^{-(c_1+1)} \sum_{\alpha} \hat{\boldsymbol{e}}_{\alpha,x} f_{\alpha}^{(\text{eq})} \exp\left(-c_2 \hat{\boldsymbol{e}}_{\alpha,x} - c_3 \hat{\boldsymbol{e}}_{\alpha,y}\right), \\ &\sum_{\alpha} \hat{\boldsymbol{e}}_{\alpha,y} f_{\alpha}^{(\text{eq})} = e^{-(c_1+1)} \sum_{\alpha} \hat{\boldsymbol{e}}_{\alpha,y} f_{\alpha}^{(\text{eq})} \exp\left(-c_2 \hat{\boldsymbol{e}}_{\alpha,x} - c_3 \hat{\boldsymbol{e}}_{\alpha,y}\right). \end{split}$$

The results are  $c_1 = -1$ , and  $c_2 = c_3 = 0$ . Therefore,  $f_{\alpha}^* = f_{\alpha}^{(eq)}$ .

Now, we can conclude that  $\{f_{\alpha}^{(eq)}\}$  is a stable fixed point of the system, and the system is irreversibly approaches the fixed point (equilibrium). This completes the proof of the local H-theorem for homogeneous systems.

### 5.3.2 The Global H-Theorem for Spatially Inhomogeneous Systems

We now turn to the system

$$\frac{\partial f_{\alpha}}{\partial t} + \hat{\boldsymbol{e}}_{\alpha} \cdot \nabla f_{\alpha} = -\frac{1}{\tau} (f_{\alpha} - f_{\alpha}^{(eq)}), \tag{5.3.7}$$

where the equilibrium distribution function  $f_{\alpha}^{(eq)}$  depends on  $\boldsymbol{x}$  and t only through the thermodynamical variables  $\rho$  and  $\boldsymbol{v}$ , that is,  $f_{\alpha}^{(eq)} = f_{\alpha}^{(eq)}(\rho, \boldsymbol{v})$ .

Define

$$H = \int d\boldsymbol{x} \sum_{\alpha} f_{\alpha} \ln(f_{\alpha}/f_{\alpha}^{(eq)}). \tag{5.3.8}$$

Then,

$$\frac{dH}{dt} = \int d\boldsymbol{x} \sum_{\alpha} \frac{\partial f_{\alpha}}{\partial t} \ln(f_{\alpha}/f_{\alpha}^{(eq)}) + \int d\boldsymbol{x} \sum_{\alpha} \frac{\partial f_{\alpha}}{\partial t} - \int d\boldsymbol{x} \sum_{\alpha} \frac{f_{\alpha}}{f_{\alpha}^{(eq)}} \frac{\partial f_{\alpha}^{(eq)}}{\partial t}$$

$$= -\int d\boldsymbol{x} \sum_{\alpha} \left( \hat{\boldsymbol{e}}_{\alpha} \cdot \nabla f_{\alpha} + \frac{1}{\tau} (f_{\alpha} - f_{\alpha}^{(eq)}) \right) \ln(f_{\alpha}/f_{\alpha}^{(eq)}) - \int d\boldsymbol{x} \sum_{\alpha} \frac{f_{\alpha}}{f_{\alpha}^{(eq)}} \frac{\partial f_{\alpha}^{(eq)}}{\partial t}.$$

If the system size is infinite, or finite with periodic boundary conditions, then

$$\int d\boldsymbol{x} \sum_{\alpha} \ln(f_{\alpha}/f_{\alpha}^{(eq)}) \hat{\boldsymbol{e}}_{\alpha} \cdot \nabla f_{\alpha} = -\int d\boldsymbol{x} \sum_{\alpha} f_{\alpha} \hat{\boldsymbol{e}}_{\alpha} \cdot \nabla \ln(f_{\alpha}/f_{\alpha}^{(eq)})$$

$$= \int d\boldsymbol{x} \sum_{\alpha} f_{\alpha} \left( \frac{1}{f_{\alpha}^{(eq)}} \hat{\boldsymbol{e}}_{\alpha} \cdot \nabla f_{\alpha}^{(eq)} - \frac{1}{f_{\alpha}} \hat{\boldsymbol{e}}_{\alpha} \cdot \nabla f_{\alpha} \right)$$

$$= \int d\boldsymbol{x} \sum_{\alpha} \frac{f_{\alpha}}{f_{\alpha}^{(eq)}} \hat{\boldsymbol{e}}_{\alpha} \cdot \nabla f_{\alpha}^{(eq)}.$$

It follows immediately that

$$\frac{dH}{dt} = -\frac{1}{\tau} \int d\boldsymbol{x} \sum_{\alpha} (f_{\alpha} - f_{\alpha}^{(eq)}) \ln(f_{\alpha}/f_{\alpha}^{(eq)}) - \int d\boldsymbol{x} \sum_{\alpha} \frac{f_{\alpha}}{f_{\alpha}^{(eq)}} \left( \frac{\partial f_{\alpha}^{(eq)}}{\partial t} + \hat{\boldsymbol{e}}_{\alpha} \cdot \nabla f_{\alpha}^{(eq)} \right).$$

In the above equation, it is apparent that the first term is non-positive for any positive  $f_{\alpha}$  and  $f_{\alpha}^{(eq)}$ , and the second one is identical to zero due to Eq. (5.3.7). Therefore, we have shown

$$\frac{dH}{dt} \le 0.$$

Following the same steps in the proof of the local H-theorem, we can also show that  $H_0 = H(f_{\alpha}^{(eq)})$  is the lower bound of H. Thus, we have proved the global H-theorem.

A few remarks are in order regarding the *H*-theorems. First, the conditions for the *H*-theorems should be restated: (1)  $\{f_{\alpha}\}$  and  $\{f_{\alpha}^{(eq)}\}$  are positive; (2)  $\{f_{\alpha}^{(eq)}\}$  are functions of  $\rho$  and  $\boldsymbol{v}$ . For the choice of  $f_{\alpha}^{(eq)}$  here, *i.e.*,  $f_{\alpha}^{(eq)}$  is a second degree polynomial of  $\boldsymbol{v}$ , the magnitude of  $\boldsymbol{v}$  (or Mach number) must be small to keep  $f_{\alpha}^{(eq)}$  positive. Second, in the proof, only the Krook operator is used for the collision

operator. However, it is straightforward to extend the proof to the full linear collision operator, J. Thus, the theorems are also true for the linear Boltzmann equation with collision operator, J. Third, the H-theorems proved here are for the systems with continuous space and time, instead of lattice space and discrete time. Thus, the theorems are only applicable to lattice systems in the hydrodynamic limit,  $\mathbf{k} \to 0$  and  $\omega \to 0$ . Since the differences between the systems with continuous space and time and those with lattice space and discrete time are the higher order derivatives (or equivalently, the higher order terms in  $\mathbf{k}$  and  $\omega$  in Fourier space). Thus, the local gradient and time variation should be small for the system to maintain the stability supported by the H-theorem, and thus to contract to the desired equilibrium.

# CHAPTER SIX

# FLOW IN A 2-D SYMMETRIC SUDDEN-EXPANSION CHANNEL

In this chapter, a numerical study of nonlinear flow phenomena in a two-dimensional symmetric sudden-expansion channel by using the lattice Boltzmann equation method is presented. The reason this system is chosen is that, not only does it exhibit an array of interesting nonlinear flow phenomena, but also it has been studied both experimentally [145–148] and numerically [149,148,150] using some traditional methods, so that a comparative study between the lattice Boltzmann method and other traditional methods can be conducted quantitatively.

In the past two decades, it has been of great interest to study certain flow systems experiencing transition to turbulence. One popular example is Taylor-Couette flow [151, 152]. The flow in a symmetric sudden-expansion channel serves as another example. It has been observed experimentally that, below a certain critical value of the Reynolds number, which depends upon the geometric configuration of the channel, the flow pattern in a symmetric sudden-expansion channel is symmetric. The two recirculation regions behind the steps are symmetrically located with respect to the channel center plane. The flow is steady (time-independent) and two-dimensional. The symmetric flow becomes unstable once the Reynolds number exceeds the critical value, and a pair of steady asymmetric flows are observed as one recirculation region grows at the expense of the other — a symmetry-breaking bifurcation has taken

place. The flow is still two-dimensional at this point. As the Reynolds number is increased further, various instabilities may be observed, depending upon the geometric configuration of the channel. The flow may become first three-dimensional and then oscillatory or *vice versa*. Ultimately, the flow becomes turbulent as the Reynolds number increases further. Studies have shown that flow asymmetry and hence solution multiplicity remains a feature of flows in the turbulent regime.

In what follows, we shall describe the boundary conditions for the numerical simulations in §6.1. In §6.2, we shall present the numerical results of the simulations.

# 6.1 The Description of the System and the Arrangement of the Simulation

Figure (6.1.1) shows a schematic two-dimensional plot (in xy-plane) of the flow channel in the experiment [148]. The three-dimensional geometry of the channel used



Figure 6.1.1: A schematic two-dimensional plot of the flow channel in the experiment.

in the experiment [148] is now described. The flow-channel consists of two sections. The long entry section before the expansion channel provides sufficient length for the required parabolic entry (velocity) profile to develop fully. To ensure that the entry flow is two-dimensional, that is, to minimize the three-dimensional flow effects induced by the side walls, the width (in z direction) of the entry section is set much larger than its height (24:1). After the entry section, the fluid then flows through an 1:3 symmetric, plane expansion into a section 80 step-heights in length and of aspect ratio 8:1. Experimental observations have shown that the low Reynolds num-

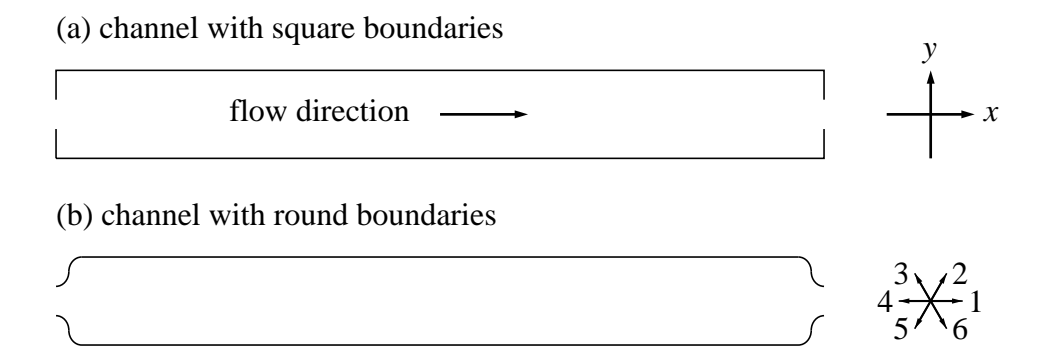


Figure 6.1.2: Geometry of boundary walls used in the simulations.

ber flow ( $R_e \leq 140$ ) is nominally two-dimensional in a channel with such an aspect ratio [146, 148].

The Reynolds number for the system is defined by

$$R_e = \frac{hU_0}{2\nu},\tag{6.1.1}$$

where h is the height of the entry section,  $U_0$  the maximum inlet velocity and  $\nu$  the kinematic viscosity. The Reynolds number is tuned by changing  $U_0$  in experiments with fixed  $\nu$ .

To test the validity of the lattice Boltzmann method, this algorithm is employed to study the occurrence of the symmetry-breaking bifurcation of the flow in the symmetric sudden-expansion channel. Because the bifurcation occurs at a critical Reynolds number at which the flow is two-dimensional, the two-dimensional lattice BGK equation with triangular lattice space is used for the simulations. There are two boundary geometries used in the simulations, as shown in Fig. (6.1.2). At the entry, the flow velocity is prescribed in the following fashion. The x-component of velocity,  $v_x$ , has a parabolic profile with a maximum,  $U_0$ , while the y-component,  $v_y$ , is zero. This entry profile is fixed for all time. At the boundary walls, velocity is always set to be zero. In the algorithm used here, the number of rest particles equals the number

of moving particles. Thus the sound speed,  $c_s$ , is  $\frac{1}{2}$ , and the Reynolds number is

$$R_e = \frac{4hU_0}{2\tau - 1},\tag{6.1.2}$$

where  $h = \frac{\sqrt{3}}{2}N_0$ ,  $N_0$  is the number of lattice sites in the  $\boldsymbol{y}$ -direction at the entry. The Reynolds number is varied by changing  $\tau$ , with both h and  $U_0$  fixed.

# 6.2 Numerical Results for the Steady State Symmetry-Breaking Bifurcation

In the simulations, the system size is  $N_x \times N_y = 2048 \times 256$ . The height of the entry section is 86 lattice sites (in  $\mathbf{y}$ -direction), thus  $h = 43\sqrt{3}$ . The maximum speed at entry  $U_0 = 0.15$ . The sinusoidal boundary walls are prescribed by  $y = \pm f(x)$ , where

$$f(x) = \begin{cases} \frac{h}{2} + \frac{(L_y - h)}{2} (1 - \cos((x - 1)\pi/64)), & 1 \le x \le 64, \\ \frac{L_y}{2}, & 65 \le x \le L_x - 64, \\ \frac{h}{2} + \frac{(L_y - h)}{2} (1 - \cos((L_x - x)\pi/64)), & L_x - 63 \le x \le L_x. \end{cases}$$

Note that the values of y are integers. With the configuration of the channel shown in Fig. (6.1.2), the expansion ratio is  $\frac{86}{256} \approx \frac{1}{3}$ . With the given h and  $U_0$ , the Reynolds number is

$$R_e = \frac{25.8\sqrt{3}}{2\tau - 1}.$$

The initial conditions for the velocity field in our simulations are set to be asymmetric with respect to the symmetric x-axis of the channel,  $v_x(y > 0) = 0.01$ ,

 $v_x(y < 0) = 0$ , and  $v_y = 0$ . The asymmetry of the initial condition determines the branch the asymmetric final state reaches. The simulation is run until a steady state is achieved.

We define the stream function,

$$\psi(x, y) = \int_0^y v_x(x, y') dy', \tag{6.2.1}$$

and a variable of state,  $\chi$ , to measure the asymmetry:

$$\chi^{2} = \frac{\int dx dy \left(\psi(x, y) + \psi(x, -y)\right)^{2}}{\int dx dy}.$$
 (6.2.2)

It is obvious that when the flow pattern is symmetric about the x-axis,  $\chi = 0$ . In the simulations,  $\chi$  is measured as a function of  $R_e$ .

Figures (6.2.1) and (6.2.2) are contours of the steady-state stream function for different values of  $R_e$ . The symmetric flow pattern for  $R_e$  below the symmetry-breaking bifurcation and the asymmetric ones for  $R_e$  above the bifurcation are shown clearly in Figures (6.2.1) and (6.2.2).

Figure (6.2.3) is the bifurcation diagram for the symmetry-breaking bifurcation in the channel flow. The diagram clearly shows the existence of the symmetry-breaking bifurcation at the critical Reynolds number,  $R_e^*$ . For the channel with square boundaries, we found that  $R_e^* = 46.19$ . For the channel with the sinusoidal boundaries,  $R_e^* = 50.12$ . To test the stability of the solutions, random noise is added to  $v_x$  and  $v_y$  at the entry. The results indicate that solutions are stable under the disturbance.

In Ref. [148], a channel with square boundaries was used in both numerical simulations and laboratory experiments. The value of the critical Reynolds number obtained from their simulations was  $R_e^* = 40.45$ , and that measured from the exper-

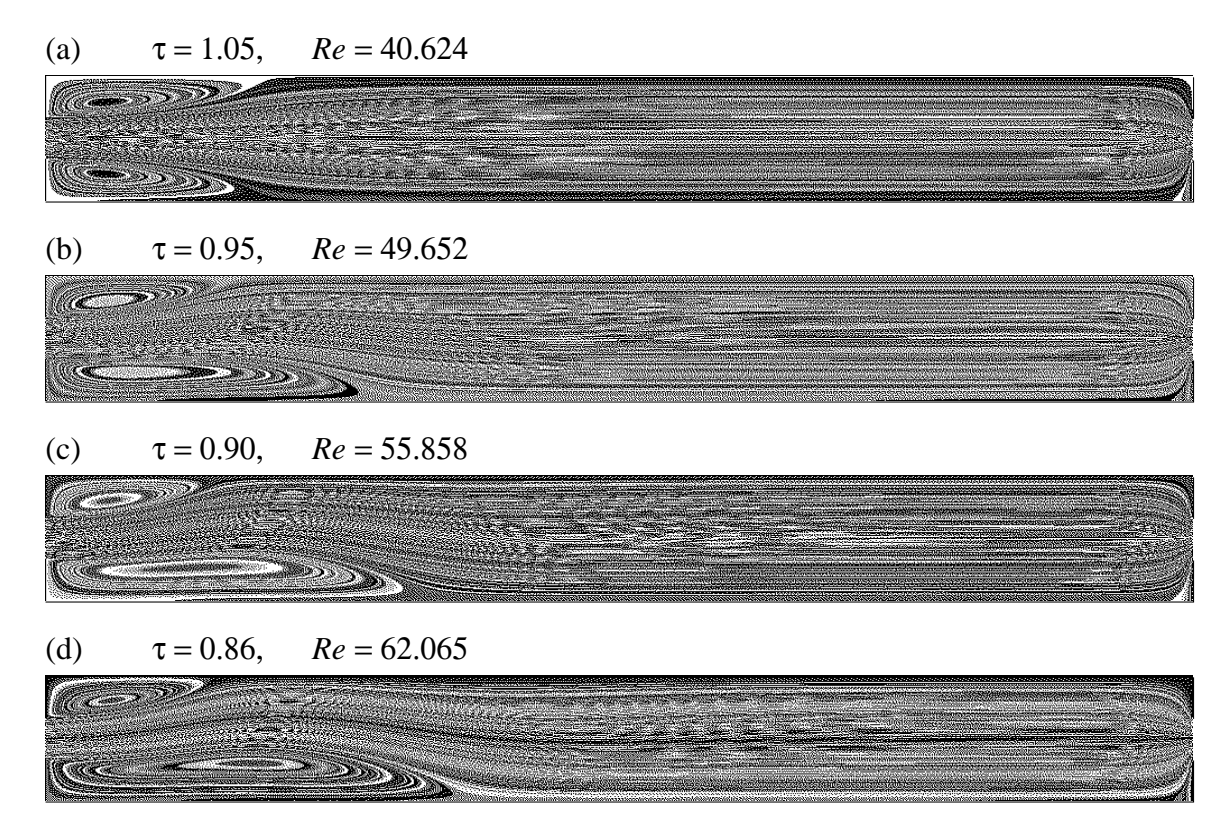


Figure 6.2.1: The contours of the stream function for the channel flow with square wall. Fig. (a) illustrates the symmetric flow pattern before the symmetry-breaking bifurcation occurs. Figs. (b), (c) and (d) illustrate the asymmetric flow patterns developed after the symmetry-breaking bifurcation occurs.

iment was  $R_e^* = 47.3$ . Our results not only reconfirm the existence of the symmetry-breaking bifurcation for flow in the 2-D symmetric sudden-expansion channel, but also agree with the existing results in Ref. [148] quantitatively. In Ref. [149], the value of  $R_e^* = 5.95$  was obtained for the channel with the sinusoidal walls. Despite the difference in the definition of the Reynolds number,  $R_e$ , the quantitative disagreement cannot be resolved between two sets of results in Ref. [148] and in Ref. [149].

In the simulations, when the Reynolds number is close to the critical value, the system is very slow to converge to the final steady state. This phenomenon is well understood: as  $R_e$  approaches  $R_e^*$ , the time to reach the final state increases exponentially. Since the algorithm used here is based upon a kinetic model, it is expected

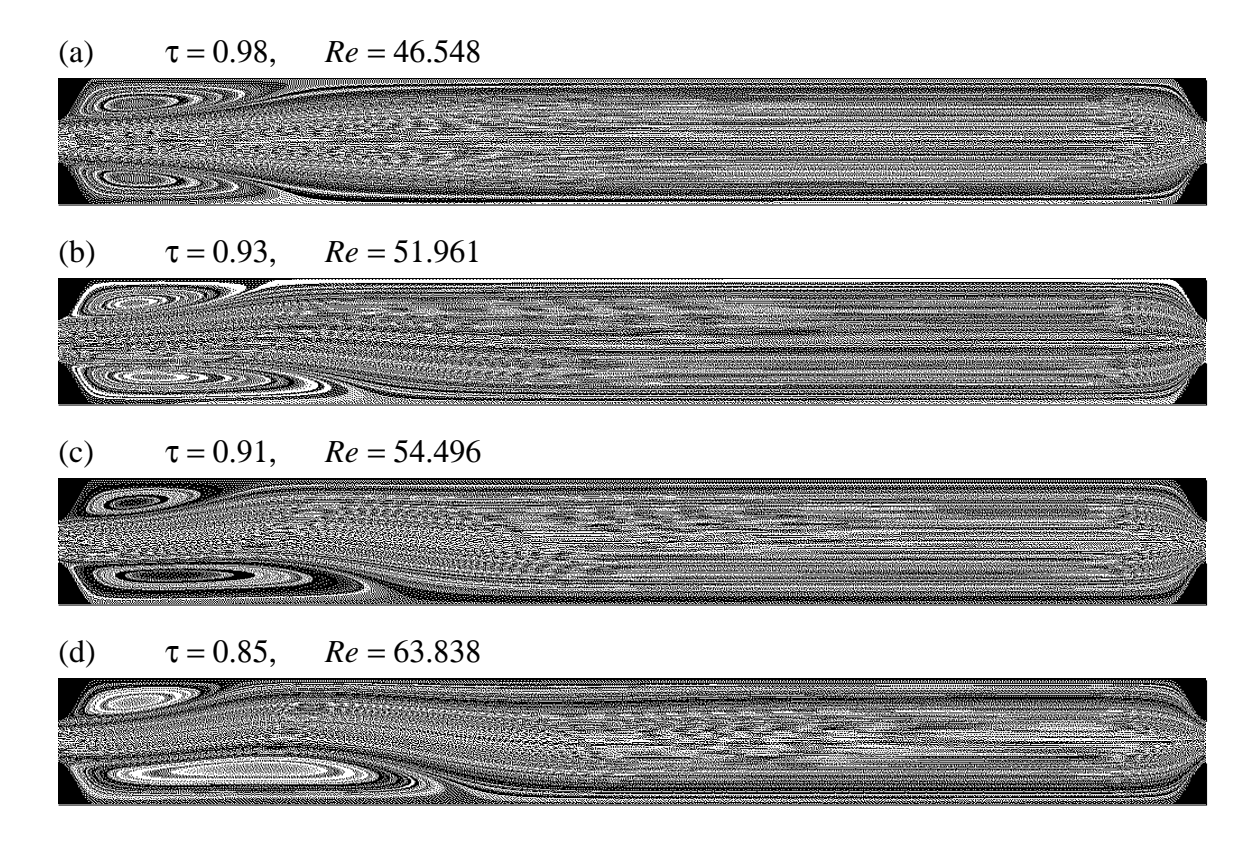


Figure 6.2.2: The same as the Fig. (6.2.1), with the sinusoidal walls.

that the number of time steps of iteration is much larger than that in standard numerical methods for solving the Navier-Stokes equations, such as finite-difference or finite-element methods, because the time steps here are on the kinetic, or microscopic, scale, while that in standard methods are on the hydrodynamic, or macroscopic, scale. Thus, the lattice-gas or the lattice Boltzmann methods might not be superior to those standard methods in terms of computing time for this particular problem. This is because, with the regular boundary geometries used here, standard methods can handle the problem in a straightforward fashion. If, however, the geometry of boundaries were more complicated, standard methods may be very inefficient in dealing with such boundaries. Then the advantages of the lattice-gas or the lattice Boltzmann methods become immediately self evident, because complicated boundary geometries do not slow down the algorithm at all.

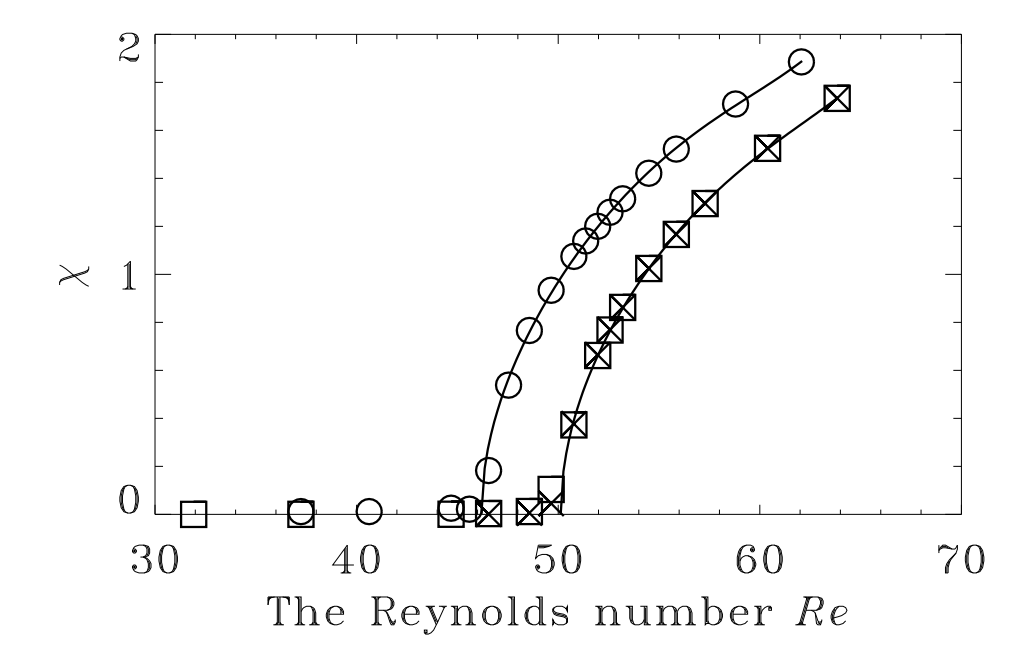


Figure 6.2.3: Bifurcation diagram of the symmetry-breaking bifurcation for flow in the symmetric sudden-expansion channel.  $\times$  represents the values of  $\chi$  with the sinusoidal walls;  $\square$  represents  $\chi$  with the sinusoidal walls and with random force at the entry;  $\bigcirc$  represents  $\chi$  with the square walls.

As shown in the results, the value of  $R_e^*$  sensitively depends upon the boundary conditions. The values of  $R_e^*$  for two sets of boundaries, *i.e.*, the square and the sinusoidal walls illustrated in Fig. (6.1.2), are significantly different. One would expect the stability of the symmetric mode (or the asymmetric modes) in the problem to depend upon the boundary conditions. This boundary condition sensitivity could also contribute, at least in part, to the difference between the results here and that obtained by the standard methods. Although, in the limit of an infinitely large lattice system, the lattice-gas or the lattice Boltzmann algorithms should converge to the Navier-Stokes equation. But, with the finite-size system, differences between kinetic models and PDE's are visible. It is hoped that the relative convergence rates can be investigated in more detail in the near future.

# CHAPTER SEVEN

# CONCLUSION AND DISCUSSION

In this thesis, the theory of the FHP lattice-gas automata and lattice Boltzmann equations is thoroughly reviewed. The linearized lattice Boltzmann equation is analytically solved. Generalized hydrodynamics of the FHP lattice-gas automata, *i.e.*, the dispersion relations of transport coefficients, is studied via the linearized lattice Boltzmann equation. The solutions for some simple flows, such as Poiseuille flow and plane Couette flow, are obtained. These solutions of the linearized Boltzmann equation are valid for the entire range of the Knudsen number,  $K_n$ . That is, the solutions not only contain a hydrodynamic component, but also contain a kinetic component. This is important in quantitative study of the kinetic effects in the simulations by the lattice-gas methods. Although we only solved the linearized lattice Boltzmann equation for a FHP 6-bit model, the method is applicable to any other lattice-gas models.

The original study of the symmetry-breaking bifurcation in a 2-D symmetry sudden-expansion channel provides convincing evidence to support the validity of the simulation techniques of the lattice Boltzmann equation. This example is valuable especially when the general convergence of the lattice Boltzmann method is not fully understood, and the quantitative numerical evidence is scarce.

Although the hydrodynamic equations can be derived from the lattice-gas and the lattice Boltzmann models, the discrepancy between the simulation by directly solving the Navier-Stokes equations and by using the methods of the lattice-gas automata and the lattice Boltzmann equations has not been quantitatively studied. One possible way of analyzing this discrepancy is to use the method of approximate inertial manifolds [153–156]. The theory of inertial manifolds provides a rigorous connection between certain evolution partial differential equations and low-dimensional dynamical systems. The restriction of the flow of the partial differential equation to the inertial manifold is given by a *finite* set of ordinary differential equations called an inertial form, which captures the long-time dynamic behavior of the partial differential equation. One can certainly apply this method to study long-time dynamics of the lattice-gas automata and the lattice Boltzmann equations, and make close comparisons with that of the Navier-Stokes equations.

The lattice-gas automata and the lattice Boltzmann equations are very simple algorithms for simulating complex physical systems. Because of their simplicity, there are some inherent shortcomings in these models. For instance, with the small number of speeds allowed, it is difficult to simulate temperature. Although this difficulty can be overcome by allowing more speeds in the model, this will increase the complexity of the model and thus decrease its numerical efficiency. Therefore, there is a trade-off between the complexity and the efficiency of these methods. This issue also deserves further study.

In closing, we have studied, in both theory and applications, the methods of the lattice-gas automata and the lattice Boltzmann equations. We have demonstrated that these methods can be utilized to solve difficult problems.

# References

- L. D. Landau and E. M. Lifshitz. Fluid Mechanics, volume 6 of Landau and Lifshitz Course of Theoretical Physics. Pergamon Press, Oxford, 2nd edition, 1987.
- [2] Victor L. Peterson. Computational challenges in aerospace. Future Generation Computer Systems, 5(2/3):243–258, 1989.
- [3] George Em Karniadakis and Steven A. Orszag. Nodes, modes and flow codes. Computers in Physics, 46(3):34–42, March 1993. This issue of Physics Today is a special issue on high-performance computing and physics.
- [4] Berni J. Alder. Challenges in computational statistical mechanics. Future Generation Computer Systems, 5:191–195, 1989.
- [5] W. Daniel Hillis. *The Connection Machine*. The MIT Press, Cambridge, Massachusetts, 1985.
- [6] Philip Elmer-Dewitt. Machines from the lunatic fringe. *Time*, pages 74–75, 1991. (November 11th issue).
- [7] Shiyi Chen and Xiaowen Shan. High-resolution turbulent simulations using the Connection Machine-2. Computers in Physics, 6(6):643-646, November/December 1992.
  - The speed cited in this article was 77 seconds per-time-step on a Connection Machine-2. Improvement has been made for the code run on a CM-200.
- [8] Stanislaw M. Ulam. Random processes and transformations. In Proceedings of the International Congress of Mathematicians, pages 264–275, Providence. RI, 1952. AMS.

[9] John von Neumann. Theory of Self-Reproducing Automata. University of Illinois Press, Urbana, IL, 1966. Edited and completed by A. W. Burks.

- [10] E. F. Codd. Cellular Automata. Academic Press, New York, 1968.
- [11] Martin Gardner. The fantastic combinations of John Conway's new solitaire game "life". Scientific American, 223(4):120–123, October 1970.
- [12] Martin Gardner. On cellular automata, self-reproduction, the Garden of Eden and the game "life". Scientific American, 224(2):112–117, February 1971.
- [13] Martin Gardner. How to triumph at nim by playing safe, and John Horton Conway's game "Hackenbush". Scientific American, 226(1):104–107, January 1972.
- [14] Brian Hayes. The cellular automata offers a model of the world and a world unto itself. Scientific American, 250(3):12–21, March 1984.
- [15] Stephen Wolfram. Statistical mechanics of cellular automata. Review of Modern Physics, 55:601–644, 1983.
- [16] Stephen Wolfram. Cellular automata as models of complexity. Nature, 311:419–424, 1984.
- [17] G. Y. Vichniac. Simulating physics with cellular automata. Physica D, 10:96– 116, 1984.
- [18] Tommaso Toffoli. Cellular automata as an alternative to (rather than an approximation of) differential equations in modeling physics. *Physica D*, 10:117–127, 1984.
- [19] Tommaso Toffoli and Norman Margolus. Cellular Automata Machines. The MIT Press, Cambridge, MA, 1987.
- [20] Doyne Farmer, T. Toffoli, and S. Wolfram, editors. Cellular Automata, volume 10 of Physica D. North-Holland, 1984.

Proceedings of an Interdisciplinary Workshop, held at Los Alamos, New Mexico 87545, USA, March 7–11, 1983. This special issue is a collection of papers on various aspects of cellular automata and their applications.

- [21] Stephen Wolfram, editor. Theory and Applications of Cellular Automata, volume 1 of Advanced Series on Complex Systems. World Scientific, Singapore, 1986.
  - A collection including selected papers on cellular automata 1983–1986.
- [22] P. Manneville, N. Boccara, G. Y. Vichniac, and R. Bidaux, editors. Cellular Automata and Modeling of Complex Physical Systems, Berlin, 1989. Springer-Verlag.
  - This volume contains the proceedings of an International Winter Workshop held at the Centre de Physique des Houches, February 21–28, 1989.
- [23] James E. Broadwell. Study of rarefied shear flow by the discrete velocity method. *Journal of Fluid Mechanics*, 19:401–414, 1964.
- [24] James Clerk Maxwell. On the dynamical theory of gases. In W. D. Niven, editor, The Scientific Papers of James Clerk Maxwell, volume II, pages 26-78. Dover Publications, Inc., New York, 1952. This paper was originally published in the Philosophical Transactions, Vol. CLVII.
- [25] R. Gatignol. Théorie Cinétique des Gaz à Répartition Discrète de Vitesses, volume 36 of Lecture Notes in Physics. Springer-Verlag, Berlin, 1975.
- [26] Tadeusz Płatkowski and Reinhard Illner. Discrete velocity models of the Boltzmann equation: A survey on the mathematical aspects of the theory. SIAM Review, 30(2):213-255, June 1988.

[27] Balasubramanya T. Nadiga. A Study of Multi-Speed Discrete-Velocity Gases. PhD thesis, California Institute of Technology, Pasadena, California, February 1992.

- [28] Joseph O. Hirschfelder, Charles F. Curtiss, and R. Byron Bird. Molecular Theory of Gases and Liquids. John Wiley & Sons, Inc., New York, 1954.
- [29] M. H. Ernst. Nonlinear model-Boltzmann equations and exact solutions. Physics Reports, 78(1):1–171, November 1981.
- [30] S. K. Godunov and U. M. Sultangazin. On discrete models of the kinetic Boltz-mann equation. Russian Mathematical Surveys, 26(3):1-55, May/June 1971. The English translation of Uspekhi Matematicheskikh Nauk.
- [31] T. Carleman. Problémes Mathèmatiques dans la Théorie Cinétique des Gaz. Almqvist and Wiksells, Uppsala, 1957.
- [32] H. P. McKean. An exponential formula for solving Boltzmann's equation for a Maxwellian gas. *Journal of Combinatorial Theory*, 2:358–382, 1967.
- [33] H. P. McKean. Application of Brownian motion to the equation of Kolmogorov-Petrovskii-Piskunov. Communications on Pure and Applied Mathematics, 28:323-331, 1975.
- [34] Henri Cornille. Exact solutions in 1 + 1 dimensions of the general two-velocity discrete Illner model. Journal of Mathematical Physics, 28(7):1567–1579, July 1987.
- [35] Reinhard Illner. Global existence for two-velocity models of the Boltzmann equation. Mathematical Methods in the Applied Sciences, 1:187–193, 1979.
- [36] Reinhard Illner. Mild solutions of hyperbolic systems with  $L_+^1$  and  $L_+^\infty$  initial data. Transport Theory and Statistical Physics, 13(3/4):431-453, 1984.

[37] James E. Broadwell. Shock structure in a simple discrete velocity gas. *Physics of Fluids*, 7(8):1243–1247, August 1964.

- [38] Leo P. Kadanoff and Jack Swift. Transport coefficients near the critical point: A master-equation approach. *Physical Review*, 165(1):310–322, January 1968.
- [39] J. Thomas Beale. Large-time behavior of solutions of the Broadwell model of a discrete velocity gas. Communications in Mathematical Physics, 102:217–235, 1985.
- [40] Shuichi Kawashima. Large-time behavior of solutions of the discrete Boltzmann equation. Communications in Mathematical Physics, 109:563–589, 1987.
- [41] Henri Cornille. Exact solutions of the broadwell model in 1 + 1 dimensions.

  Journal of Physics A, 20:1973–1988, 1987.
- [42] Henri Cornille. Exact 1 + 1-dimensional solutions of discrete planar velocity Boltzmann models. *Journal of Statistical Physics*, 48(3/4):789-811, 1987.
- [43] Henri Cornille. 2D and 3D exact shock wave solutions with specular reflection to the discrete Boltzmann models. *Journal of Physics A*, 22:4787–4796, 1989.
- [44] Uriel Frisch, Brosl Hasslacher, and Yves Pomeau. Lattice-gas automata for the Navier-Stokes equation. *Physical Review Letters*, 56(14):1505–1508, April 1986.
- [45] Stephen Wolfram. Cellular automaton fluids 1: Basic theory. *Journal of Statistical Physics*, 45(3/4):471–526, November 1986.
- [46] Uriel Frisch, D. d'Humières, B. Hasslacher, P. Lallemand, Yv. Pomeau, and J.-P. Rivet. Lattice gas hydrodynamics in two and three dimensions. *Complex Systems*, 1(4):649-707, August 1987.
- [47] Brosl Hasslacher. Discrete fluids. Los Alamos Science, Special Issue(15):175–217, 1987.

This special issue of Los Alamos Science is also published as From Cardinals to Chaos by Cambridge University Press, Cambridge, 1988.

- [48] Gary D. Doolen, editor. Complex Systems, volume 1, August 1987.
  The articles in this issue are mostly based in part on presentations given at the "Workshop on Large Nonlinear Systems", held in Santa Fe, New Mexico, on October 27–29, 1986.
- [49] Gary D. Doolen, editor. Lattice Gas Methods for Partial Differential Equations, volume IV of A Proceedings Volume in the Santa Fe Studies in the Sciences of Complexity, Redwood City, CA, 1989. Addison-Wesley.
  - A volume of lattice gas reprints and articles, including selected papers from the workshop on large nonlinear systems, held August, 1987 in Los Alamos, New Mexico.
- [50] Gary D. Doolen, editor. Lattice Gas Methods for PDE's: Theory, Applications and Hardware, volume 47 of Physica D. North-Holland, 1991.
   Proceedings of the NATO Advanced Research Workshop held at the Center for Nonlinear Studies, Los Alamos National Laboratory, Los Alamos, NM 87545,
- [51] Daniel H. Rothman and Jeffrey M. Keller. Immiscible cellular-automaton fluids.

  Journal of Statistical Physics, 52(3/4):1119–1127, August 1988.

USA, September 6-8, 1989.

- [52] Daniel H. Rothman and Stéphane Zaleski. Spinodal decomposition in a latticegas automaton. *Journal de Physique*, 50(16):2161–2174, August 1989.
- [53] Andrew K. Gunstensen and D. H. Rothman. A lattice-gas model for three immiscible fluids. *Physica D*, 47:47–52, 1991.

[54] Andrew K. Gunstensen, D. H. Rothman, S. Zaleski, and G. Zanetti. Lattice Boltzmann model of immiscible fluids. *Physical Review A*, 43(8):4320–4327, April 1991.

- [55] S. Chen, G. D. Doolen, K. Eggert, D. Grunau, and E. Y. Loh. Local lattice-gas model for immiscible fluids. *Physical Review A*, 43(12):7053-7056, June 1991.
- [56] Andrew K. Gunstensen and D. H. Rothman. Microscopic modeling of immiscible fluids in three dimensions by a lattice Boltzmann method. Europhysics Letters, 18(2):157–161, February 1992.
- [57] Andrew K. Gunstensen. Lattice-Boltzmann Studies of Multiphase Flow Through Porous Media. PhD thesis, Massachusetts Institute of Technology, Cambridge, Massachusetts, June 1992.
- [58] Xiaowen Shan and Hudong Chen. A lattice Boltzmann model for simulating flows with multiple phases and components. *Physical Review E*, 47(3):1815– 1819, March 1993.
- [59] David Dab, Anna Lawniczak, Jean-Pierre Boon, and Raymond Kapral. Cellular-automaton model for reactive systems. *Physical Review Letters*, 64(20):2462-2465, May 1990.
- [60] Anna Lawniczak, David Dab, Raymond Kapral, and Jean-Pierre Boon. Reactive lattice gas automata. Physica D, 47:132–158, 1991.
- [61] Raymond Kapral, Anna Lawniczak, and Paul Masiar. Oscillations and waves in a reactive lattice-gas automaton. *Physical Review Letters*, 66(19):2539–2542, May 1991.
- [62] Raymond Kapral, Anna Lawniczak, and Paul Masiar. Reactive dynamics in a multispecies lattice-gas automaton. *Journal of Chemical Physics*, 96(4):2762– 2775, February 1991.

[63] Raymond Kapral. Discrete models for chemical reacting systems. preprint, 1992.

- [64] Xiao-Guang Wu and Raymond Kapral. Catalytic *CO* oxidation on *Pt* surfaces: A lattice-gas cellular automaton model. *Physica A*, 188(1–3):284–301, 1992.
- [65] B. Hasslacher, R. Kapral, and A. Lawniczak. Molecular Turing structures in the biochemistry of the cell. preprint, 1992.
- [66] H. Chen, S. Chen, G. D. Doolen, Y. C. Lee, and H. Rose. Multithermodynamic phase lattice-gas automata incorporating interparticle potentials. *Physical Re*view A, 40(5):2850–2853, September 1989.
- [67] S. Chen, H. Chen, G. D. Doolen, Y. C. Lee, and H. Rose. Lattice gas automata models for nonideal gas fluids. *Physica D*, 47:97–111, 1991.
- [68] Cécile Appert and Stéphane Zaleski. A lattice gas with a liquid-gas transition. Physical Review Letters, 64:1, 1990.
- [69] Cécile Appert, Daniel H. Rothman, and Stéphane Zaleski. A liquid-gas model on a lattice. *Physica D*, 47:85–96, 1991.
- [70] Hudong Chen and William H. Matthaeus. New cellular automaton model for magnetohydrodynamics. *Physical Review Letters*, 58(18):1845–1848, May 1987.
- [71] S. Succi, M. Vergassola, and R. Benzi. Lattice Boltzmann scheme for twodimensional magnetohydrodynamics. *Physical Review A*, 43(8):4521–4524, April 1991.
- [72] Shiyi Chen, Hudong Chen, Daniel Martínez, and William Matthaeus. Lattice Boltzmann model for simulation of magnetohydrodynamics. *Physical Review Letters*, 67(27):3776–3779, December 1991.

[73] Shiyi Chen, Daniel Martínez, William Matthaeus, and Hudong Chen. Magnetohydrodynamics computations with lattice gas automata. *Journal of Statistical Physics*, 68(3/4):533-556, August 1992.

- [74] M. G. Ancona. Lattice-gas approach to semiconductor device simulation. Solid-State Electronics, 33(12):1633–1642, 1990.
- [75] K. Kometer, G. Zandler, and P. Vogl. Lattice-gas cellular-automaton method for semiclassical transport in semiconductors. *Physical Review B*, 46(3):1382– 1394, July 1992.
- [76] Bruce M. Boghosian and C. David Levermore. A cellular automaton for Burgers' equation. *Complex Systems*, 1:17–30, August 1987.
- [77] Hudong Chen, Shiyi Chen, Gary Doolen, and Y. C. Lee. Simple lattice gas models for waves. *Complex Systems*, 2:259–267, 1988.
- [78] Hudong Chen, W. H. Matthaeus, and L. W. Klein. Theory of multicolor lattice gas: A cellular automaton Poisson solver. *Journal of Computational Physics*, 88:433-466, 1990.
- [79] S. Ponce-Dawson, S. Chen, and G. D. Doolen. Lattice Boltzmann computations for reaction-diffusion equations. *Journal of Chemical Physics*, 98(2):1514–1523, January 1993.
- [80] J. Hardy and Yv. Pomeau. Thermodynamics and hydrodynamics for a model fluid. *Journal of Mathematical Physics*, 13:1042–1051, 1972.
- [81] J. Hardy, Yv. Pomeau, and O. de Pazzis. Time evolution of a two-dimensional classical lattice system. *Physical Review Letters*, 31:276–279, 1973.
- [82] J. Hardy, Yv. Pomeau, and O. de Pazzis. Time evolution of a two-dimensional model system. I. Invariant states and time correlation functions. *Journal of Mathematical Physics*, 14:1746–1759, 1973.

[83] J. Hardy, O. de Pazzis, and Yv. Pomeau. Molecular dynamics of a classical lattice gas: Transport properties and time correlation functions. *Physical Review* A, 13:1949–1961, 1976.

- [84] D. d'Humières, P. Lallemand, and U. Frisch. Lattice gas models for 3D hydrodynamics. *Europhysics letters*, 2:291, 1986.
- [85] G. R. McNamara and G. Zanetti. Use of the Boltzmann equation to simulate lattice-gas automata. *Physical Review Letters*, 61(20):2332-2335, November 1988.
- [86] R. Benzi, S. Succi, and M. Vergassola. The lattice Boltzmann equation: Theory and applications. *Physics Reports*, 222(3):145–197, December 1992.
- [87] Christopher M. Teixeira. Continuum Limit of Lattice Gas Fluid Dynamics. PhD thesis, Massachusetts Institute of Technology, Cambridge, Massachusetts, September 1992.
- [88] I. G. Currie. Fundamental Mechanics of Fluids. McGraw-Hill, New York, 1974.
- [89] Michael E. O'Neill and Frank Chorlton. Viscous and Compressible Fluid Dynamics. Ellis Horwood Limited, Chichester, West Sussex, England, 1989.
- [90] Stewart Harris. An Introduction to the Theory of the Boltzmann Equation. Holt, Rinehart and Winston, Inc., New York, 1971.
- [91] Carlo Cercignani. The Boltzmann Equation and Its Applications, volume 67 of Applied Mathematical Sciences. Springer-Verlag, New York, 1988.
- [92] Richard L. Liboff. Kinetic Theory. Prentice Hall, Englewood Cliffs, New Jersey, 1990.
- [93] E. M. Lifshitz and L. P. Pitaevskii. Physical Kinetics, volume 10 of Landau and Lifshitz Course of Theoretical Physics. Pergamon Press, Oxford, 1981.

[94] Richard L. Liboff. *Introduction to the Theory of Kinetic Equations*. John Wiley and Sons, Inc., New York, 1969.

- [95] Ludwig Boltzmann. Lectures on Gas Theory. University of California Press, Berkeley and Los Angeles, 1964. Translated by Stephen G. Brush.
- [96] James A. McLennan. Introduction to Non-Equilibrium Statistical Mechanics. Prentice Hall, Englewood Cliffs, New Jersey, 1989.
- [97] Kerson Huang. Statistical Mechanics. John Wiley & Sons, Inc., New York, 1963.
- [98] Sydney Chapman and T. G. Cowling. The Mathematical Theory of Non-Uniform Gases. The Cambridge University Press, Cambridge, 2nd edition, 1953.
- [99] S. T. Choh. The Kinetic Theory of Phenomena in Dense Gases. PhD thesis, University of Michigan, 1958.
- [100] George E. Uhlenbeck and George W. Ford with E. W. Montroll. Lectures in Statistical Mechanics, volume I of Lectures in Applied Mathematics. American Mathematical Society, Providence, Rhode Island, 1963. Proceedings of the Summer Seminar, Boulder, Colorado, 1960.
- [101] Joel Keizer. Statistical Thermodynamics of Nonequilibrium Processes. Springer-Verlag, New York, 1987.
- [102] Uriel Frisch. Lectures on turbulence and lattice gas hydrodynamics. In Jackson R. Herring and James C. McWilliams, editors, Lecture Notes on Turbulence, pages 219–278. World Scientific, Singapore, 1989. Lecture Notes from the NCAR-GTP Summer School, June 1987.

[103] A. Despain, C. E. Max, G. D. Doolen, and B. Hasslacher. Prospects for a lattice-gas computer. In Gary D. Doolen, editor, Lattice Gas Methods for Partial Differential Equations, pages 211–218, Redwood City, CA, 1989. Addison-Wesley.

- [104] R. Monaco, editor. Discrete Kinetic Theory, Lattice Gas Dynamics and Foundations of Hydrodynamics, Singapore, 1989. World Scientific.
  Proceedings of the workshop held in Torino, Italy, September 20–24, 1988.
- [105] Gianluigi Zanetti. Hydrodynamics of lattice-gas automata. Physical Review A, 40(3):1539-1548, August 1989.
- [106] Leo P. Kadanoff, G. R. McNamara, and G. Zanetti. From automata to fluid flow comparisons of simulation and theory. *Physical Review A*, 40:4527–4541, 1989.
- [107] D. d'Humières, Y.-H. Qian, and P. Lallemand. Invariants in lattice gas models. In R. Monaco, editor, Discrete Kinetic Theory, Lattice Gas Dynamics and Foundations of Hydrodynamics, pages 102–113, Singapore, 1989. I.S.I., World Scientific.
- [108] Gianluigi Zanetti. Counting hydrodynamic modes in lattice gas automata models. *Physica D*, 47(1/2):30-35, 1991.
- [109] David B. Goldstein. Investigations of a Discrete Velocity Gas. PhD thesis, California Institute of Technology, Pasadena, California, 1990.
- [110] Edwin Schrödinger. Statistical Thermodynamics. Dover Publications, Inc., New York, 2nd edition, 1989.
- [111] R. K. Pathria. Statistical Mechanics, volume 45 of International Series in Nature Philosophy. Pergamon, Oxford, England, 1984.

[112] L. E. Reichl. A Modern Course in Statistical Physics. University of Texas Press, Austin, Texas, 1980.

- [113] K. Diemer, K. Hunt, S. Chen, T. Shimomura, and G. D. Doolen. Density and velocity dependence of reynolds number for several lattice gas models. In Gary D. Doolen, editor, Lattice Gas Methods for Partial Differential Equations, pages 137-177. Addison-Wesley, Redwood City, CA, 1989.
- [114] Li-Shi Luo, Hudong Chen, Shiyi Chen, G. D. Doolen, and Y.-C. Lee. Generalized hydrodynamic transport in lattice-gas automata. *Physical Review A*, 43(12):7097-7100, June 1991.
- [115] H. L. Royden. Real Analysis. Macmillan Publishing Company, New York, 3rd edition, 1988.
- [116] D. d'Humières and P. Lallemand. Numerical simulations of hydrodynamics with lattice gas automata in two dimensions. Complex Systems, 1(4):599-632, August 1987.
- [117] Berni J. Alder and T. E. Wainwright. Decay of the velocity autocorrelation function. *Physical Review A*, 1(1):18, January 1970.
- [118] Washington Taylor, IV and Bruce M. Boghosian. Renormalization of lattice gas transport coefficients. preprint, September 1991.
- [119] Steven A. Orszag and Victor Yakhot. Reynolds number scaling of cellular-automaton hydrodynamics. *Physical Review Letters*, 56(16):1691–1693, April 1986.
- [120] W. Daniel Hillis. Richard Feynman and the Connection Machine. *Physics Today*, 42(2):78–83, February 1989.
- [121] Berni J. Alder and W. Edward Alley. Generalized hydrodynamics. *Physics Today*, 37(1):56–63, January 1984.

[122] W. Edward Alley and Berni J. Alder. Generalized transport coefficients for hard spheres. *Physical Review A*, 27(6):3158–3173, June 1983.

- [123] W. Edward Alley and Berni J. Alder. The neutron scattering function for hard spheres. *Physical Review A*, 27(6):3174–3186, June 1983.
- [124] Daniel H. Rothman. Cellular-automaton fluids: A model for flow in porous media. *Geophysics*, 53(4):509–518, April 1988.
- [125] S. Chen, K. Diemer, G. D. Doolen, K. Eggert, C. Fu, S. Gutman, and B. J. Travis. Lattice gas automata for flow through porous media. *Physica D*, 47:72–84, 1991.
- [126] P. J. Davis. Circulant Matrices. Wiley, New York, 1974.
- [127] G. A. Korn and T. M. Korn. Mathematical Handbook for Scientists and Engineers. McGraw-Hill, New York, 2nd edition, 1968.
- [128] J. P. Rivet and U. Frisch. Lattice gas automata in the Boltzmann approximation. In Gary D. Doolen, editor, Lattice Gas Methods for Partial Differential Equations, pages 443-449. Addison-Wesley, Redwood City, CA, 1990. This article originally appeared in Comptes Rendus, 302(II):267, 1986.
- [129] Patrick Grosfils, Jean-Pierre Boon, and Pierre Lallemand. Spontaneous fluctuation correlations in thermal lattice-gas automata. *Physical Review Letters*, 68(7):1077-1080, February 1992.
- [130] S. P. Das, H. J. Bussemaker, and M. H. Ernst. Generalized hydrodynamics of lattice gas automata. preprint, 1993.
- [131] D. K. Bhattacharya and G. C. Lie. Molecular-dynamics simulations of nonequilibrium heat and momentum transport in very dilute gases. *Physical Review Letters*, 62(8):897–900, February 1989.

[132] Leo P. Kadanoff, G. R. McNamara, and G. Zanetti. A Poiseuille viscometer for lattice gas automata. *Complex Systems*, 1(4):791–803, August 1987.

- [133] R. Cornubert, D. d'Humières, and D. Levermore. A Knudsen layer theory for lattice gases. *Physica D*, 47:241–259, 1991.
- [134] F. J. Higuera and S. Succi. Simulating the flow around a circular cylinder with a lattice Boltzmann equation. *Europhysics Letters*, 8(6):517–521, March 1989.
- [135] F. J. Higuera and J. Jiménez. Boltzmann approach to lattice gas simulations. Europhysics Letters, 9(7):663-668, August 1989.
- [136] S. Succi, E. Foti, and F. Higuera. Three-dimensional flows in complex geometries with the lattice Boltzmann method. Europhysics Letters, 10(5):433–438, November 1989.
- [137] Yue-Hong Qian. Gaz sur Réseaux et Théorie Cinétique sur Réseaux Appliquée à l'Equation de Navier-Stokes. PhD thesis, de l'Université Pierre et Marie Curie, January 1990.
- [138] F. J. Higuera. Lattice gas method based on the Chapman-Enskog expansion. Physics of Fluids A, 2(6):1049–1051, June 1990.
- [139] R. Benzi and S. Succi. Two-dimensional turbulence with the lattice Boltzmann equation. *Journal of Physics A*, 23:L1–L5, 1990.
- [140] R. Benzi, S. Succi, and M. Vergassola. Turbulence modelling by nonhydrodynamics variables. *Europhysics Letters*, 13(8):727–732, December 1990.
- [141] M. Vergassola, R. Benzi, and S. Succi. On the hydrodynamic behaviour of the lattice Boltzmann equation. *Europhysics Letters*, 13(5):411–416, November 1990.

[142] Yue-Hong Qian, D. d'Humières, and P. Lallemand. Lattice BGK models for Navier-Stokes equation. *Europhysics Letters*, 17(6):479–484, February 1992.

- [143] Hudong Chen, Shiyi Chen, and W. H. Matthaeus. Recovery of the Navier-Stokes equations using a lattice-gas Boltzmann method. *Physical Review A*, 45(8):R5339-5342, April 1992.
- [144] P. L. Bhatnagar, E. P. Gross, and M. Krook. A model for collision processes in gases. I. Small amplitude processes in charged and neutral one-component systems. *Physical Review*, 94(3):511–525, May 1954.
- [145] F. Durst, A. Melling, and J. H. Whitelaw. Low Reynolds number flow over a plane symmetric sudden expansion. *Journal of Fluid Mechanics*, 64:111–128, 1974.
- [146] W. Cherdron, F. Durst, and J. H. Whitelaw. Asymmetric flows and instabilities in symmetric ducts with sudden expansion. *Journal of Fluid Mechanics*, 84:13– 31, 1978.
- [147] Ian J. Sobey. Observation of waves during oscillatory channel flow. Journal of Fluid Mechanics, 151:395-426, 1985.
- [148] R. M. Fearn, T. Mullin, and K. A. Cliffe. Nonlinear flow-phenomena in a symmetric sudden-expansion. *Journal of Fluid Mechanics*, 211:595–608, 1990.
- [149] Ian J. Sobey and Philip G. Drazin. Bifurcations of two-dimensional channel flows. Journal of Fluid Mechanics, 171:263-287, 1986.
- [150] Lambros Kaiktsis. Break of symmetry and early transition in a symmetric sudden expansion flow. preprint, May 1992.
- [151] R. C. DiPrima and H. L. Swinney. Instabilities and transition in flow between concentric rotating cylinders. In H. L. Swinney and J. P. Gullob, editors, *Hydro-dynamic Instabilities and the Transition to Turbulence*, volume 45 of *Topics in*

- Applied Physics, chapter 6, pages 139–180. Springer-Verlag, Berlin, 2nd edition, 1985.
- [152] T. Mullin and K. A. Cliffe. Symmetry breaking and the onset of time dependence in fluid mechanical systems. In S. Sarker, editor, Nonlinear Phenomena and Chaos, pages 97–112. Adam Hilger, 1986.
- [153] Lawrence Sirovich. Turbulence and the dynamics of coherent structures Part
   I: Coherent structures. Quarterly of Applied Mathematics, XLV(3):561-571,
   October 1987.
- [154] H. S. Brown, M. S. Jolly, I. G. Kevrekidis, and E. S. Titi. Use of approximate inertial manifolds in bifurcation calculations. In D. Roose et. al., editor, Continuation and Bifurcations: Numerical Techniques and Applications, pages 9-23. Kluwer Academic Publishers, 1990.
- [155] M. S. Jolly, I. G. Kevrekidis, and E. S. Titi. Approximate inertial manifolds for the Kuramoto-Sivashinsky equation: Analysis and computations. *Physica* D, 44:38–60, 1990.
- [156] A. E. Deane, I. G. Kevrekidis, G. E. Karniadakis, and S. A. Orszag. Low-dimensional models for complex geometry flows: Application to grooved channels and circular cylinders. *Physics of Fluids A*, 3(10):2337–2354, October 1991.

### VITA

Li-Shi Luo was born on April 11th, 1958 (in the year of the Dog, at the apogee of the Great Leap Forward) in Xiamen City, in the Fujian Province of China. He is the oldest son of Mr. Wei-Jin Luo and Ms. Xiu-E Tong. He received his elementary education in Zhangzhou City, Fujian. After his graduation from Zhangzhou Third Middle School in the fall of 1975, Mr. Luo was sent by Chairman Mao to the countryside to be re-educated by peasants of the poor, lower and middle class. In 1977, at the end of the Cultural Revolution, the re-educated Mr. Luo passed the first post-Revolutionary university entrance examination, gaining admission to the Department of Electrical Engineering of Fuzhou University. He began his studies there in Spring of 1978, and was graduated with a BSc degree in Spring 1982. In May 1982 Mr. Luo traveled to London, Canada, where in September of that year he began study as a special student in the Department of Physics, University of Western Ontario. A year and a half later, he entered the graduate school to pursue his Master's degree under the supervision of Prof. John Nuttall. Mr. Luo studied large order perturbation theory and Padé approximants for his Master's thesis. After obtaining his MSc degree from the University of Western Ontario, he came to the School of Physics of the Georgia Institute of Technology in October of 1986, to pursue his PhD degree. In April 1989 he came to Los Alamos National Laboratory to complete his thesis work. He has been working with Dr. Gary D. Doolen in the field of lattice-gas automata and lattice Boltzmann equations since then.

Li-Shi Luo married Dr. Jianing Huang in 1988. Their daughter Lara was born in November 1992.